Characterization of Apoptosis and DNA Damage Response in Human Induced Pluripotent Stem Cells

Dissertation

der Mathematisch-Naturwissenschaftlichen Fakultät

der Eberhard Karls Universität Tübingen

zur Erlangung des Grades eines

Doktors der Naturwissenschaften

(Dr. rer. nat.)

vorgelegt von

Dipl.-Biochem. Simon Lehle

aus Stuttgart

Tübingen

2013

Tag der mündlichen Qualifikation:	05.07.2013
Dekan:	Prof. Dr. Wolfgang Rosenstiel
1. Berichterstatter:	Prof. Dr. Klaus Schulze-Osthoff
2. Berichterstatter:	Prof. Dr. Sebastian Wesselborg

TABLE OF CONTENTS

ABBREVIATIONS

AP	Alkaline phosphatase
APC	Allophycocyanin
APE1	Apurinic/apyrimidinic endonuclease 1
APS	Ammonium persulfate
ASK1	Apoptosis signal-regulating kinase 1
ATF	Activating transcription factor
ATM	Ataxia-telangiectasia mutated
ATP	Adenosine triphosphate
ATR	Ataxia-Telangiectasia mutated Rad-3 related
BAD	Bcl-2 associated death promoter
BAK	Bcl-2 homologous antagonist killer
BAX	Bcl-2 associated X protein
BCA	Bicinchoninic acid
BH	Bcl-2 homology domain
BID	BH3 interacting-domain death agonist
BIK	Bcl-2 interacting killer
BIM	Bcl-2 interacting mediator of cell death
BiP	Binding immunoglobulin protein
BIR	Baculovirus inhibitor of apoptosis protein repeat
Bleo	Bleomycin
BMF	Bcl-2-modifying factor
bp	Base pair
BSA	Bovine serum albumine
BSO	Buthionine sulfoximine
CaMKII	Ca^{2+}/calmodulin-dependent protein kinase II
CAT	Catalase
CD	Cluster of differentiation
CDK	Cyclin dependent kinase
ChIP	Chromatin immunoprecipitation
Chk	Checkpoint kinase
CHOP	C/EBP homologous protein
C_p	Crossing point
C_t	Threshold cycle
Ctrl	Control
d	Day
DAPI	4’,6-Diamidino-2-phenylindole
DED	Death effector domain
DISC	Death-inducing signaling complex
DMEM	Dulbecco's Modified Eagle Medium
DMF	Dimethyl fumarate
DMSO	Dimethylsulfoxide
DNA	Deoxyribonucleic acid
dNTP	Deoxyribonucleotide
DR	Death receptor
DSB	Double strand break
dsDNA	Double-stranded deoxyribonucleic acid
DTNB	5,5'-Dithiobis-(2-nitrobenzoic acid) / Ellman’s reagent
DTT	Dithiothreitol
E	Amplification efficiency

EB	Embryoid body
ECL	Enhanced chemoluminescence
ECM	Extracellular matrix
EDTA	Ethylenediaminetetraacetic acid
eIF2α	Eukaryotic translation initiation factor 2A
ELISA	Enzyme-linked immuno sorbent assay
ER	Endoplasmic reticulum
ES	Embryonic stem
ESC	Embryonic stem cell
Eto	Etoposide
FACS	Fluorescence-activated cell sorting
FADD	Fas-associated protein with death domain
FCS	Fetal calf serum (Fetal bovine serum)
FGF	Fibroblast growth factor
Fib	Fibroblasts
FITC	Fluorescein isothiocyanate
g	Standard gravity units
GAPDH	Glycerinaldehyde 3-phosphate dehydrogenase
Grp78	78 kDa glucose-regulated protein
GSH	Glutathione (reduced form)
GSH-OEt	Glutathione O-ethyl ester
GSSG	Glutathione (oxidized form)
GSx	Total glutathione (sum of reduced and oxidized form)
GTP	Guanosine triphosphate
Gy	Gray
HDAC	Histone deacetylase
HEK	Human embryonic kidney
HEPES	4-(2-hydroxyethyl)-1-piperazineethanesulfonic acid
hES	Human embryonic stem
hFib	Human (primary) fibroblast(s)
HGF	Hepatocyte growth factor
hiPS	Human induced pluripotent stem
HPLC	High-performance liquid chromatography
HRP	Horseradish peroxidase
HRK	Activator of apoptosis harakiri
IAP	Inhibitor of apoptosis
IP3R1	Inositol 1,4,5-trisphosphate receptor-1
iPS cells	Induced pluripotent stem cells
IR	Ionizing radiation (gamma radiation)
IRE1	Inositol requiring protein-1
JNK	c-Jun N-terminal kinase
K	Kelvin
kd	Knock down
ko	Knock out
LB	Lysogeny broth
LIF	Leukemia inhibitory factor
LORD-Q	Long run real-time PCR-based DNA damage quantification
M	Mole/liter
MAP3K	Mitogen-activated protein kinase kinase kinase
MAPK	Mitogen-activated protein kinase
MAPKKK	Mitogen-activated protein kinase kinase kinase

MCL-1	Induced myeloid leukemia cell differentiation protein
MDM2	Mouse double minute 2 homolog
MEF	Murine embryonic fibroblast
MOI	Multiplicity of infection
MOMP	Mitochondrial outer membrane permeabilization
MPTP	1-Methyl-4-phenyl-1,2,3,6-tetrahydropyridine
mRNA	Messenger ribonucleic acid
NADH	Nicotinamide adenine dinucleotide
NADPH	Nicotinamide adenine dinucleotide phosphate
NOXA (PMAIP)	Phorbol-12-myristate-13-acetate-induced protein 1
OMM	Outer mitochondrial membrane
PARP-1	Poly [ADP-ribose] polymerase-1
PBS	Phosphate buffered saline
PCD	Programmed cell death
PCR	Polymerase chain reaction
PE	Phycoerythrin
PerCP	Peridinin chlorophyll
PERK	Protein kinase RNA (PKR)-like ER kinase
PIPES	Piperazine-N,N′-bis(2-ethanesulfonic acid)
PMSF	Phenylmethanesulfonylfluoride
pRb	Retinoblastoma protein
PSC	Pluripotent stem cell
PTEN	Phosphatase and tensin homolog
PUMA	p53 upregulated modulator of apoptosis
PVDF	Polyvinylidene fluoride
qPCR	Quantitative PCR
R	Purine
RNA	Ribonucleic acid
ROS	Reactive oxygen species
rpm	Revolutions per minute
RPMI	Roswell Park Memorial Institute medium
rtPCR	Real-time PCR
RT-PCR	Reverse transcription PCR
SCID	Severe combined immunodeficiency
SDS	Sodium dodecyl sulfate
SDS-PAGE	Sodium dodecyl sulfate polyacrylamide gel electrophoresis
shRNA	Small hairpin RNA
siRNA	Small interfering RNA
SMAC/DIABLO	Second mitochondria derived activator of caspases/ Direct IAP binding protein with low pI
SOD	Superoxide dismutase
SSA	5-Sulfosalicylic acid
SSB	Single strand break
ssDNA	Single-stranded deoxyribonucleic acid
STS	Staurosporine
tBID	Truncated Bid
TAE	Tris, acetic acid, EDTA
TBS	Tris-buffered saline
TE	Tris/EDTA
TEMED	Tetramethylethylenediamine
TNFα	Tumor necrosis factor α

TNFR	TNF receptor
TRADD	TNF receptor type 1-associated death domain protein
TRAF2	TNF receptor-associated factor 2
TRX	Thioredoxin
U	Unit
UNG	Uracil N-glycosylase
UPR	Unfolded protein response
UV	Ultraviolet
UVR	Ultraviolet radiation
v	Volume
w	Weight
W	Adenine/Thymine
XBP1	X-box binding protein 1
Y	Pyrimidine
γH2AX	Phosphorylated histone H2AX

1. INTRODUCTION

Apoptosis is a fundamental and indispensable process involved in maintenance of cellular homeostasis and clearance of dysfunctional cells. Execution of apoptosis involves characteristic hallmarks, such as changes in cellular morphology, activation of key executioner proteases (caspases) and loss of the plasma membrane bilayer asymmetry. Responses to apoptotic stimuli vary with strength of the stimulus, cell type and activation status of a cell. In many tissues, DNA damage caused by genotoxic stimuli or endogenous stress provides a potent stimulus of apoptosis. Alternatively, DNA repair or cellular senescence may be induced e.g. depending on the strength and the duration of the genotoxic insult.

Human induced pluripotent stem (hiPS) cells represent a recently described cell type with a yet poorly defined response to apoptotic and genotoxic stimulation. These cells constitute embryonic stem-like cells that can be generated by forced expression of a few defined factors in somatic cells. This new cell type (first described in 2006[1]) is able to give rise to tissues and cells of all three germ layers. For this reason, hiPS cells are promising candidates for individualized stem cell and tissue replacement therapies employing patient-specific isogenic cells. However, little is known about DNA damage signaling and apoptotic response in hiPS cells. In order to develop safe stem cell applications, hiPS cells need to be thoroughly examined in terms of their balance of life and death. This is of prime importance since all pluripotent stem cells exhibit tumorigenic potential and thus entail the risk of carcinogenesis.

The first aim of the current project was a comprehensive characterization of apoptotic responses in hiPS cells upon defined extrinsic, intrinsic and ER stress stimuli. Second, cell type-specific acquisition of DNA damage during genotoxic treatment and its correlation to induction of apoptosis in hiPS cells was investigated. In this context, a method for DNA damage quantification was developed. Third, potential DNA-protective mechanisms in iPS cells were addressed.

The current chapter outlines the three main apoptotic signaling pathways, common types of DNA lesions, current DNA damage detection methods, signaling pathways activated by genotoxic impact and the relation between DNA damage and apoptosis. Human iPS cells are introduced and the current state of knowledge about DNA damage and apoptotic responses in these cells is explained.

1.1. Apoptosis

1.1.1. Definition and hallmarks of apoptosis

Programmed cell death (PCD), first termed apoptosis (greek: *apoptosis*, "to fall off") in 1972[2], is an evolutionary conserved form of programmed cell death. It is essential to control tissue homeostasis in higher and population size in primitive organisms[3,4]. In addition, it is involved in embryonic development[5], selection of germ cells[6] and activation-induced elimination of autoreactive lymphocytes[7].

Insufficient apoptosis is an essential property of most tumors, as many mutations in human cancers interrupt or impair death signaling[8]. Contrariwise, excessive apoptosis is associated with degenerative pathologies, such as neurodegeneration or autoimmune diseases[9]. A detailed understanding of apoptotic processes and disease-specific dysregulations is therefore an essential prerequisite for the development of any therapeutic application.

In contrast to traumatic (necrotic) cell death, apoptosis constitutes a highly orchestrated process. After initiation by extrinsic death ligands, ER stress (e.g. by accumulation of unfolded proteins) or intrinsic stimuli (e.g. DNA damage, replicative or oxidative stress), apoptosis is executed in a cascade of events, finally leading to activation of a set of cysteine-dependent aspartate-directed proteases (caspases) by limited proteolysis of procaspases. Two classes of caspases can be distinguished, named initiator (caspase-8 and -9) and downstream effector caspases (caspase-3, -6 and -7).

Caspases cleave their substrates within tetrapeptide consensus sequences of which the C-terminal amino acid is aspartate. Hundreds of substrates can be activated (such as the caspase-activated DNase, CAD) or inactivated (e.g. poly(ADP ribose)polymerase-1, PARP-1) by a few key executing proteases, which, in this way, control the progression of PCD[10]. Caspases initiate processes such as cleavage of the nuclear lamina (leading to nuclear shrinkage) or CAD-dependent fragmentation of nuclear DNA (yielding a characteristic DNA “ladder” of about 180 bp fragments)[11,12], attraction of professional phagocytes[13,14] and exposure of phosphatidylserine to the outer leaflet of the cell membrane, which constitutes a clearance signal for phagocytes[15].

Cells undergoing apoptosis exhibit characteristic changes in cellular morphology. Cytosolic acidification, cell shrinkage and nuclear condensation occur. ROCK (Rho-

associated (coiled-coil containing) protein kinase)-mediated rearrangements of the cytoskeleton result in chaotic budding of the cell membrane, so-called blebbing[16]. At the last stage of apoptosis, the blebbing cell is dissected into apoptotic bodies which are internalized and digested by phagocytes. In contrast to necrosis, apoptosis constitutes an anti-inflammatory process in which cellular integrity is maintained. However, if proper clearance fails, apoptotic bodies become secondary necrotic and perforate, leading to release of cytosolic content to the extracellular lumen and promotion of inflammatory immune responses[14].

Different cell types exhibit specific resistance or susceptibility to stimulation with potential inducers of apoptosis. For instance, B cells display inducible resistance to treatment with the death ligand CD95L (Fas ligand)[17], while neurons resist numerous internal apoptotic stimuli, such as high levels of oxidative stress[18]. In contrast, human ES cells prove hypersensitive to apoptosis induced by ionizing radiation[19].
Despite this heterogeneity of responses to apoptotic stimuli, three main apoptotic pathways have been described, namely the extrinsic, intrinsic and endoplasmic reticulum-mediated pathways. Fig. 1.1 depicts a schematic overview of extrinsic and intrinsic pathways.

1.1.2. Extrinsic apoptosis signaling pathway

The extrinsic apoptosis signaling pathway is a mechanism to respond to extracellular death signals. It is essential for the elimination of autoreactive T and B cells, killing of virally infected cells and removal of malignant cells[20]. Trimeric death ligands bind to specific transmembrane receptor proteins[21]. Death ligands comprise tumor necrosis factors alpha and beta (TNFα, TNFβ), CD95 ligand (CD95L / FasL) and TNFα-related apoptosis inducing ligand (TRAIL). Upon ligand binding, the monomeric receptors TNF-R1 (CD120a), TNF-R2 (CD120b), CD95 (Fas), TRAIL-RI (DR4) or TRAIL-RII (DR5) trimerize (Fig. 1.1). The trimeric receptors consequently serve as docking platforms for adaptor proteins, predominantly Fas-associated protein with death domains (FADD) for CD95 interaction and TNF receptor-associated protein with death domains (TRADD) binding to TNF-R1/2[21]. The resulting complex composed of receptors and adaptor proteins provides a scaffold for recruitment of procaspase-8 (or procaspase-10) molecules, so-called initiator caspases, leading to induced proximity and autoproteolysis. Procaspase-8 molecules are cleaved, yielding a long and a short fragment, both of which arrange with another cleaved

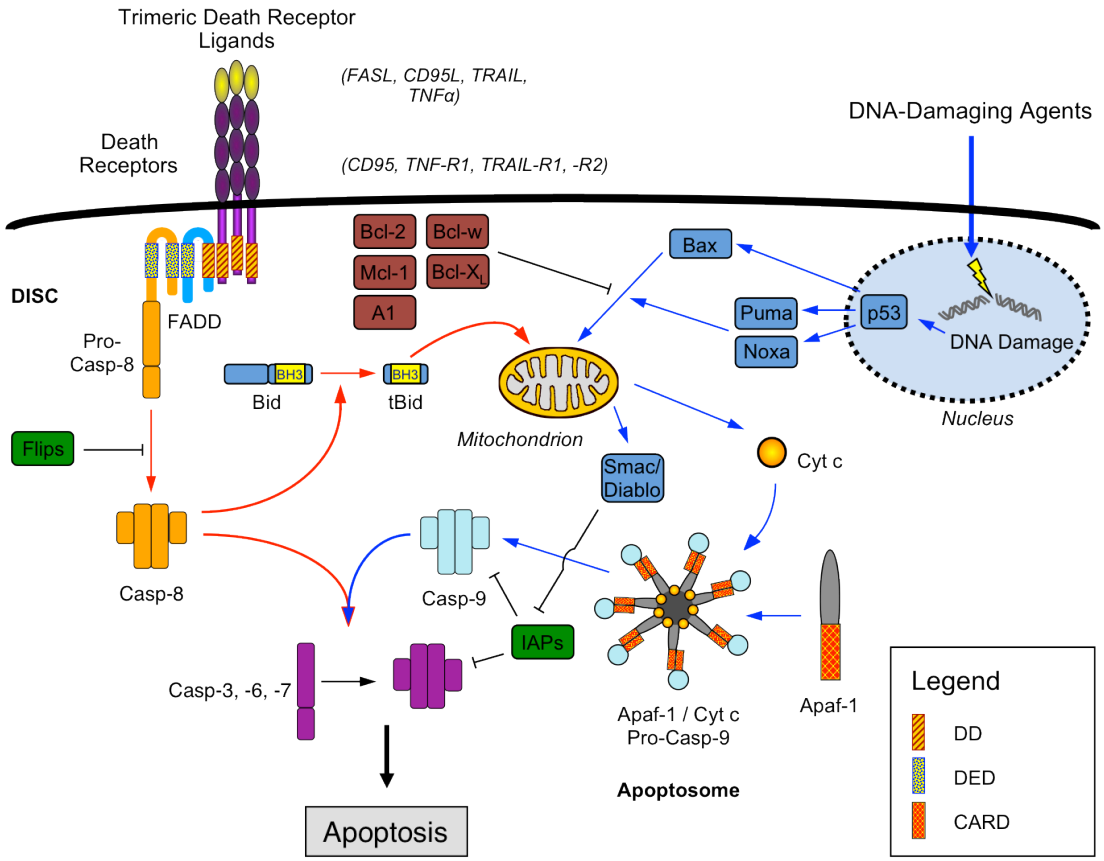

Fig. 1.1: Simplified schematic illustration of extrinsic and intrinsic apoptosis pathways.

Trimeric death ligands (CD95L, TRAIL, TNFα) bind to specific death receptors (CD95, TNF-R1, TRAIL-R1, TRAIL-R2) and initiate extrinsic apoptosis signaling (red arrows) by trimerization of the respective receptors (left). Subsequently, the adaptor protein FADD or TRADD (not shown) binds to the trimeric receptors, followed by recruitment of procaspase-8 molecules. The resulting protein complex (DISC) causes proximity-induced autoproteolytic activation of the procaspase-8 molecules. The long and short fragments of caspase-8 form heterotetramers that constitute active initiator caspases. Downstream effector caspases (caspase-3, -6, -7) are activated by caspase-8 and execute apoptosis.
Intrinsic stimuli (right, blue arrows) like genotoxic radiation, xenobiotics or ROS induce DNA damage. Thereupon, p53 is activated, leading to upregulation of pro-apoptotic target genes such as Bax and Puma. In turn, Bax and Bak initiate MOMP and cytochrome c release from the mitochondrial intermembrane space into the cytosol. Cytochrome c, dATP and Apaf-1 form apoptosomes which activate procaspase-9 to yield active initiator caspase-9. Similar to caspase-8, caspase-9 activates downstream effector caspases. The gap between extrinsic and intrinsic pathway is bridged by truncated (t)Bid, which, following cleavage of Bid by caspase-8, initiates Bax/Bak-mediated MOMP and progression of the intrinsic signaling pathway. Anti-apoptotic Bcl-2 proteins (brown) inhibit Bax and Bak activation. FLIPs (FLICE-like inhibitory proteins; green) suppress caspase-8 activation whereas IAPs (inhibitors of apoptosis; green) can directly bind to and inactivate caspases-3 and 9. Smac/Diablo is an IAP inhibitor. Abbreviations: CARD: caspase recruitment domain; Casp: caspase; Cyt: cytochrome; DD: death domains; DED: death effector domains; DISC: death-inducing signaling complex. (Adapted with modifications from Los *et al.*[22])

procaspase-8 to form an active caspase-8 heterotetramer. The receptor-adaptor-caspase-8 complex is referred to as death-inducing signaling complex (DISC). Active caspase-8 cleaves and activates the downstream executioner caspase-3, which in turn activates caspase-6 and caspase-7[23].

Regulation of extrinsic apoptosis signaling

Extrinsically stimulated apoptosis underlies different levels of regulation. Depending on the cell type, receptors and other molecules involved in the pathway may be differentially expressed. In addition, several anti-apoptotic factors control the depicted activation cascade. On the receptor level, decoy receptors lacking functional intracellular signaling domains (e.g. the TRAIL decoy receptors DcRI and DcRII) bind and hence neutralize death ligands. Cells may vary their response towards extrinsic death signals by modulating the receptor to decoy receptor ratio[21].

A potent inhibitor of DISC-mediated procaspase activation is c-FLIP (cellular FADD-like IL-1β-converting enzyme inhibitory protein). Cell lines overexpressing c-FLIP show inhibition of extrinsic apoptotic stimulation by inactivation of the DISC[24]. Accordingly, several human cancers evade cell death by overexpression of c-FLIP, whereas different γ-herpes viruses transduce a viral form of the protein, v-FLIP, into the host cell to prevent apoptosis[25].

Another control mechanism is provided by cellular inhibitors of apoptotic proteins (cIAPs). IAPs bind to and inhibit caspase-3, -7 and -9[26] (see also section 1.1.1.2).

Bid constitutes a link between extrinsic and intrinsic apoptosis pathway

Besides caspase-3 activation and direct cleavage of target proteins, caspase-8 also bridges the gap between extrinsic and intrinsic apoptosis pathway. It cleaves the BH3-only protein BID to yield active truncated BID (tBID), which translocates to the outer mitochondrial membrane, resulting in activation of Bcl-2–associated X protein (BAX) and Bcl-2 homologous antagonist/killer (BAK)[27]. Activated BAX and BAK in turn initiate the intrinsic pathway (see section 1.2.1.2).

Alternative signaling by death receptors

Death ligand signaling does not necessarily induce programmed cell death. TNFα and other death ligands can initiate cross-talk of "competitive" signaling pathways and cellular responses depending on the transcriptional and/or the adaptor protein status of the cell. Exemplarily, TNF-R1 recruits FADD molecules to its TRADD adapter proteins which subsequently interact with receptor-interacting protein (RIP),

cIAP1/2 and TNFR-associated factor-2 (TRAF2). This complex can activate two anti-apoptotic pathways, namely NFκB and c-Jun N-terminal kinase (JNK) pathways[21], provoking survival and proinflammatory responses.

1.1.3. Intrinsic apoptosis signaling pathway

Intrinsic stimuli such as ultraviolet (UV) and ionizing radiation (IR), metabolic or replicative stress, toxic xenobiotics or kinase inhibition as well as caspase-8-mediated tBid activation converge on mitochondria. Hence, mitochondria represent the key organelles involved in intrinsic apoptotic signaling. Activated Bak and Bax integrate all upstream signals and execute initiation of apoptosis by pore formation and accompanied mitochondrial outer membrane permeabilization (see below).

The Bcl-2 protein family

Intrinsic apoptotic stimuli often result in upregulation of pro-apoptotic proteins: DNA damage leads to p53-dependent transcription of pro-apoptotic genes such as Noxa, Puma and Bax[28]. Bax and Bak contain four BH (Bcl-2 homology) domains (BH1-4). Bad, Bid, Bik, Bim, Bmf, Hrk, Noxa and Puma belong to the BH3-only protein family, exhibiting a single BH3 domain. All of the designated proteins belong to the Bcl-2 protein family.

Bim and tBid form heterodimers by binding to five different anti-apoptotic BH3 multidomain proteins of the Bcl-2 family (Bcl-2, Bcl-X_L, Bcl-W, Mcl-1 and A1)[29,30]. In this way, Bim and tBid are sequestered in an inactive state on the surface of mitochondria[30]. Other pro-apoptotic BH3-only proteins (so-called “sensitizers”) bind to the anti-apoptotic Bcl-2 proteins, thereby replacing and releasing tBid and Bim (“activators”) from the heterodimers[31]. Bim and tBid subsequently activate Bax and Bak which in turn perpetuate intrinsic apoptotic signaling. This direct-activation model, published by Certo *et al*. in 2006, bases upon experimentally determined dissociation constants of different combinations of binding domains of pro- and anti-apoptotic BH3 proteins. Bim and tBid are able to neutralize all five anti-apoptotic factors and Bad interacts with Bcl-2, Bcl-X_L and Bcl-W, while Hrk, Noxa and Puma selectively bind to Bcl-X_L, Mcl-1 and A1, respectively. These findings are similar to (but not congruent with) previous reports[32,33]. However, other publications suggest a second model of indirect activation[27], which favors activation of Bax and Bak by simply sequestering and, hence, inactivating the anti-apoptotic counterparts.

Mitochondrial outer membrane permeabilization (MOMP)

Activated Bak and/or Bax oligomerize and form pores that integrate into the outer mitochondrial membrane (mitochondrial outer membrane permeabilization, MOMP)[34,35]. These pores enable release of cytochrome c and Smac/Diablo from the mitochondrial intermembrane space into the cytosol (Fig. 1.1). Cytochrome c, dATP and Apaf-1 form a high-molecular complex, called the apoptosome, which provides a scaffold for recruitment and subsequent proximity-induced autoactivation of procaspase-9. Active caspase-9 is inhibited by IAPs (cIAP1/2, XIAP or survivin). However, the IAP inhibitor Smac/Diablo binds to BIR domains of IAPs[26], thereby releasing active initiator caspase-9, which in turn proteolytically activates effector caspases-3, -6 and -7 (Fig. 1.1).

1.1.4. Endoplasmic reticulum pathway (type III)

The endoplasmic reticulum is the main cellular organelle involved in protein folding and protein sorting. Disturbances such as excessive protein synthesis, overloading of chaperons' refolding capacities or defective calcium homeostasis generate ER stress which triggers ER stress response, generally referred to as unfolded protein response (UPR). UPR initiates pro-survival pathways and transcriptional readjustment which may rescue the cell[36]. Albeit, if remaining unsolved, ER stress can alternatively initiate apoptosis. UPR comprises three key players, namely IRE1, PERK and ATF6, which initiate three pathways:

Inositol-requiring protein-1 (IRE1) possesses both a kinase and a nuclease activity. IRE1α (the predominant form of IRE1 in most cell types) is activated by e.g. dissociation of the chaperone BiP/Grp78 or by direct binding of unfolded proteins[37]. Consequently, an mRNA encoding XBP1 is spliced and the protein is translated. XBP1 is a “critical transcription factor”[36] for induction of numerous genes involved in UPR.

PERK is a kinase which is activated similar to IRE1; it phosphorylates and thereby inactivates eIF2α[38]. This globally arrests initiation of translation. However, expression of the downstream factor CHOP is initiated. Likewise, CHOP is a target gene of ATF6. On transient ER stress conditions, CHOP is a negative regulator of UPR and restores translation levels by re-activation of eIF2α[39].

Prolonged IRE1 and CHOP activation can result in induction of apoptosis. IRE1 recruits TRAF2 and initiates a cascade comprising the MAP kinase kinase kinase (MAPKKK) ASK1 and JNK. Sustained JNK activation mediates apoptosis via Bax

and Bax expression, which in turn may amplify IRE1 signaling in a positive-feedback loop[36]. CHOP initiates apoptosis by simultaneous upregulation of pro-apoptotic factors such as TRAIL-R2 and Bim and downregulation of anti-apoptotic Bcl-2, thus promoting Bax/Bak-mediated MOMP. In addition, CHOP upregulates ER oxidase 1α (ERO1α), resulting in hyperoxidation of the ER lumen[36]. Reactive oxygen species (ROS) may then provoke leakage into the cytoplasm, thereby enhancing cytoplasmic calcium levels. ERO1α additionally activates the ER calcium channel IP3R1 which hereupon mediates Ca^{2+} efflux from the ER into the cytoplasm. CaMKII (Ca^{2+}/calmodulin-dependent protein kinase II) subsequently promotes different apoptosis pathways[40].

ER stress can be experimentally applied, e.g. by chemicals such as the glycosylation inhibitor tunicamycin[41,42] or thapsigargin[41,42], which depletes ER calcium storages. Brefeldin A induces ER stress by inhibition of protein sorting. It causes defragmentation of the Golgi apparatus, thereby overloading the ER with redirected proteins[43,44].

1.2. DNA damage

Maintenance of genetic stability and prevention of mutations constitute indispensable prerequisites to avoid cellular malfunction. A vast number of studies has provided evidence that various physiological processes are tightly associated with DNA damage. These processes cover such diverse phenomena as cancer, neurodegenerative disorders and aging.
In this section, the role of DNA damage in cellular dysfunction, the different types of DNA modifications and the ways they are repaired are outlined. In addition, signaling pathways triggered by DNA damage and cellular mechanisms of antioxidative damage defense are being presented. The final subsection explicates current methods for DNA damage quantification.

1.2.1. DNA damage in cellular dysfunction and disease

Under physiological conditions, cells face roughly 10^5 DNA modifications per day, most of which are immediately and correctly removed[45]. However, if improperly repaired, DNA damage can cause mutations and malfunctions such as malignant development, accompanied by loss of cell cycle control and perpetual cell division.
DNA lesions can be caused by different factors. A major internal source of DNA modifications is the generation of ROS side products during cellular metabolism in the mitochondrial electron transport chain (ETC). While most oxygen molecules are reduced to water, a minor fraction is converted to radicals, most prominently superoxide anions and hydroxyl radicals. Besides, nitric oxide synthases (NOS) generate NO radicals, which serve as second messengers but may also provoke DNA damage[46]. Other intrinsic sources of DNA damage are replication errors causing double strand breaks (DSBs), programmed DSBs (during lymphocyte maturation) or spontaneous deamination and oxidation processes[47]. External sources for DNA modifications are high-energy radiation (e.g. ultraviolet or gamma radiation), cytostatic drugs such as cisplatin, etoposide and bleomycin or genotoxic chemicals (i.e. dimethylsulfate).

Mutations in nuclear genes that are involved in apoptosis or cell cycle control are frequently found in tumors. In this context, more than 50% of human cancers exhibit mutations in the gene encoding the tumor suppressor protein p53[48], most of which are acquired prior or during development of malignancy accompanied by

immortalizing processes such as reconstitution of telomerase activity. Many if not all developmental stages of cancer progression base upon chromosomal instability and mutations that are caused by DNA damage: While single base modifications and replication errors may cause point mutations, DSBs can lead to insertions, deletions and duplications during recombination processes[47]. DNA damage is therefore a major contributor to genomic and/or chromosomal instability[49], which is a hallmark of cancer.

On the other hand, DNA damage and accompanied mutations, especially within the mitochondrial genome, can lead to increased cell death and tissue degeneration. Numerous studies have demonstrated that mtDNA damage, mainly caused by ROS or drugs that impair oxidative phosphorylation (e.g. MPTP), plays an important role in the development and progression of neurological disorders such as Alzheimer's[50] and Parkinson's[51] disease.
Neurological pathologies are not yet fully understood; mtDNA damage may be a consequence of primary processes (such as beta-amyloid protein accumulation and increased ROS generation). However, since thirteen subunits of the five respiratory chain complexes are encoded by mtDNA, mutations in the circular genomes of these organelles can directly affect and impair cellular energy metabolism[51]. Consequently, defects in the ETC, often represented by complex I dysfunction (reviewed by Fato *et al*.[52]), lead to depletion of cellular ATP and increased ROS levels, as electrons are insufficiently transferred onto oxygen molecules. Such "leaky" ETCs are a steady source of ROS and hence even more DNA lesions, finally leading to or accelerating cellular demise[52]. For instance, in Parkinson's disease dopaminergic neurons of the *substantia nigra* degenerate. This region of the brain contains high levels of iron cations which catalyze the generation of hydroxyl radicals by Fenton's reaction. Thus, neurons within the *substantia nigra* suffer from higher ROS levels (and accompanying mtDNA damage) than neurons in regions with moderate or low iron levels[53].

Besides pathological conditions, DNA damage is thought to be a major contributor to aging processes. In the Disposable Soma model[54], the "imperfect maintenance of nuclear DNA likely represents a critical contributor to aging"[47]. DNA damage and corresponding mutations accumulate with age in mammals[47], accompanied by progressive loss of cellular self-renewal capacities.
The putative link between DNA damage and aging might be typified by the state of cellular senescence. Upon continued cell division (replicative senescence) or acute

genotoxic treatment (premature senescence), somatic cells can permanently exit the cell cycle and enter a quasi-quiescent state. This process is accompanied by considerable morphological and biochemical rearrangements, such as increase in cell size (hypertrophy), polyploidy and upregulation of p21 and lysosomal hydrolases[55,56]. In addition, senescence is a relevant physiological process involved in chronic liver diseases[57]. Besides DNA repair and induction of senescence, an alternative cellular response upon DNA damage is initiation of apoptosis (see section 1.2.4).

1.2.2. Types of DNA lesions

As previously described, various internal and external factors give rise to different types of DNA damage. Lesions can affect one or both of the complementary strands in mitochondrial and nuclear genomes. Depending on the type of lesion, different DNA damage response and repair pathways are activated.

Oxidative lesions

Oxidative lesions represent single-strand lesions that are mainly caused by reactive oxygen species (ROS) such as H_2O_2 or organic peroxides (e.g. peroxidized lipids), hydroxyl radicals, superoxide anion (O_2^-), photochemically generated singlet oxygen, nitric oxide or peroxynitrite[46,58]. To date, more than 20 types of oxidative DNA modifications have been identified[59], of which 8-oxo-dG (8-hydroxy-dG), single-strand breaks (SSBs) and abasic sites are the most frequent representatives[59].

Single-strand breaks, abasic sites & cytosine deamination

Single-strand breaks and abasic sites are mainly caused by replicative stress during continued or even uncontrolled cell proliferation[49]. Moreover, they can occur by spontaneous depurination or, less frequently, by depyrimidation and subsequent backbone cleavage carried out by apurinic/apyrimidinic endonucleases. In addition, cytosine may spontaneously deaminate to uracil yielding an abasic site after excision by uracil-DNA glycosylase. Contrarily, programmed deamination of cytosines takes place during activation-induced deaminase (AID)-mediated somatic hypermutation and class switch recombination in B cell development[60,61]. SSBs and abasic sites are likewise formed as side products of other genotoxic impacts such as UV or ionizing radiation[62] or as intermediate states during DNA repair.

Pyrimidine dimers

DNA exposure to UV radiation leads to generation of cyclobutane adducts in neighbored thymines or cytidines (cyclobutane pyrimidine dimer, CPD) by electrocyclic addition. The predominant modifications induced by UVA (320-400 nm) and UVB (290-320 nm) exposure are thymine (TT) dimers, while cytidine or mixed dimers are less frequent[63]. Alternatively, pyrimidine(6-4)pyrimidone photoproducts (6-4PP) may be formed. Both CPD and 6-4PP formations result in bulky DNA adducts which impair DNA duplication and transcription.

Alkylation & intercalation

Alkylating agents generate three-dimensional structural DNA changes via electrophilic addition to amino or oxo/hydroxyl groups. Many of these compounds are not DNA-reactive *per se* but are metabolically activated prior DNA modification. Most prominently, polyaromatic hydrocarbons (e.g. benzo[a]pyrene) are enzymatically converted into intermediate epoxide derivatives, which subsequently attack DNA bases in an electrophilic manner[64]. The most frequently occurring alkylation reactions are methylations, which, in turn, can be deliberately applied to CpG motifs by DNA methyltransferases during epigenetic gene regulation.
In contrast to alkylation, intercalating agents (e.g. acridine dyes) do not covalently modify DNA, but physically integrate between stacked bases, thereby disturbing DNA synthesis and leading to frameshifts and other kinds of mutations[65].

Double strand breaks

Double strand breaks (DSBs) are considered the most severe form of DNA lesions[47,66]. While undamaged complementary strands provide redundancy for proper DNA repair of single-strand breaks (SSBs), this information is absent in the case of DSBs. External sources of DSBs are e.g. IR and several genotoxic drugs. Major internal sources of DSBs are ROS generated during oxidative phosphorylation and replicative stress during DNA unwinding and duplication[151]. Some cytostatic drugs potentiate internal DNA stress to provoke DSB. Exemplarily, etoposide generates DSBs by inhibition of religation of topoisomerase-II-induced strand breaks[67] and torsional stress[68]. Bleomycin induces DSBs[69] by a radical-based mechanism.

Crosslinking

Different anti-tumor drugs, e.g. cisplatin, covalently crosslink DNA in an inter- or intrastrand manner[70]. Similar reactions can be provoked by gamma radiation or reactive chemicals such as formaldehyde, which may also form "mixed" adducts between DNA and proteins.

1.2.3. DNA repair

Most living cells possess the ability to repair DNA damage to a certain extent. Minimizing the number of DNA lesions is an important prerequisite for DNA synthesis during S phase of the cell cycle and proximate cell division. In this context, effective and rapid removal of DNA lesions can rescue the respective cell, while persistent DNA damage signaling provides a strong apoptotic stimulus.

Three main pathways exist for SSB repair, namely base excision repair (BER), nucleotide excision repair (NER) and mismatch repair (MMR). DSBs are primarily removed by non-homologous end joining (NHEJ) or homologous recombination (HR). The type of repair mechanism employed for DNA repair depends on the type of lesion, the respective cell type and current cell cycle phase[70]. In this context, nuclear and mitochondrial DNA must be regarded separately, as they exhibit different spectra of mechanisms to remove genomic lesions.

Base excision repair

Base modifications that do not or hardly alter the three-dimensional structure of the DNA double helix are removed via base excision repair. These modifications include oxidations, deaminations and alkylations (predominantly methylations).

Specific glycosylases (e.g. uracil-N glycosylase (UNG) and 8-oxoguanine glycosylase-1 (OGG1)) recognize and excise damaged bases by hydrolysis of the N-glycosidic bond, thereby forming an apurinic/apyrimidinic (AP) site. AP endonucleases then hydrolyze the phosphoribose backbone. In humans, polynucleotide kinase-phosphatase (PNKP) and DNA polymerase β (or the Flap endonuclease FEN1) in collaboration with ligases complement the missing nucleotide and ligate the backbone[71,72].

Nucleotide excision repair

For nucleotide excision repair (NER) in eukaryotes two pathways have been described, referred to as global genomic NER (GG-NER) and transcription-coupled NER (TC-NER)[73]. Both repair pathways recognize bulky base modifications and remove the respective nucleotide(s). CDP, 6-4PP or alkylations, all of which generate helix distortions, are subject of NER.

In GG-NER, two protein complexes, the so-called DNA-damage binding (DDB) and the XPC-Rad23b complex, permanently scan the nuclear genome for lesions. TC-NER lacks such damage recognition complexes. Instead, it uses RNA polymerases that halt during transcription because of lesions as damage signals. Actively transcribed DNA single strands are therefore faster repaired than transcriptionally silent genomic regions[73].

Following damage recognition, a protein complex - including the key enzyme transcription factor II H (TFIIH) - binds to the damaged site. TFIIH unwinds the DNA employing its helicase activity, followed by a dual incision 5' and 3' of the lesion. This dual incision subsequently leads to the removal of about 25nt of the respective single-strand. DNA polymerases re-synthesize the missing part of the single-strand while ligases finally connect the nick[73].

Mismatch repair

Mismatch repair (MMR) mainly addresses mispairing of bases (A-C, A-G, T-C or T-G) or unpaired single-stranded sequences (insertions / deletions) shortly after DNA synthesis. In prokaryotes, lack of methylation of the newly synthesized strand allows the MutS repair machinery to distinguish between the “correct” leading and the “erroneous” lagging strand. In contrast, eukaryotes synthesize the lagging strand in short Okazaki fragments. Therefore, the lagging strand carries single strand nicks, probably serving as markers for the eukaryotic MutS homologs[74].

MMR is highly conserved from prokaryotes to eukaryotes. The following annotated proteins represent the eukaryotic denotations. Successively, the different events in MMR comprise recognition of the mispaired base(s), incision, removal, resynthesis and ligation.

Base mismatches and small loops (generated by single-strand insertions / deletions) are sensed by MutSα, (Msh2/Msh6 heterodimer), while MutSβ (Msh2/Msh3 heterodimer) is mainly involved in small and large (about 10 nt) loop repair. MutL has three homologs in humans, namely MUTLα (MLH1/PMS2 heterodimer), MUTLβ (MLH1/PMS3 heterodimer) and MUTLγ (MLH1/PMS1 heterodimer). The role of the

eukaryotic MutLβ and MutLγ is yet poorly understood. MutLα has an endonuclease activity and incises the respective single strand in a PCNA-dependent manner[75], followed by DNA polymerase δ and DNA ligase-mediated termination of the repair process[74,76].

Non-homologous end joining (NHEJ)

NHEJ repairs DSBs without employing any homologous template[77], although compatible single strand overhangs at the DSB site are used for accurate match of the ends. In mammals, the Mre11-Rad50-Nbs1 (MRN) complex tethers the ends for alignment following recognition of the lesion by ATM[78]. Thereupon a Ku70/Ku80 heterodimer, mediated by DNA-PK_{cs}, binds to the DSB site and acts as a docking platform for other repair proteins such as DNA polymerases λ and μ, DNA ligase IV, XLF and XRCC4[79] which then repair the lesion[78].

NHEJ is, as compared to homologous recombination, an error-prone DNA repair pathway. If DSBs occur within repetitive sequences (such as microsatellites), deletions, insertions or translocations may be introduced by NHEJ (since this repair pathway utilizes merely complementary single-strand overhangs instead of homologous template sequences). NHEJ therefore inherits a higher risk for generation of mutations than does HR.

Homologous recombination (HR)

A variety of DNA lesions, mainly DSBs, but also single strand gaps and interstrand crosslinks can be repaired by homologous recombination (reviewed by Krejci *et al*.[66]). In principle, homologous sequences (e.g. on sister chromatids) can be bidirectionally used as template if one of the two sequences is damaged. HR is essential during the first meiotic cell division as it leads to genetic diversity through crossover and sister chromatid exchange of DNA segments[80].

The main factor involved in HR is Rad51. Initially it binds in multiple copies to the 3' end of a single-strand overlap at the lesion site and forms a Rad51-ssDNA filament, thereby stretching the DNA so that it can intersect into the dsDNA of the homologous dsDNA template. The filament displaces the undamaged complementary single strand (resulting in a "D loop") and forms a heteroduplex. Subsequently, Rad51 dissociates from the 3' end and DNA synthesis elongates the invaded ssDNA. The repair processes can be terminated in two different ways; the first of which involves a double-Holliday Junction (dHJ)[81] and yields crossover or non-crossover products, depending on the nuclease cleavage pattern. Alternatively, the elongated invading

strand is separated from the D loop, followed by annealing of both template and elongated strand to the respective complementary strands. At the former DSB site remains a ssDNA gap which is subsequently filled up and ligated by common DNA polymerases and ligases, respectively[66].

HR constitutes a repair pathway which - in stark contrast to NHEJ - is not error-prone in terms of mutations. HR is the main repair mechanism during most of the cell cycle, whereas cells at the G0/G1 stage rely mainly on NHEJ. In addition, it is the predominant DSB repair pathway in murine embryonic stem cells[82], as the homology-based mechanism avoids potentially tumorigenic deletions. However, it is also implicated e.g. in the DNA damage response regulated by the BCR-ABL translocation in chronic myeloid leukemia and is assumed, in this context, to facilitate development of chromosomal aberrations and tumor progression[83].

Mitochondrial DNA repair

Mitochondria are the main ATP-producing organelles which generate high amounts of ROS and lack of DNA-protecting mechanisms comparable to the nuclear envelope or histones. Combined, the highly oxidative environment and limited sealing of the mitochondrial genome give rise to high DNA damage incidence. Mitochondria are equipped with different repair machineries similar to the nucleus to face mtDNA stress[84].

All proteins involved in DNA repair are encoded by nuclear genes. The most important mitochondrial repair pathway is BER as the majority of lesions are oxidative modifications of DNA bases[84]. Comparable to nuclear DNA, specific monofunctional glycosylases such as UNG1 or bifunctional glycosylases, e.g. OGG1, remove the modified base. Monofunctional glycosylases are assisted by APE1, which cleaves the sugar-phosphate backbone at the apurinic/apyrimidinic site. Bifunctional glycosylases cleave both the N-glycosidic bond and the sugar-phosphate backbone of the concerning base. DNA polymerase γ1 and ligase LIG3, the sole known mitochondrial DNA polymerase and ligase, respectively, then finish the repair process[84].

Besides BER also NER, MMR and HR pathways were identified in mitochondria, although evidence for their existence decreases in the same order[84]. Upon accumulation of damaged mtDNA, a retrograde signaling to the nucleus is postulated[84], which leads to upregulation of mitochondrial DNA repair enzymes.

1.2.4. DNA damage response, cell cycle regulation and apoptosis

Irrespective of the type of lesion and kind of repair mechanism, cells respond to DNA damage in a universal manner, referred to as DNA damage response (DDR, see Fig. 1.2 for a schematic overview). DDR leads to the phosphorylation of p53, which translocates into the nucleus and initiates transcription of its target genes. Depending on the strength and duration of DDR signaling, cells can transiently undergo cell cycle arrest (mediated by upregulation of p21), initiate apoptosis (mediated by pro-apoptotic p53 target genes) or senescence (by prolonged upregulation of p21 and induction of p16/Ink4a and p19/ARF; Fig.1.2)[70].

DNA lesions, represented by phosphorylated histone (γ)H2AX and colocalized 53BP1 foci, are sensed by the MRN (Mre11-Rad50-Nbs1) complex, which subsequently phosphorylates ATM (ataxia-telangiectasia mutated). ATM and ATR (ATM and Rad3 related) transduce the damage signal to checkpoint kinases 1 and 2 (Chk1, Chk2). In addition, the sensor dimer Ku70/Ku80 and the transducer DNA-PK initiate NHEJ repair, while HR repair is mediated by the key players ATM, MRN complex, BRCA1 (breast cancer 1, early onset) and Rad51. The kinases ATM, ATR, Chk1 and Chk2, if activated, phosphorylate p53 and, in this way, prevent its ubiquitinylation-mediated degradation via the E3 ligase Mdm2 (mouse double minute 2 homolog)[85]. Phosphorylated p53 accumulates in the nucleus and initiates transcription of pro-apoptotic Bcl-2 family members, e.g. Bax, Noxa and Puma[28] (Fig. 1.2). Forced expression of these proteins can shift the balance between pro- and apoptotic signals at the outer mitochondrial membrane towards Bax/Bak oligomerization, pore formation and cytochrome c release (see section 1.1.3).

P53 activation furthermore leads to p21 and GADD45 upregulation, whereas it represses cyclin E and BRCA1[86]. P21 in turn inhibits cyclin 2 and cyclin 1 containing complexes, PCNA and several transcription factors (e.g. E2F1, STAT3 and MYC). In addition, phosphorylated p21 is prevented from translocation into the nucleus and inhibits major apoptotic executioners (caspase-3 and -8) in the cytosol[87]. Consequently, it leads to cell cycle arrest in the S and G2 phase (through cyclin 2 and E2F1 repression, respectively), global inhibition of translation and suppression of apoptosis [87].

Moreover, p53 signaling can induce differentiation in murine ES cells. Following DNA damage, (S315-phosphorylated) p53 binds to the *Nanog* promoter and represses Nanog expression[88], leading to loss of pluripotency.

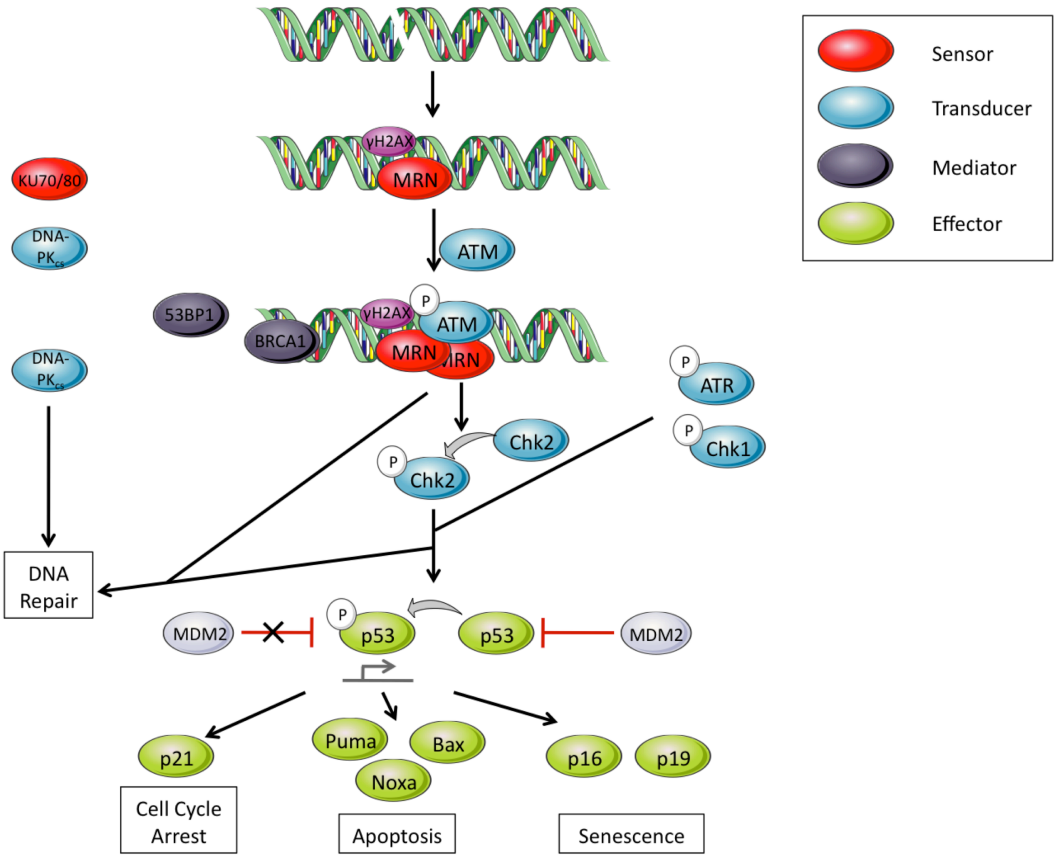

Fig. 1.2: DNA damage response pathways.

Schematic overview of DNA damage response pathways. See text for details. Figure modified from Blainpain *et al*., see Ref. 70. Figure was produced using Servier Medical Art.

1.2.5. ROS and antioxidative defense mechanisms

Most genotoxic drugs and radiation damage DNA rather by generation of ROS than by direct impact. Besides, cells generate high levels of endogenous ROS as side effect of oxidative phosphorylation and oxygen metabolisms. For this reason cells have developed a series of antioxidant defense systems to capture and neutralize ROS before they can oxidate lipids, proteins or DNA, thus preventing genomic damage and associated mutations. These defense systems comprise small molecule antioxidants, chaperones and enzymatic ROS detoxification.

Small-molecule antioxidants

Ascorbate, α–tocopherol, ubiquinone and glutathione (GSH) belong to the group of cellular small molecule antioxidants. Ascorbate (vitamin C) serves both as direct radical scavenger and as cofactor for different hydroxylases. Following oxidation, it can be reduced by thioredoxin (which is regenerated in an NADPH-dependent manner) or GSH and undergo further redox cycles[89]. α–Tocopherol (vitamin E) and lipophilic ubiquinone, a membrane-resident electron carrier of the ETC, can, upon oxidation, form radicals of low reactivity, thereby detoxifying ROS such as superoxide anions or hydroxyl radicals[89]. Ubiquinone (coenzyme Q10) protects mitochondrial membranes from lipid or protein peroxidation, as such modifications might severely interfere with cellular ATP generation.

GSH is a tripeptide (γ-glutamylcysteinylglycine) synthesized in a translation-independent two-step enzymatic process involving γ-glutamylcysteine ligase (GCL) and glutathione synthetase, of which GCL catalyzes the rate-limiting step[90]. GSH exhibits a free thiol group and can undergo spontaneous dimerization by mild oxidation to form glutathione disulfide (GSSG). GSH is substrate of numerous enzymes involved in antioxidative defense and detoxification of xenobiotics. Several cell types such as glia cells[91], but also tumor cells[92] which often suffer from metabolic and cell division stress, exhibit high GSH levels to face enhanced ROS generation or xenobiotic load. GSH levels in cells can be manipulated by inhibitors of GCL-mediated biosynthesis (such as buthionine sulfoximine), depletion by drugs which are metabolized or secreted in a GSH-dependent manner (e.g. dimethyl fumarate), replenishment by GSH derivatives (such as a cell permeable GSH O-ethyl ester) or GSH precursors like cysteine or cystine[93].

Antioxidative enzymes and proteins

Catalase (CAT) and superoxide dismutases (SODs) are enzymes that detoxify hydrogen peroxide and superoxide radical anions, respectively. CAT is localized in peroxisomes which are specialized organelles for both β-oxidation of very long fatty acids and detoxification of harmful substances, such as ethanol and H_2O_2. SODs exist in three isoforms present in the cytosol (SOD1), mitochondrial matrix (SOD2) and extracellular space (SOD3).

Peroxiredoxins are essential in several cells types and belong to the class of peroxidases that catalyze the reduction of peroxides such as H_2O_2 and peroxynitrite[94]. For instance, PRDX1 has been reported to be indispensable for antioxidative defense in erythrocytes[95]. The oxidized form of these enzymes can be

regenerated by GSH, ascorbate or thioredoxin[89]. Besides, other redox-active proteins or enzymes with free sulfhydryl groups such as thioredoxin and protein disulfide isomerases, but also chaperones (which reduce the load of stress-induced un- and misfolded proteins) contribute to the cellular antioxidative defense.

Glutathione-dependent enzymes

Three classes of enzymes use GSH as substrate: First, GSH peroxidases (GPXs) peroxidate two molecules of GSH to yield the disulfide form, GSSG, thereby reducing H_2O_2 or organic peroxides[89]. At least seven isoenzymes exist in humans.
Second, GSH transferases (GSTs) transfer GSH onto ROS or xenobiotics such as paracetamol to form GSH conjugates[96]. In addition, GSH-dependent xenobiotic excretion has been reported, e.g. of the natural compound vincristine[97]. While conjugation of xenobiotica with GSH und subsequent secretion leads to GSH depletion, GSH-dependent ROS detoxification yields GSSG which can be recycled by glutathione reductases (see below). Several classes of mammalian GSTs exist (GST α, μ, σ, π, τ, ζ and microsomal GST (MGST) classes) which each comprise between one and five isoenzymes[97]. GST classes and isoenzymes are differentially expressed in different tissues and cell types, thereby providing a broad spectrum of combinations and a precisely adjusted and cell type-specific antioxidative defense.
Third, glutathione reductase converts GSSG and $NADPH/H^+$ into two molecules of GSH and $NADP^+$, thereby regenerating the GSH pool. Under normal culturing conditions, the cellular *in vitro* GSH:GSSG ratio is > 50:1[93].

Other antioxidative mechanisms

Various other factors are at least partially involved in antioxidant defense. To mention only a few, the osmolyte taurine, uric acid, melatonin and polyunsaturated molecules, e.g. carotene derivatives, constitute antioxidative molecules. Further proteins involved in antioxidative defense are represented by apolipoproteins (in particular apopliporotein E[98]) which decrease the rate of lipid peroxidation.

1.2.6. Additional DNA damage-preventing mechanisms

Besides antioxidative (hence biochemical) protection of the DNA against ROS, cells use physical methods to protect DNA. For instance, topoisomerases sense and ease DNA over- or underwinding, thereby preventing torsion stress-induced strand

breakage. Second, the hierarchical chromatin organization of the nuclear DNA into nucleosomes, 30-nm-fibres, active chromosomes and meta-phase chromosomes reduces torsion stress and provides another line of defense by “packaging of DNA in chromatin to shield the genetic material by providing alternative targets”[58]. Similarly, tightly packed heterochromatin may provide better protection compared to loose euchromatin by burying the genetic material in a compact protein-rich environment. Likewise, the nuclear envelope provides another physical barrier for the protection of the nuclear genome.

1.2.7. DNA damage detection and quantification methods

In order to investigate DNA repair capacities or DNA-protective mechanisms in a certain cell type, suitable methods for detection and quantification of DNA lesions are needed. Current methods comprise immunostaining for γH2AX[99] and single cell gel electrophoresis assay[100] (comet assay) for DSB visualization, immunostaining for thymine dimers[101], 8-oxo-dG detection (quantifiable e.g. by mass spectrometry or ELISA[102]) or quantitative (endpoint) qPCR-based DNA damage determination[103]. However, all of these methods suffer from different disadvantages. Several techniques are labor-intense and hardly high-throughput compatible in standard life science laboratories. For instance, comet assay and γH2AX staining require manual recording and evaluation of a multitude of pictures for determination of "head-to-tail ratios" of single cells in comet assay or counting of γH2AX foci. ELISA-based assays are accurate and specific for a certain type of lesion, but may require enormous amounts of sample DNA (100-500 µg per sample)[104].

Other methods are merely semi-quantitative (e.g. thymine dimer immunostaining assays, comet assay) or undefined regarding the detected types of lesions (qPCR[103]) or the localization of the damage (all non-PCR / sequencing methods). Thus, these assays are unable to analyze DNA damage in distinct regions of the genome, e.g. loci encoding proto-oncogenes or tumor suppressor proteins. Accordingly, mtDNA damage is not distinguishable from nuclear (n)DNA damage by such methods.

A current method to quantify DNA lesions is a real-time PCR (rtPCR)-based approach as first described by Rothfuss *et al*[105]. This assay employs 1 kb mtDNA probes which are amplified by rtPCR. The principle of the assay relies on the inhibition of the employed polymerase by DNA lesions.

1.3. Pluripotent stem cells

Pluripotent stem cells (PSCs) are immortal and possess the ability to give rise to all somatic cells types. They are, for this reason, a promising tool for future applications in regenerative medicine. However, PSCs intrinsically possess a substantial tumorigenic potential. Besides, if PSCs are obtained from human embryos (embryonic stem cells; ESCs), their employment in scientific and therapeutic applications raises ethical issues. Moreover, xenograft rejection may occur upon transplantation of ESC-derived tissues.

An exciting newly discovered cell type, induced pluripotent stem (iPS) cells, avoids host-engraft rejections and ethical implications. Nonetheless, iPS cell properties need to be globally characterized in terms of e.g. signaling pathways, apoptosis and their response to toxic or genotoxic treatment prior development of safe stem cell therapies.

1.3.1. Overview: Stem cells

During embryogenesis, embryonic stem cells (ESCs) build the inner cell mass (ICM) of blastocyst-stage embryos (Fig. 1.3). ESCs are pluripotent stem cells that possess the ability to differentiate into all three germ layers and, thus, to generate all cell types, tissues and organs within the developing organism. In contrast to totipotent cells, namely zygotes and cells at the morula stage, PSCs lack the ability to form extraembryonic placenta tissue.

Differentiation of pluripotent stem cells towards unipotent somatic cells is accomplished in a stepwise process. Following division into the three germlayers (ectodermal, endodermal and mesodermal layer), PSCs give rise to multipotent progenitor cells (Fig. 1.3), e.g. hematopoietic stem cells (HSCs), mesenchymal stem cells (MSCs) or neural stem cells (NSCs), which still exhibit the ability to generate all cell types of the respective lineage, but not of other lineages.

The subsequent stage is represented by oligopotent cells which are progenitor cells as well, i.e. HSC-derived common lymphoid progenitor (CLP) cells which give rise to natural killer (NK) cells, T and B lymphocytes. However, multipotent cells can generate cells of different lineages, while progenitors such as CLPs can generate cells of the lymphoid lineage, but not myeloid cell types such as granulocytes.

Progenitors differentiate into precursors, e.g. hepatoblasts, which finally form terminally differentiated somatic cells such as hepatocytes. Both precursor and

terminally differentiated cells are designated “unipotent” since they exclusively generate or regenerate a single cell type.

PSCs express telomerase to maintain the length of their telomeres which would otherwise shorten per cell division (comparable to somatic cells which finally reach the Hayflick limit[106] and become senescent, thereby permanently exiting the cell cycle[107]). As a result of sustained telomerase activity, PSCs exhibit unlimited self-renewal capacity and are thus considered immortal[108]. ES cells can be isolated from blastocysts and both cultivated and differentiated *in vitro*. Alternatively, pluripotent cells can be obtained by reprogramming of target cells to induced pluripotent stem

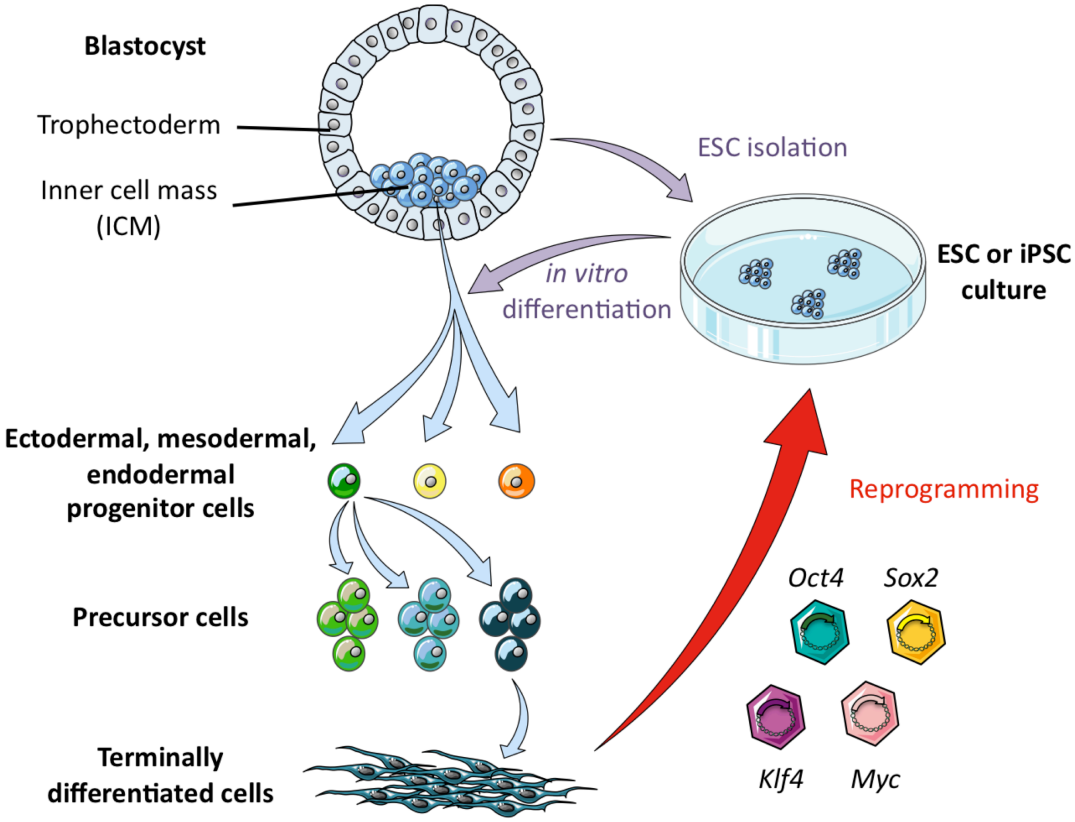

Fig. 1.3: Plupipotent stem cells, differentiation and reprogramming.

Embryonic pluripotent stem cells (ESCs) constitute the inner cell mass of embryos at the blastocyst stage. During embryonic development (blue arrows) ESCs differentiate into progenitor cells of all three germ layers (ectoderm, mesoderm and endoderm) which give rise to precursor cells of different lineages. The final step of differentiation leads to terminally differentiated cells, e.g. fibroblasts. ESCs can be isolated from blastocysts, followed by *in vitro* culture and differentiation (violet arrows). Paralleling embryonic development, *in vitro* differentiation of PSCs gives rise to cells of all three germ layers. Alternatively, pluripotent stem cells can be induced by transduction of the four transcription factors Oct4, Sox2, Klf4 and c-Myc (red arrow), thereby inverting the natural direction of development. Figure was produced using Servier Medical Art.

(iPS) cells: Following forced expression of defined transcription factors (e.g. Oct4, Sox2, Klf4 and c-Myc[1] or OSKM, "Yamanaka factors") by viral transduction of somatic cells, ESC-like pluripotent stem cell colonies arise (Fig. 1.1).
The key marker and "gatekeeper" of pluripotency is Nanog[109] whose repression initiates differentiation[88]. In addition to Nanog, both Oct4 and Sox2 expression were shown to be of prime importance for the attainment and maintenance of pluripotency[110].

1.3.2. Scientific, medical and ethical aspects of PSCs

1.3.2.1. Scientific potential of PSCs

Pluripotent stem cells offer a plethora of scientific possibilities. Due to their ability to self-renew both ESCs and iPSCs (see section 1.3.3) display an infinite source of cells which can be differentiated into all cell types (except totipotent cells). They are therefore a valuable tool for elucidation of critical factors for directed differentiation. Exemplarily, successful generation of functional neurons and hepatocyte-like cells from PSCs revealed the roles of critical factors such as retinoic acid[111] in neural and HGF in hepatocellular differentiation[112]. Thus, PSCs enable *in vitro* investigations of differentiation routes, involvement of cytokines and growth factors as well as studies that illuminate the orchestration of embryonic and subsequent developmental processes[113].
Another important scientific application of PSCs concerns toxicology. Various primary human cells can only scarcely be won. For instance, hepatocytes must be isolated from liver resections. Obtaining viable human cardiomyocytes and neurons proves even more difficult. In contrast, these cell types are of major interest for toxicological screenings, as most pharmaceutical drugs are metabolized in liver and, concurrently, many side effects of drugs implicate cardio- and/or neurotoxicity. In future aspects, PSCs could provide an unlimited source for toxicological screening approaches[114] and reduce the need for animal experiments[115].

1.3.2.2. Therapeutic potential of PSCs

Various dysfunctions and diseases such as neurodegenerative disorders or loss of cardiomyocytes following infarction are yet irreversible and uncurable as the regarding tissues do not (or hardly) regenerate *in vivo*. Pluripotent stem cells epitomize the hope to replace such cells and even tissues[116,117].

To date, several stem cell-based therapies were tested in animal studies. In models of Parkinson's disease, functional iPSC- or ESC-derived dopaminergic neurons were successfully engrafted in mice[118,119]. Beating cardiomyocytes derived from human ESCs were able to improve function in infarcted hearts in animal experiments[120]. Shiba *et al*. recently reported overcoming of roadblocks in cardiomyocyte transplantation, such as arrhythmias, thereby raising hope that PSC-derived cardiomyocytes might prove useful to improve human heart functions as well[121]. Other potential targets of future stem cell therapies comprise liver diseases[122,123] or endocrine disorders, e.g. diabetes[124-126].

Furthermore, iPS cell-derived cells and tissues can be employed in disease models. This is of significant importance if primary cells prove inaccessible, e.g. human neurons that are involved in pathogenesis[127]. Analogous patient-specific iPSC-derived neurons can be generated from somatic cells of individuals suffering from neurological disorders. Such neurons are already being employed to investigate the influence of genetic aberrations on cellular functions, clinical symptoms and etiopathology[127,128].

1.3.2.3. Tumorigenic potential of PSCs

Stem cells share several similarities with cancer cells

Pluripotent stem cells share several characteristic properties with cancer cells: First, they are immortal and can therefore give rise to an unlimited number of daughter cells, comparable to cancer cells. If control over cell division is lost in stem cells, teratomas may form. In these stem cell tumors cells differentiate into all three germ layers in an uncontrolled manner, thereby forming tissue- and organ-like structures[129]. Second, tumor cells exhibit differentiation capacity which is a hallmark of PSCs. In particular, poorly differentiated tumors have been associated with aggressive progression[129]. Third, ESC-like epigenetic imprintings have been described in aggressive human tumors[129]. Moreover, key factors for pluripotency and reprogramming such as c-MYC, KLF4, SOX2, OCT4 or NANOG were found to be involved in tumor signaling and tumorigenesis[129-131] and their activation targets were reported to be frequently overexpressed in poorly differentiated tumors[129]. For instance, *c-Myc* is a proto-oncogene that has been shown to promote tumorigenesis[132]. Similarly, expression and/or activation of SOX2 have been implicated in various cancer types such as breast cancer[131], prostate cancer[133] and sinonasal cancer[134].

These parallels between tumors and stem cells are reflected by the perception of

cancer stem cells (CSCs). While stem cells build and regenerate tissues and organs, CSCs are likewise postulated to generate tumors by exhibition of remarkable self-renewal and differentiation potential[129]. According to this theory, CSCs can enter a quiescent state, called dormancy[135]. They survive chemo- and radiation therapies (which target rapidly dividing tumor cells, but not dormant CSCs) in so-called stem-cell niches[135] and give rise to recrudescence and formation of metastases. These properties parallel normal stem cells (such as progenitor and precursor cells), which regenerate e.g. hair or the immune system following chemo- and radiotherapies. Irrespective of its correctness, the theory of cancer stem cells demonstrates the parallels between multi- or oligopotency and tumorigenicity.

Tumorigenic potential mediated by use of retroviruses

Another source for tumorigenic potential is provided by the use of retroviruses during induction of pluripotent stem cells following the original reprogramming protocol published by Takahasi *et al*.[136] (see section 1.3.3). Retroviral gene transduction implies random insertion of viral DNA into the genome of the host cell, thereby stochastically disrupting critical genes for cell cycle or apoptosis control. This is of particular significance, as p53 deficiency or uncontrolled cell divisions may provide advantageous selection criteria during reprogramming and under cell culturing conditions[137]. Consequently, reprogramming methods that avoid genomic alterations in the target cells, such as mRNA[138] - or protein-based[139] methods, need to be leveraged.

Incomplete differentiation of PSC-derived cells may conserve tumorigenic potential

Directed *in vitro* differentiation of human PSCs does not necessarily end up with the favored cell types. For instance, recent studies in hepatic differentiation demonstrated that the resulting cells are merely “hepatocyte-like” cells, but not identical with primary hepatocytes[140]. Exemplarily, hepatocyte-like cells express hepatocyte-specific markers such as albumin but slightly diverge from primary hepatocytes in terms of e.g. global expression profiles as confirmed by microarray analyses[112]. This phenomenon can be referred to as incomplete differentiation. In addition, no differentiation protocol published so far is able to induce directed differentiation in all treated cells of a given culture batch, therefore yielding a mixture of different (and often unidentified) cell types and differentiation stages. In a recent study, it was reported that “less than 5% of the cells remained Oct4-positive”, providing direct evidence for significant amounts of residual undifferentiated stem or

progenitor cells[140].

Hence, incomplete terminal differentiation on both the cellular and the colony level (remaining oligo-, multi- or pluripotent cells) and, accordingly, a remaining tumorigenic potential, cannot be ruled out for (i)PSC-derived cells. The control of the PSC fate is, however, a basic requirement to make stem cells safe and applicable for future stem cell therapies[141]. Likewise, a detailed understanding of apoptosis and survival regulation in PSCs upon potentially cytotoxic (particularly genotoxic) stimuli is of prime necessity to minimize risks concerning tumor formation by therapeutically applied cells.

1.3.2.4. Ethical issues in ES cell science

Before hiPS cells were first described in 2007[136], human PSCs were exclusively won from human embryos at the blastocyst stage. Such embryos arise during *in vitro* fertilization (IVF), when isolated oocytes and sperm cells are combined *ex vivo*. However, only few of these embryos are transplanted into the uterus of the patient. Hence, reproductive medicine yields a multitude of excessive human embryos that are flash-frozen and stored in liquid nitrogen.

As described above, ES cells can be isolated from the inner cell mass of human embryos. During this procedure, the embryos are irreversibly damaged and destroyed. Ethical issues converge from the fact that, before destruction, the embryos would have been viable following transplantation and orderly pregnancy. In this context, questions about the onset of dignity of life arise. It is yet questionable whether human embryos may be sacrificed for scientific use, even though research might provide insights that could finally lead to therapies and cure of yet incurable disorders.

The controversial debate about the preparation and use of ES cells in science has led to comprehensive legal protection of human embryos in most western countries. In Germany, the situation is governed by the embryo protection law (Embryonenschutzgesetz, ESchG) and stem cell law (Stammzellgesetz, StZG), which regulate the application of *in vitro* fertilization, the generation, import and scientific use of ES cells. Briefly, ES cell import and use in science are generally prohibited although exceptional rules exist. Such exceptions require official approval and both the compliance of a due day (until 2008: Jan 1st, 2002. Since 2008: Feb 1st 2007) and the prove of "high-ranking scientific aims" *(“… Forschungsarbeiten an embryonalen Stammzellen dürfen nur durchgeführt werden, wenn … sie hochrangigen Forschungszielen … dienen ...”,* §5 StZG). In addition, ES cells must

have been isolated from excessive IVF embryos.

Taken together, the scientific use of ES cells in Germany is significantly restricted due to ethical issues concerning dignity of life and the need to protect human embryos. Since iPS cells are generated from somatic cells of adult humans, they are not object of the German ESchG or StZG. Thus, iPS cells offer an ethically uncomplicated way to study human PSCs without the need to destroy viable embryos.

1.3.3. Induced pluripotent stem cells

Since ES cells were discovered and isolated, scientists searched for alternative techniques to generate pluripotent cells, thereby circumventing ethical implications accompanying human ES cell usage in research (see section 1.3.2.4). For many years a procedure designated somatic cell nuclear transfer (SCNT) has been the gold standard to generate ES-like cells in animal cloning. In SCNT somatic cells are fused with enucleated oocytes. Such "re-nucleated" oocytes are then electrically stimulated, whereupon few of them divide and, after several rounds of mitotic divisions, reach the blastocyst stage[142,143]. A recent report describes the first successful SCNT approach employing human cells[144]. Other ways to generate pluripotent-like cells comprise parthenogenesis[142] and fusion of a somatic with a pluripotent cell[143,145]. However, none of these techniques is ethically accepted for generation of human pluripotent cells. In contrast, neither human embryos nor oocytes or human cloning are needed for iPS cell generation.

1.3.3.1. Generation and properties of induced pluripotent stem cells

Generation of human pluripotent stem cells

In August 2006, Kazutoshi Takahashi and Shinya Yamanaka, Nobel laureate of 2012, first described a method for the generation of induced pluripotent stem (iPS) cells from murine embryonic and adult fibroblasts[1,146], thereby converting somatic into pluripotent cells. The following year, the successful generation of human iPS cells (hiPS cells, hiPSCs) from human adult fibroblasts was published[136]. In both cases, fibroblasts were retrovirally transduced with four transcription factors (the so-called “Yamanaka factors” or OSKM), namely *Oct3/4*, *Sox2*, *Klf4 and c-Myc*[1,146]. Subsequently, the cells were transferred onto cell cycle-arrested feeder MEFs (murine embryonic fibroblasts) and cultivated for roughly 30 days until visible

colonies arose. Meanwhile, numerous groups reported successful reprogramming of various somatic sources, e.g. hepatocytes[147], circulating T cells[148] or even urine samples[149]. IPSCs have likewise been generated from different species such as rats[150] and rhesus monkeys[151].

Paralleling reprogramming cells of diverse tissues and species, the process of iPS cell induction was diversified. Yamanaka and colleagues established a protocol omitting the tumor promoting factor *c-Myc*[152], while other groups reported iPSC generation from neural stem cells employing only two[153,154] or even solely *Oct3/4* as single reprogramming factor[155]. However, relinquishment of one ore more of the OSKM factors led to reductions in reprogramming efficiency, and exclusive use of *Oct3/4* for reprogramming, as stated above, to date merely succeeded in (endogenously Sox2-expressing) NSCs. Apparently, *Oct3/4* is indispensable for nuclear reprogramming. It has thus also been designated the “gatekeeper” for any reprogramming process towards pluripotency[156].

Cellular fate does astonishingly not only depend on the transcription factor “cocktail“ applied to the cells of origin, but also on the culturing conditions. This was impressively demonstrated by Efe *et al.* who converted fibroblasts into neurons (so-called transdifferentiation) by using the four Yamanaka factors, but different culturing conditions compared to previous reprogramming approaches[157]. This led to the hypothesis that short OSKM expression may induce an “erasure“ of epigenetic imprinting, while subsequent forced expression of lineage-specific characteristic transcription factors then converts the cells into the respective cell type[158].

Morphology of human iPS cells

Murine iPS cells strongly resemble mES cells derived from the inner cell mass of murine embryos. They form spherical or dome-shaped colonies, which require leukemia-inhibitory factor (LIF) in the culture medium to maintain pluripotency[159]. In contrast, human iPSC (hiPSC) form flat, round colonies exhibiting distinct borders. They exhibit an “epithelial character with a clear apico-basal polarity”[160] similar to epiblasts[161], thereby representing a second form of pluripotent cells besides ES cells. During embryonic development, ES cells differentiate into primitive endoderm and epiblasts. A single layer of epiblasts covers the proamniotic cavity[159]. Ohgushi *et al*. hence refer to mES and miPS cells as “ICM-type”, exhibiting LIF dependency and “naïve pluripotency”. In contrast, cultured hES or hiPS cells represent an “epiblast-type” and “primed pluripotency”[159].

ES cells and epiblasts are in principle interconversible (depending on the culturing

conditions), although human ES cells proved not to be stable under most culture conditions and quickly differentiate into epiblasts. However, recent publications describe successful (albeit sophisticated) cultivation of LIF-dependent hiPS cells which exhibit morphological similarity to mESCs[162,163].

Generation of iPS cells without use of retroviruses

In view of the therapeutic aspirations associated with iPS cell generation, concerns about the safety of virally generated iPS cell lines were raised[164,165]. Retroviruses may lead to insertional mutations, thereby stochastically inactivating tumor suppressor or other critical genes involved in cell cycle regulation (see section 1.3.2.3). In addition, incomplete silencing of the viral reprogramming factors might be accompanied by incomplete differentiation. This might increase both the heterogeneity of iPS cell lines and the risk of tumorigenesis following directed differentiation[164].

In this context, less tenuous reprogramming methods were developed. To date, successful approaches employing lentiviral vectors[166,167], excisable transposon elements[168], non-integrating adeno- (DNA) or Sendai (RNA) viruses[148,169] and transient plasmid[170], mRNA[138] or protein delivery[139,171] were reported. However, retroviral transduction of OSKM yields efficiencies of about 0.1% reprogrammed fibroblasts and most alternative methods are even less efficient[165]. Numerous projects therefore focus on improving the rate of conversion of somatic into pluripotent cells, thereby elucidating critical factors of nuclear reprogramming.

Roadblocks and enhancers of nuclear reprogramming

Dedifferentiation during conversion of somatic into pluripotent cells is an extrinsically forced process. Spontaneously occurring dedifferentiation *in vivo* is associated with cellular dysfunctions such as cancer (see section 1.3.2.3), while different mechanisms prevent dedifferentiation in healthy cells. The tumor suppressor protein p53 constitutes one of the major roadblocks for induced pluripotency. In 2008, five groups reported in *Nature* simultaneously that transient or permanent inhibition of p53 was essential for iPS cell generation[172-176]. The authors concluded that the initiation of both apoptosis by p53 and senescence by its target gene *p21* must be blocked to induce pluripotency, thereby highlighting the important role of p53 in reprogramming.

For the same reason, inhibitors of stem cell-specific apoptosis pathways (see section 1.3.4), e.g. the ROCK inhibitor Y-27632, enhance reprogramming efficiencies[160].

Interestingly, two main apoptotic caspases, namely caspase-3 and -8, are both activated in an Oct4-dependent manner and their suppression impairs the reprogramming process[177]. Likewise, antioxidative additives (e.g. vitamin C[178]) and hypoxia enhance reprogramming efficiencies[179], presumably because antioxidative environmental conditions impede induction of senescence as a competing process of nuclear reprogramming.

1.3.3.2. Characterization of iPSC

The pluripotency of iPS cells must be verified prior use in any scientific, medical or therapeutic context. An overview about commonly applied methods for characterization of pluripotent stem cells is outlined in Table 1.1.

Given that reprogramming was achieved by retroviral transduction of transcription factors, e.g. OSKM, expression of these exogenous factors in turn triggers expression of the corresponding endogenous factors. Relative mRNA levels of pluripotency factors can be determined employing RT-PCR[1].

Several days after viral infection, the concerning cells silence the viral promoters by CpG methylation. Silencing can be monitored using bisulfite sequencing which specifically detects CpG methylation sites within the respective viral promoters[1]. In addition, putative iPS cells can be stained for pluripotency-specific surface (e.g. SSEA-1 for murine and SSEA-4 for hiPS cells) or nuclear (e.g. Nanog) markers and

Table 1.1: Commonly applied methods for characterization of cellular pluripotency.

Method	Detected attribute / property
Alkaline phosphatase staining	Intracellular alkaline phosphatase activity
Bisulfite sequencing	CpG methylation of viral promoters
Flow cytometry	Expression of pluripotency markers
Immunofluorescence	Expression of pluripotency markers
PCR	Viral integration into host cell genome
RT-PCR	Expression of pluripotency markers
Teratoma formation	Teratoma formation in SCID mice
Tetraploid complementation	Chimera formation
Undirected differentiation	Generation of cells of all three germlayers

analyzed by flow cytometry or fluorescence microscopy[146]. Furthermore, examination of alkaline phosphatase activity provides a widely accepted pluripotency flash test method[1].

To date, there are two gold standards for definite confirmation of pluripotency; one of which is tetraploid complementation[180,181]. In this assay, miPS cells are injected into the inner cell mass of blastocyst-staged murine embryos. Injection of pluripotent cells will give rise to chimeric mice[180,181]. This technique is yet not suitable for human PSCs as ethical and legal issues permit chimera formation.

The second method of choice is teratoma formation. Exclusively pluripotent and totipotent cells are able to form teratoma that comprise tissues of all three germlayers. The respective cells are subcutaneously injected into SCID (severe combined immunodeficiency) mice[182]. After 3-6 weeks, mice are sacrificed and teratomas are analyzed[183]. However, teratoma formation is a time-consuming and expensive method which is therefore not suitable for routine screenings of large numbers of iPSC clones. IPSCs can, for this reason, be alternatively differentiated into the three germ layers *in vitro* in a so-called undirected differentiation approach and subsequently be analyzed by immunostaining. In their initial publication, Yamanaka and colleagues chose smooth muscle actin (mesoderm), α-fetoprotein (endoderm) and βIII-tubulin (ectoderm) as germlayer markers[1].

1.3.3.3. Differences between hiPS and hES cells

A key question concerning the possible replacement of hES cells by hiPS cells in science and therapy is the extent of congruence between iPS and ES cells. It is undoubted that most properties of both cell types are strikingly similar. However, several differences have been reported. Virally reprogrammed cells, unless integration-free viruses were employed, bear enhanced risks of tumorigenesis (see section 1.3.2.3). First, this is due to prolonged “leaky“ expression of the virally transduced pluripotency factors, which have been discussed to exhibit oncogenic potential (even in terminally differentiated progeny) and by the possibility of reactivation of e.g. the formerly silenced *c-Myc* transgene[184]. Second, insertion-associated mutagenesis in critical cell cycle-regulating genes or tumor suppressors such as p53 could give rise to selection advantage while promoting tumorigenesis. Third, the reprogramming process itself positively selects cells which evade apoptosis and senescence[172-176], thereby strongly enriching “suspicious“ cells exhibiting abnormalities in terms of karyotype[185], cell cycle regulation[176] or copy number of pluripotency genes[186].

IPS and ES cells vary in several terms of their epigenomes[187]. Obviously, the erasure of the original methylation pattern during reprogramming is incomplete, thus iPSC keep a "memory" of origin at the epigenetic level[188,189]. Different groups reported that such remnants could lead to increased differentiation affinity towards the cell type of origin[188-190]. The same phenomenon was observed in miRNA[191] and non-coding RNA[192] patterns. Besides, differences in functional properties of iPS cells depending on the donor cell type were described, in particular in iPSCs of early passages[193]. Accordingly, varying efficiencies concerning the generation of specific differentiated cell types were reported for hiPSCs and hESCs[194].

1.3.3.4. The promise of hiPS cells

Both ES and hiPS cells can give rise to virtually any cell type applicable in clinical use. However, possible applications of ES cell-based therapies are downsized by imminent transplant rejections (exceptions are transplantations at immunoprivileged sites such as brain or eyes). Unlike ESCs, iPSCs can be generated from patient cells. Tissues derived from such patient-specific iPS cells may avoid MHC (major histocompatibility complex) incompatibilities upon transplantation since donor and recipient are identical, although recent findings provoked controversy about the immunogenicity of isogenic iPSCs[195].

However, iPSCs promise for numerous possible therapeutic applications. To name but a few, patient-specific dopaminergic neurons could be prospectively engrafted in the *substantia nigra* in Parkinson's disease. Hematopoietic stem cells derived from iPSCs might be used to cure immunodeficient patients[196]. Similarly, iPSC-derived natural killer (NK) cells, T or B cells might be applied during immune therapies[196].

Patient-derived iPSCs may, moreover, be used to develop customized therapies. Once differentiated into the cell type of interest, these cells can be employed to model the patient-specific pathophysiological dysfunction *in vitro*, thereby facilitating screenings for drug candidates[116].

In case that mutations are the known source of dysfunction, gene targeting[197] or zinc finger nucleases could be employed to exercise a gene correction in the patient-specific iPS cells, followed by expansion and directed differentiation into the desired cell type[198]. For instance, iPSCs derived from a patient suffering from hereditary Parkinson's disease caused by the common point mutation G2019S in the *Lrrk2* locus[199] were gene-corrected employing a customized zinc finger nuclease[200]. Similarly, iPSCs from individuals with α-thalassemia[201], sickle cell anemia[202],

laminopathy[203], gyrate atrophy[204], chronic granulomatosis[205] and Fanconi Anemia[198] were genetically corrected.

Despite the fact that such "repaired" iPS or iPS-derived cells are not yet suitable for therapeutic applications, they represent groundbreaking progress towards customized therapies. IPS cells epitomize the promise for future individualized therapies to cure yet irremediable diseases. However, the basis for any clinical employment of iPS cells is, on the one hand, to standardize and steady iPS cell generation to ensure safe applications and, on the other, a global functional understanding of this new cell type. It is therefore of prime importance that processes such as cell cycle regulation, responses upon cellular stress conditions, e.g. DNA damage, and apoptosis are in-depth elucidated.

1.4. DNA damage, DNA repair & apoptosis in PSCs

Pluripotent stem cells can result in the development of complete organisms. Decisions about apoptosis and survival in PSCs must, for this reason, be elaborately balanced, as they can be fatal for the future individual: Increased apoptosis may lead to death of the embryo and abort, while insufficient apoptosis, e.g. following genotoxic impact, may cause spreading of mutations to the entire organism including germ cells and, subsequently, offsprings. In stark contrast, acquisition of mutations in somatic cells affects the respective individual (by potential degenerative or tumorigenic disorders within affected tissues) but not future generations.

For this reason, it is essential that cells of the highest potency levels (toti- and pluripotent cells) minimize the rate of deleterious mutations and preceding acquisition of DNA lesions. Different mechanisms have evolved to ensure these requirements for proper organismal development. First, while somatic cells can undergo either senescence or apoptosis following DNA damage, the senescence-related oxidative stress pathway is blocked in PSCs as reported by Prigione *et al.*[206]. Consequently, PSCs which have faced irreparable DNA damage need to initiate apoptosis. Second, human iPSCs and ESCs exhibit low mitochondrial content and mtDNA copy numbers, according to little endogenous ROS production, dependence on anaerobic glycolysis and low oxidative stress levels[206]. Elevated ROS levels have been associated with initiation of differentiation in PSCs[207-209].

Both human[210] and murine ESCs[211,212] show increased expression of various DNA repair enzymes[212]. Human PSCs have likewise been reported to exhibit enhanced DNA repair capacities[210]. Luo *et al*. found, however, solely accelerated execution of BER in hESC[19]. Surprisingly, the NER complex XPC has recently been shown to be a coactivator of Sox2/Oct4 in murine ES cells, thus implicating a role for DNA repair mechanisms in maintenance of both genome integrity and pluripotency[213].

Despite elevated expression of factors involved in DNA repair, human PSCs have been shown to be extremely vulnerable to DNA damage, as treatment with ionizing radiation (IR) leads to rapid and massive apoptosis after few hours[214]. Murine ES cells were reported to be hypersensitive to the base modification O6-methylguanine[215].

The exact mechanisms by which PSCs respond to DNA damage are still unknown. Filion *et al*.[216] and Momcilovic *et al*.[214] reported that human PSCs, unlike most other cell types, lack a G1 cell cycle phase arrest and stop in G2 phase after experiencing DNA damage[214,216]. Accordingly, lack of p21 upregulation upon IR treatment was

stated[216]. However, controversy arose concerning the existence of a G1 phase arrest in human ESCs[217]. Nonetheless, it is generally accepted that, if a G1 phase arrest exists in human PSCs, it is short-lived.

Similar to their peculiar cell cycle regulation, human PSCs were shown to have several extraordinary properties in terms of apoptosis. When human ESC or iPSC colonies are dissociated into single cells (e.g. by incubation in trypsin), hPSCs quickly initiate blebbing and, subsequently, programmed cell death. Ogushi *et al*. showed that apoptosis was induced by a Rho- and ROCK-dependent myosin hyperactivation-mediated mechano-chemical process and that ROCK inhibition by Y-27632 was able to suppress dissociation-induced apoptosis[159,160].
Albeit caspases (in particular caspase-3) represent the executioners of apoptosis, they play a yet cryptic role during reprogramming and iPSC generation as well, possibly by proteolytic inactivation of the tumor suppressor Rb protein[177]. Moreover, another important step of the apoptotic cascade is exclusively altered in human PSCs: While BAX is only activated and oligomerized upon apoptotic stimulation in other cell types, in hiPSCs and hESCs it resides at the Golgi apparatus in a pre-activated form, enabling an accelerated induction of apoptosis[218]. Upon suitable stimulation BAX is released from the Golgi by a yet unknown mechanism and translocates to the mitochondrion, leading to MOMP and cytochrome c release[218].

2. AIMS OF THE PROJECT

Human iPS cells epitomize the hope for future clinical therapies in the field of regenerative medicine. They give rise to all differentiated cell types and can be individually generated from patient-derived cells, thereby avoiding host-engraft rejection after transplantation. A thorough and comprehensive analysis of pluripotent stem cell function and properties during survival and apoptotic processes is an essential prerequisite for the development of therapeutic applications. Numerous studies have investigated self-renewal capacity, tumorigenicity and directed differentiation of iPS and ES cells; however, iPS cells have hardly been characterized in terms of cell death responses following different stimuli such as genotoxic chemicals or oxidative stress.

The first part of this thesis aimed to characterize the still largely unknown apoptosis pathways in human iPS cells. For this purpose, I established the reprogramming of primary human dermal fibroblasts to iPS cells and confirmed their pluripotent state on the cellular and molecular level. The generated iPS cells were subsequently exposed to various stimuli triggering the extrinsic, intrinsic and ER stress apoptosis pathways. To investigate their apoptotic susceptibility, induction of cell death was compared to the apoptotic responses of isogenic and non-isogenic fibroblasts as well as a control cell line. In these analyses, human iPS cells were found to be highly sensitive to apoptosis induced in particular by genotoxic treatment, whereas fibroblasts initiated quiescence or senescence upon severe DNA damage.

To investigate the mechanisms underlying the different apoptosis susceptibility of iPS cells and differentiated fibroblasts, the second part of the project explored DNA damage responses and a potential link between apoptosis induction and the DNA lesion rate. In this context, I developed a novel highly sensitive and accurate method for the detection and quantification of DNA lesions in the nuclear and mitochondrial genomes. This method, which we called LORD-Q for long-run real-time PCR-based DNA damage quantification, was thoroughly analyzed and found to be suitable for various applications. LORD-Q was further employed to compare iPS cells and fibroblasts regarding the acquisition of DNA lesions, DNA repair capacities and locus-specific damage frequencies.

Quantification of the DNA lesions uncovered a strong resistance of iPS cells to DNA damage. The last part of this work therefore aimed to explore the cell type-specific differences between pluripotent and differentiated cells and the molecular mechanisms underlying the high resistance and repair capacity of DNA damage in human iPS cells.

3. MATERIALS & METHODS

3.1. Materials

3.1.1. Cell lines & media

3.1.1.1. Cell lines and ES cell mRNA

Human K3, K7 and K22 dermal fibroblasts were used for the generation of hiPS cells by retroviral reprogramming. The human Jurkat T cell leukaemia cell line was a kind gift of the group of Prof. Wesselborg, University of Düsseldorf. Messenger RNA derived from H1 and H9 hES cell lines was kindly provided by Prof. Marek Los, Linkoping University, Sweden.

3.1.1.2. Media and solutions for cell culture

All media were supplemented with 1x penicillin/streptomycin.

Freezing solution

FCS	80% (v/v)
DMSO	20% (v/v)

Freezing solution (stem cells)

Serum replacement	80% (v/v)
DMSO	20% (v/v)

Human ectodermal differentiation medium

Neurobasal Medium	250 mL
DMEM F12	250 mL
B-27 Serum-Free Supplement (50X)	10 mL
Glutamine (100x)	5 mL
MEM non-essential amino acids (100x)	5 mL
N-2 Plus Media Supplement (100x)	2.5 mL
2-Mercaptoethanol (25 mM)	0.5 mL
Y-27632 (Wako),	10 µM
BSA	0.075 g

Human embryonic stem (hES) cell medium

Knockout DMEM	500 mL
Serum replacement	100 mL
Glutamine (100x)	5 mL
MEM non-essential amino acids (100x)	5 mL
2-Mercaptoethanol (25 mM)	0.5 mL
Basic FGF (10 µg/mL)	0.2 mL

Human endodermal/mesodermal differentiation medium

Knockout DMEM	500 mL
FCS	100 mL
Glutamine (100x)	5 mL
MEM non-essential amino acids (100x)	5 mL
2-Mercaptoethanol (25 mM)	0.5 mL

Human fibroblast (hFib) medium

RPMI 1640	500 mL
FCS	50 mL
Sodium pyruvate (100x)	5 mL

Jurkat medium

RPMI 1640	500 mL
FCS	50 mL

Murine embryonic fibroblast (MEF) medium

DMEM	500 mL
FCS	50 mL
Glutamine (100x)	5 mL

3.1.2. Reagents

3.1.2.1. Chemicals

Reagent	Provider
Acrylamide (Rotiphorese Gel 29:1)	Carl Roth
Agarose	Carl Roth

Ammonium persulfate (APS)	Carl Roth
Ampicillin	Carl Roth
Bromophenol blue	Sigma-Aldrich
BSA (fraction V)	Carl Roth
Calcium chloride (dihydrate)	Merck
Deoxycholic acid sodium salt	Sigma-Aldrich
Disodium phosphate dihydrate	Merck
DMSO	NeoLab
DTNB	Sigma-Aldrich
ECL chemiluminescence film	Amersham Biosciences
EDTA	Carl Roth
Ethanol	Merck
Glacial acetic acid	Carl Roth
Glutathione reductase	Roche
Glycerol	AppliChem
Glycine	AppliChem
HEPES	Carl Roth
Isopropanol	Merck
Lithium chloride	Sigma-Aldrich
Magnesium chloride (dihydrate)	AppliChem
2-Mercaptoethanol	Sigma-Aldrich
Methanol	Merck
Midori Green Advance	Biozym Scientific
Monosodium phosphate monohydrate	Merck
NADPH	Sigma-Aldrich
Nonidet P-40	AppliChem
PIPES	Carl Roth
PMSF	Merck
Potassium dihydrogen phosphate	Carl Roth
Potassium monohydrogen phosphate	Merck
PVDF membrane	GE Healthcare
Sodium bicarbonate	Carl Roth
Sodium chloride	Carl Roth
Sodium dodecyl sulfate	AppliChem
Sodium deoxycholate	Carl Roth
SSA	Sigma-Aldrich
TEMED	Carl Roth

Tris	AppliChem
Triton X-100	Carl Roth
Tween 20	Merck

3.1.2.2. Cell culture reagents

Reagent	Provider
Accumax	Millipore
Accutase	Millipore
Accustain	Sigma-Aldrich
B-27 Serum-Free Supplement (50X)	Invitrogen
Basic FGF	Peprotech
Bleomycin (sulfate)	Medac
BSO	Sigma-Aldrich
Cisplatin	Sigma-Aldrich
Collagenase / Dispase	Roche
DMEM	PAA
DMEM F12	Invitrogen
Dimethyl fumarate	Sigma-Aldrich
Etoposide	Sigma-Aldrich
FCS	PAA
Glutamine (100x)	Life Technologies (Gibco)
GSH-OEt	Sigma-Aldrich
Hydrogen peroxide	AppliChem
Knockout DMEM	Life Technologies (Gibco)
LIF	Biomol
MEM non-essential amino acids (100x)	PAA
Mitomycin c	Biotrend
N-2 Plus Media Supplement (100x)	R&D Systems
Neurobasal Medium	Gibco
PBS (1x)	PAA
Penicillin / Streptomycin (100x)	PAA
Q-IETD-OPH	MP Biomedicals
Q-LEHD-OPH	MP Biomedicals
Q-VD-OPH	MP Biomedicals
RPMI 1640	PAA
Serum replacement	Life Technologies (Gibco)

Sodium pyruvate (100x)	Life Technologies (Gibco)
Staurosporine	Sigma-Aldrich
TeSR1 medium	Stem Cell Technologies
Trypsin (0.05%) / EDTA	PAA
Y-27632 (Rock inhibitor)	Wako

3.1.2.3. PCR reagents

Reagent	Provider
APE1	New England Biolabs
Buffer 4 (5x)	New England Biolabs
KAPA 2G Hot Start Polymerase Mastermix (2x)	KAPA Systems
dNTP Mix (100 mM each)	Fermentas GmbH
Oligonucleotides	Sigma-Aldrich
ResoLight (20x)	Roche
SYBR Green Mastermix (2x)	Fermentas
UNG	New England Biolabs
Water (HPLC grade)	VWR

3.1.3. Buffers & solutions

ChIP cellular lysis buffer

85 mM	KCl
5 mM	PIPES pH 8.0
0,5 %	Nonidet P-40 (v/v)

ChIP dilution buffer

150 mM	NaCl
20 mM	Tris-HCl pH 8.0
2 mM	EDTA
1 %	Triton X-100 (v/v)

ChIP elution buffer

100 mM	$NaHCO_3$
1 %	SDS (w/v)

ChIP nuclear lysis buffer

50 mM	Tris-HCl pH 8.0
10 mM	EDTA
1 %	SDS (w/v)

ChIP wash buffer 1

150 mM	NaCl
20 mM	Tris-HCl pH 8.0
2 mM	EDTA
1 mM	PMSF
1 %	Triton X-100 (v/v)
0.1 %	SDS (w/v)

ChIP wash buffer 2

500 mM	NaCl
20 mM	Tris-HCl pH 8.0
2 mM	EDTA
1 mM	PMSF
1 %	Triton X-100 (v/v)
0.1 %	SDS (w/v)

ChIP wash buffer 3

250 mM	LiCl
10 mM	Tris-HCL pH 8.0
1 mM	EDTA
1 %	Sodium deoxycholate (v/v)
1 %	Nonidet P-40 (v/v)

FACS buffer

500 mL	PBS
25 mL	FCS

GSH buffer

100 mM	Na_2HPO_4 / NaH_2PO_4
1 mM	EDTA
pH = 7.5	

Laemmli buffer (4x) 10 mL

4.0 mL	Glycerol
2.5 mL	1 M Tris pH 6.8
2.0 mL	20% SDS
1.0 mL	2-Mercaptoethanol
0.5 mL	H_2O
~ 0.01 %	Bromophenol blue (w/v)

RIPA lysis buffer

150 mM	NaCl
50 mM	HEPES pH 7.4
1 %	Nonidet P-40 (v/v)
0.5 %	Sodium deoxycholate (w/v)
0.1 %	SDS (w/v)

TAE buffer (1x)

40 mM	Tris
1 mM	EDTA (pH 8.0)
0.12 %	Glacial acetic acid (v/v)

TBS/T

150 mM	NaCl
20 mM	Tris-HCl
0.05 %	Tween-20 (v/v)
pH 7.4	

TE buffer

10 mM	Tris
1 mM	EDTA
pH = 8.0	

Western blot transfer buffer

20 %	Methanol (v/v)
200 mM	Glycine
25 mM	Tris

3.1.4. Commercial kits

Kit	Application	Provider
Alkaline Phosphatase Detection Kit	AP staining	Millipore
BCA Kit	Protein quantif.	Thermo Scientific
DNeasy Blood & Tissue Kit	DNA isolation	Qiagen
GeneJET Gel Extraction Kit	PCR purification	Fermentas
GeneJET PCR Purification Kit	PCR purification	Fermentas
GeneJET Plasmid Miniprep Kit	Plasmid isolation	Thermo Scientific
Human and Murine PSC Kit	Flow Cytometry	BD Biosciences
OxiSelect Total Glutathione Kit	GSx quantification	Cell Biolabs
QuantiTect Primer Assay Kit	Real-time PCR	Qiagen
RNeasy Mini Kit / QIAshredder	RNA isolation	Qiagen

3.1.5. Antibodies & flow cytometry reagents

Reagent (conjugated fluorophore)	Provider
Annexin V (FITC)	BD Biosciences
Dihydrorhodamine 123	Sigma-Aldrich
Propidium iodide	AppliChem

Species	Specificity (conjugated fluorophore)	Provider
Rabbit	Acetylated histone H3 K9/K14	Millipore
Mouse	Actin	Sigma-Aldrich
Mouse	BAD	BD Transduction Laborat.
Rabbit	BAK	Millipore NT (Upstate)
Mouse	BAX	Trevigen
Mouse	BCL-2	Santa Cruz
Rabbit	BCL-X	BD Pharmingen
Goat	BID	R&D Systems
Rabbit	BIM	Stressgen
Rabbit	Caspase-9	AG Prof. Wesselborg
Rabbit	phospho-Chk2 Thr68	Cell Signaling
Mouse	α-Fetoprotein	Sigma-Aldrich
Bovine	Goat IgG (HRP)	Santa Cruz
Mouse	MCL-1	BD Pharmingen

Goat	Mouse IgG (Alexa Fluor 546)	Invitrogen
Goat	Mouse IgG (HRP)	Promega
Rabbit	NANOG	Abcam
Mouse	p21	BD Pharmingen
Mouse	p53	Calbiochem
Mouse	PARP1	BD Pharmingen
Chicken	Rabbit IgG (Alexa Fluor 594)	Invitrogen
Goat	Rabbit IgG (HRP)	Promega
Mouse	α-Smooth muscle actin	Abcam
Rabbit	SOX2	Abcam
Mouse	β3-Tubulin	Sigma-Aldrich

3.1.6. Oligonucleotides

All listed oligonucleotides for PCR and real-time PCR experiments were purchased from Sigma-Aldrich. All oligonucleotides which are not listed were purchased from Qiagen in the QuantiTect Primer Kit format (pre-mixed, tested primer pairs).

3.1.6.1. Primers for LORD-Q Assay

Denotation	Sequence
AS2.F	5′-GGCCACAGCACTTAAACACA-3′
AS2.R	5′-TGGTTAGGCTGGTGTTAGGG-3′
CL5.F	5′-ATCGTAGCCTTCTCCACTTC-3′
COL1A1.F (52)	5′-TGCAGGGTGAGAAACATGAC-3′
COL1A1.F (3578)	5′-ATTATCGGGACATCGGTGAA-3′
COL1A1.R	5′-CCACCAAAGCTTTCTTCTGC-3′
P53.F	5′-CATAACCGCAAATGGGAAAC-3′
P53.R (45)	5′-CGTCCTTTTGATGGCCTTT-3′
P53.R (3075)	5′-CGGGACGTGAAAGGTTAGAA-3′
OCT4.F (68)	5′-CTGCTGCCCATTTTCCTAGT-3′
OCT4.F (3438)	5′-GCAGGCCTAGGAGATGTGAG-3′
OCT4.R	5′-AAGAGGGTGGTGTTGAGTGG-3′

3.1.6.2. Primers for semi-long run DNA damage quantification

Denotation	Sequence
AL4.F	5′-CTGTTCTTTCATGGGGAAGC-3′
AS2.F	5′-GGCCACAGCACTTAAACACA-3′
AS2.R	5′-TGGTTAGGCTGGTGTTAGGG-3′

3.1.6.3. Oligonucleotides carrying modified base / insertion

General sequence:

5′-CCCTTCGCCCTATTCTTCATACGATTA[X]GCACAGCACCCTAACACCAGCCTA
ACCA-3′

Denotation	Insertion [X]
Abasic site	Abasic site
1 x AGCT	5′-AGCT-3′
1 x AGUT	5′-AGUT-3′
3 x AGCT	5′-AGCTAGCTAGCT-3′
3 x AGUT	5′-AGUTAGUTAGUT-3′
Control	-
7-Deaza-dA	7-Deaza-2'-deoxyadenosine
7-Deaza-dG	7-Deaza-2'-deoxyguanosine
5-HMdC	5-Hydroxymethyl-2'-deoxycytosine
5-Me-dC	5-Methyl-2'-deoxycytosine
N6-Me-dA	N6-Methyl-2'-deoxyadenosine
O6-Me-dG	O6-Methyl-2'-deoxyguanosine
8-Oxo-dA	8-Oxo-2'-deoxyadenosine
8-Oxo-dG	8-Oxo-2'-deoxyguanosine
TT dimer	cis-Thymine dimer

Primers used for LORD-Q analysis of the respective modified templates:

Denotation	Sequence
DL1.F	5′-CCCTTCGCCCTATTCTTCAT-3′
AS2.R	5′-TGGTTAGGCTGGTGTTAGGG-3′

3.1.6.4. Primers for rtPCR-based mRNA level determination

Denotation	Sequence
ACTB.F	5'-CATGTACGTTGCTATCCAGGC-3'
ACTB.R	5'-CTCCTTAATGTCACGCACGAT-3'
ALAS1.F	5'-CGCCGCTGCCCATTCTTAT-3'
ALAS1.R	5'-TCTGTTGGACCTTGGCCTTAG-3'
APOA1.F	5’-CCCTGGGATCGAGTGAAGGA-3’
APOA1.R	5’-CTGGGACACATAGTCTCTGCC-3’
APOA2.F	5’-CTGTGCTACTCCTCACCATCT-3’
APOA2.R	5’-CTCTCCACACATGGCTCCTTT-3’
APOA4.F	5’-CTCAAGGGACGCCTTACGC-3’
APOA4.R	5’-GTCCTGAGCATAGGGAGCCA-3’
APOB.F	5’-ACACACTGGACGCTAAGAGGA-3’
APOB.R	5’-ACTTGTGCTACCATCCCATACT-3’
APOC1.F	5’-TCCAGTGCCTTGGATAAGCTG-3’
APOC1.R	5’-GGCTGATGAGTTCCCGAGC-3’
APOE.F	5'-GTTGCTGGTCACATTCCTGG-3'
APOE.R	5'-GCAGGTAATCCCAAAAGCGAC-3'
CAT.F	5'-TGTTGCTGGAGAATCGGGTTC-3'
CAT.R	5'-TCCCAGTTACCATCTTCTGTGTA-3'
Endo OCT4.F	5’-GGCTCTCCCATGCATTCAAAC-3’
Endo OCT4.R	5’-CATGGCCTGCCCGGTTATTA-3’
Endo SOX2.F	5’-GCACACTGCCCCTCTCACAC-3’
Endo SOX2.R	5’-CACCAGACCAACTGGTAATGGTAGC-3’
ESG1.F	5’-ATATCCCGCCGTGGGTGAAAGTTC-3’
ESG1.R	5’-ACTCAGCCATGGACTGGAGCATCC-3’
GAPDH.F	5'-GGAGCGAGATCCCTCCAAAAT-3'
GAPDH.R	5'-GGCTGTTGTCATACTTCTCATGG-3'
GCLC.F	5'-GGAGGAAACCAAGCGCCAT-3'
GCLC.R	5'-CTTGACGGCGTGGTAGATGT-3'
GCLM.F	5'-TGTCTTGGAATGCACTGTATCTC-3'
GCLM.R	5'-CCCAGTAAGGCTGTAAATGCTC-3'
GDF3.F	5’-GCCATCAAAGAAAGGGAACA-3’
GDF3.R	5’-TCTGGCACAGGTGTCTTCAG-3’
GPX1.F	5'-CAGTCGGTGTATGCCTTCTCG-3'

GPX1.R	5'-GAGGGACGCCACATTCTCG-3'
GPX2.F	5'-GGTAGATTTCAATACGTTCCGGG-3'
GPX2.R	5'-TGACAGTTCTCCTGATGTCCAAA-3'
GPX3.F	5'-AGAGCCGGGGACAAGAGAA-3'
GPX3.R	5'-ATTTGCCAGCATACTGCTTGA-3'
GPX4.F	5'-GAGGCAAGACCGAAGTAAACTAC-3'
GPX4.R	5'-CCGAACTGGTTACACGGGAA-3'
GPX7.F	5'-CCCACCACTTTAACGTGCTC-3'
GPX7.R	5'-GGCAAAGCTCTCAATCTCCTT-3'
GSR.F	5'-TTCCAGAATACCAACGTCAAAGG-3'
GSR.R	5'-GTTTTCGGCCAGCAGCTATTG-3'
GSTA1.F	5'-CTGCCCGTATGTCCACCTG-3'
GSTA1.R	5'-AGCTCCTCGACGTAGTAGAGA-3'
GSTA2.F	5'-TACTCCAATATACGGGGCAGAA-3'
GSTA2.R	5'-TCCTCAGGTTGACTAAAGGGC-3'
GSTA4.F	5'-CCGGATGGAGTCCGTGAGAT-3'
GSTA4.R	5'-GGGCACTTGTTGGAACAGC-3'
GSTM1.F	5'-TCTGCCCTACTTGATTGATGGG-3'
GSTM1.R	5'-TCCACACGAATCTTCTCCTCT-3'
GSTM2.F	5'-TGTGCGGGGAATCAGAAAAGG-3'
GSTM2.R	5'-CTGGGTCATAGCAGAGTTTGG-3'
GSTM3.F	5'-TCGTGCGAGTCGTCTATGGT-3'
GSTM3.R	5'-TCTCCTCATAAGAGGTATCCGTG-3'
GSTM4.F	5'-AGAGGAGAAGATTCGTGTGGA-3'
GSTM4.R	5'-TGCTGCATCATTGTAGGAAGTT-3'
GSTM5.F	5'-CCATCCTGCGCTACATTGC-3'
GSTM5.R	5'-CCAGCTCCATGTGGTTATCCAT-3'
GSTO1.F	5'-GAACGGCTGGAAGCAATGAAG-3'
GSTO1.R	5'-TGCCATCCACAGTTTCAGTTT-3'
GSTO2.F	5'-TGCCCCTATTCTCACAGGACC-3'
GSTO2.R	5'-TCCAGGTACTCACAAGCAATAAC-3'
GSTT1.F	5'-TGCCGCGCTGTTTACATCTT-3'
GSTT1.R	5'-GTGCTGACCTTTAATCAGATCCA-3'
GSTT2.F	5'-TGGCATCCCCTTAGAGCTG-3'
GSTT2.R	5'-CTTGAGCGTCGGCAGTTTC-3'

GSTZ1.F	5'-GCCCAGAACGCCATCACTT-3'
GSTZ1.R	5'-CTACACAGTATATGCCCGCTG-3'
LDLR.F	5′-TCTGCAACATGGCTAGAGACT-3′
LDLR.R	5′-TCCAAGCATTCGTTGGTCCC-3′
LRP1.F	5′-AGCCAGCTATGCACCAACAC-3′
LRP1.R	5′-CCTTGCAGGAGCGGTTATC-3′
LRP2.F	5′-GGCCTGCTATAACACCAGTCA-3′
LRP2.R	5′-ACTCATTGTGCAAGCATATCTCA-3′
LRP8.F	5′-GCCAAGGATTGCGAAAAGGAC-3′
LRP8.R	5′-GTGGTCTAAGCAGTCATCGTC-3′
MGST1.F	5'-ATGACAGAGTAGAACGTGTACGC-3'
MGST1.R	5'-TACAGGAGGCCAATTCCAAGA-3'
MGST2.F	5'-TCGGCCTGTCAGCAAAGTTAT-3'
MGST2.R	5'-TGCCCGAAATACTCTCTCAAAC-3'
MGST3.F	5'-GGCCCACCTAGCCATCAATG-3'
MGST3.R	5'-CGCTGAATGCAGTTGAAGATGT-3'
NANOG.F	5′-ACTCTCCAACATCCTGAACCTC-3′
NANOG.R	5′-GCCTTCTGCGTCACACCA-3′
PRDX1.F	5'-CATTCCTTTGGTATCAGACCCG-3'
PRDX1.R	5'-CCCTGAACGAGATGCCTTCAT-3'
PRDX2.F	5'-GAAGCTGTCGGACTACAAAGG-3'
PRDX2.R	5'-TCGGTGGGGCACACAAAAG-3'
PRDX3.F	5'-GAGACTACGGTGTGCTGTTAGA-3'
PRDX3.R	5'-GTTGACGCTCAAATGCTTGATG-3'
PRDX4.F	5'-AGAGGAGTGCCACTTCTACG-3'
PRDX4.R	5'-GGAAATCTTCGCTTTGCTTAGGT-3'
PRDX6.F	5'-GTTGCCACCCCAGTTGATTG-3'
PRDX6.R	5'-TGAAGACTCCTTTCGGGAAAAGT-3'
REX1.F	5′-CAGATCCTAAACAGCTCGCAGAAT-3′
REX1.R	5′-GCGTACGCAAATTAAAGTCCAGA-3′
TERC.F	5′-CTAACCCTAATGAGAAGGGCGTA-3′
TERC.R	5′-GGCGAACGGGCCAGCAGCTCACATT-3′
VLDLR.F	5′-CTGGGTATGCGACGATGATG-3′
VLDLR.R	5′-CTTGGTGTGTATGACTGGCTG-3′

3.1.7. Instruments / Systems

Instrument	Application	Manufacturer
AggreWell plates	EB generation	Stemcell Technol.
Epgradient S Mastercycler	PCR cycler	Eppendorf
Gammacell 40 Exactor	Gamma irradiation (IR)	MDS Nordion
Infinite M200	96 Well plate reader	Tecan
LightCycler 480 II	Real-time PCR cycler	Roche
LSR II	Flow cytometer	BD Biosciences
NanoDrop 1000	Spectrometer	Peqlab
SNAP Protein Detection System	Western blot system	Millipore
UV Stratalinker 2400	UVC irradiation (UVR)	Stratagene

3.2. Methods

3.2.1. Cell culture

3.2.1.1. Culturing conditions

With exception of primary MEFs (see section 3.2.1.6), cells were cultured at 37°C, 5% CO_2 in the respective media (see materials section for compositions). Human pluripotent stem cells were grown on MEF feeder layers in hES medium supplemented with 10% TeSR1 medium and 5 ng/mL basic FGF. Human primary fibroblasts were grown in hFib medium supplemented with 5 ng/mL basic FGF.
During cultivation of Jurkat and pluripotent cells, medium was exchanged daily. Media of MEFs and human fibroblasts were exclusively changed during passaging.

3.2.1.2. Detachment of cells

Human fibroblasts and MEFs were detached using 1x trypsin/EDTA (PAA), while hiPS cells were detached by collagenase/dispase (Roche) treatment (30 min at 37°C, 1 mg/mL in PBS). Human cells were passaged 1:2 to 1:10, depending on the cell density. MEFs were passaged 1:3 after reaching a confluent state every 3-5 days.

3.2.1.3. Freezing and storage of cells

For storage, cells were pelletized and gently resuspended in a mixture of 50% culture medium and 50% freezing solution and steadily cooled down (1K/min) to -80°C. After several days, the vials containing the frozen cells were transferred to liquid nitrogen.

3.2.1.4. Thawing of cells

Cells were washed in 10 mL of warm cell culture medium, pelletized (5 min, 200 x g) and resuspended in appropriate volumes of prewarmed cell culture medium before seeding.

3.2.1.5. Isolation of MEFs from murine embryos

Pregnant BL6 mice were a kind gift of Benjamin Schmid (Hertie Institute for Clinical Brain Research, Tübingen). Mice were sacrificed on day E13.5 and MEFs were prepared as follows. After opening the abdomen the mice's uteri were isolated. Uteri were opened up, tissues surrounding the embryos were removed and the umbical

cords were cut. The isolated embryos were then put into fresh cold PBS. The livers were minutely removed to exclude hepatocytes. Each embryo was transferred into a single reaction vial containing 100 µL cold PBS and was cut into small pieces. 900 µL of trypsin/EDTA solution were added per vial. Next, the suspension was thoroughly resuspended and incubated under cell culture conditions (37°C, 5% CO_2) for 5 min. This resuspension / incubation step was repeated twice. The DNA clots that had formed were carefully removed with a pipet tip and the remaining cell suspensions were transferred into vials containing 10 mL of MEF medium. The cells were then centrifuged at 150 x g for 5 min and the supernatants were removed. Each pellet was resuspended in 2-5 mL MEF medium (depending on the assumed cell density) and the suspension was transferred to a single well of a 6-well plate or a 25 cm^2 flask (likewise depending on the assumed cell density). Cells were kept under low oxygen conditions (37°C, 5% O_2, 5% CO_2) and passaged 1:3 after reaching a confluent state. The MEFs of each embryo were cultivated separately until passage 3 to reduce the risk of contaminations.

3.2.1.6. Generation of MEF feeder cells

MEFs were kept under low oxygen conditions (37°C, 5% O_2, 5% CO_2) and passaged 1:3 every 3-5 days by trypsin detachment after reaching confluency. At passage 8, the confluent cells were incubated for 3 h in MEF medium supplemented with 10 µg/mL mitomycin c. Cells were washed with PBS twice, detached by incubation with trypsin/EDTA, then frozen as described above and stored in liquid nitrogen until usage.

3.2.1.7. Derivation of primary human dermal fibroblasts

Human primary fibroblasts (designated K3, K7 and K22) were derived from punch biopsies (diameter: 6 mm) of the skin (volar forearm) of healthy donors. The biopsies were fragmented into pieces of some 4 mm^2, each transferred into a single well of a 6-well plate and kept under cell culture conditions in hFib medium for 10-14 days. The cellular outgrowth was detached by trypsin/EDTA treatment and further cultivated in a 25 cm^2 cell culture flask.

The cells were grown to 80-90% confluence, followed by detachment (by incubation with trypsin/EDTA) and expansion in new cell culture dishes or flasks.

3.2.1.8. Generation of human iPS cells

Human induced pluripotent stem cells were generated by retroviral transduction of human dermal fibroblasts with the four Yamanaka factors *Oct4, Sox2, Klf4* and *c-Myc* (Addgene) as previously described[146]. Five days post-transduction, cells were detached with trypsin/EDTA and seeded onto MEF feeder cells. Human transduced cells were grown in hES medium supplemented with 10% TeSR1 medium and 5 ng/mL basic FGF. Medium was exchanged daily. Visible colonies emerged 20-30 days after transduction. Single colonies were manually picked and further cultivated as described above.

3.2.1.9. Embryoid body-mediated *in vitro* differentiation of iPS cells

Human iPS cells were detached and singularized by incubation with 1 mg/mL collagenase/dispase (30 min at 37°C) followed by accutase treatment. The cells were then transferred to AggreWell plates (Stemcell Technologies) and cultured two days in hES medium devoid of basic FGF and 2-mercaptoethanol to induce embryoid body formation. Next, the cells were cultured in ectodermal or endodermal/mesodermal differentiation media. The respective medium was exchanged daily. After 8 days, the cells were fixed by incubation in accustain (30 s). The cells were gently washed with PBS and permeabilized with 1 % Triton X-100. Finally, the cells were incubated for 1 h with the primary mouse antibodies anti-α-fetoprotein (1:100 in TBS-T), anti-α-smooth muscle actin (1:200 in TBS-T) or anti-β3-tubulin (1:500 in TBS-T). Following extensive washing with PBS, the cells were stained with Alexa Fluor 546-conjugated anti-mouse secondary antibody (1:1,000) for 30 min. Cellular nuclei were stained with 100 ng/µL DAPI.

3.2.2. DNA damage quantification

3.2.2.1. Induction of DNA damage

For induction of DNA damage the cells were irradiated (with UVC or ionizing radiation) or chemically treated before harvest. The cells were UV-irradiated in cell culture dishes (diameter 10 cm) at volumes of 10 mL medium or PBS per sample.
For chemical induction of DNA damage, cells were incubated with H_2O_2 (5 min), bleomycin (20 min) treatment, etoposide and cisplatin (both 16 h).
After stimulation, cells were washed with cold PBS and immediately harvested by scraping off the plates, then transferred to appropriate vials and pelletized (400 x g,

5 min, 4°C). Subsequently, cell pellets were snap-frozen in liquid nitrogen.
During DNA repair experiments, following stimulation the cells were allowed to recover for 2 h in fresh medium prior harvest.

3.2.2.2. DNA isolation

Prior DNA damage analysis, total DNA from pelletized cells (exposed to genotoxic stimuli or controls) was isolated using the DNeasy Blood & Tissue Kit (Qiagen) following the manufacturer's instructions. After elution, DNA concentrations were determined by optical density (OD) measurement at a wavelength of 260 nm using a Nanodrop 1000 spectrometer and ND-1000 software (Peqlab). OD260/OD280 ratios (generally > 1.80) were employed to confirm high DNA purities. Undiluted DNA was stored at -20°C prior use.

3.2.2.3. Agarose gel electrophoresis

0.5 – 2 % Agarose (w/v) was suspended in 0.5x TAE buffer and boiled until a clear, homogeneous solution was yielded. The solution was chilled for several minutes. 3 µL Midori Green Advance were added per 100 mL and mixed followed by transfer of the solution into a standard electrophoresis gel chamber (Peqlab) employing combs suitable to generate 10 – 24 gel pockets. After chilling to RT, the gel chamber was filled with 0.5x TAE buffer. 5 volumes of DNA samples were mixed with 1 volume of 6x Orange loading dye and 5 – 25 µL were applied per pocket. Electrophoresis was carried out at 100 – 150 V for 30 – 90 min. DNA fragments were subsequently visualized under UV light (254 nm).

3.2.2.4. Real-time PCR

15 µL reaction mixture and 5 µL diluted sample DNA (containing 50 ng whole-cell DNA) were applied per well. The reaction mixture contained 10 µL of 2x KAPA2G Fast Hot Start Polymerase kit, each 1 µL (corresponding to 10 pmol) of forward (sense) and reverse (antisense) primer, 2.95µL water (HPLC grade) and 0.05 µL 20x ResoLight dye (Roche). Every sample was analyzed in triplicate for each fragment.
After adding the reaction mixture and diluted sample DNA to the wells, the 96 well plates were sealed with a LightCycler 480 sealing foil (Roche) and analyzed. A pre-heating phase (95°C, 5 min) was followed by 35-50 cycles consisting of melting (95°C, 10 s), annealing (60°C, 10 s) and elongation step (72°C; expression analyses: 10 s; LORD-Q: Long fragments 2:15 min, short fragments 1 s; semi-long run method:

Long fragments 50 s, short fragments 10 s). To confirm PCR product sizes and purities, a melting curve analysis was performed and respective PCR reactions were analyzed by agarose gel electrophoresis (see 3.2.2.3).

Table 3.1: Genomic loci and corresponding primers, amplicon lengths and primer efficiencies employed in LORD-Q assays.

Gene / Locus	Fragment	Primer Forward	Primer Reverse	Length bp	Efficiency
mtDNA	Long	CL5.F	AS2.R	3,723	1.643
	Short	AS2.F	AS2.R	50	1.989
TP53	Long	TP53.F	TP53.R(3075)	3,075	1.649
	Short	TP53.F	TP53.R(45)	45	1.991
Oct4	Long	Oct.F(3438)	Oct.R	3,438	1.660
	Short	Oct.F(68)	Oct.R	68	1.995
Col1a1	Long	Col1A1.F(3578)	Col.R	3,578	1.641
	Short	Col1A1.F(52)	Col.R	52	1.990

3.2.2.5. Determination of primer pair efficiencies

For all primer pairs used for LORD-Q analysis, amplification efficiencies (E) were determined. DNA of untreated human Jurkat cells was serially diluted in buffer AE (DNeasy Blood & Tissue Kit, Qiagen) to yield final concentrations of 20, 10, 5 and 2.5 ng/µL. These dilutions (5 µL/well) were then used for LORD-Q analysis (see 3.2.4). C_p (crossing point) values were plotted against $\log_2$(DNA concentration) and efficiencies of the reactions were calculated by linear regression analysis following the equation $E^{-m} = 2$, in which m is the slope of the regression curve. All primer pair efficiencies were determined in ≥ 3 independent experiments.

3.2.2.6. Long-run rtPCR-based DNA damage quantification assay

Quantification of DNA damage rates by long-run rtPCR was carried out on a LightCycler 480 II system (Roche) in white nontransparent 96 well plates (Roche).

For each analyzed genomic locus both a long (3,000 – 4,000 bp) and a small nested amplicon (40 – 75 bp) were amplified in separate runs. All investigated genomic loci and the corresponding primers are listed in Table 3.1.

Prior analysis, DNA samples were diluted in buffer AE (Qiagen) to yield a final concentration of 10 ng/µL. RtPCR was carried out as described above employing specific elongation times for long and short fragments, respectively. Following completion of the respective PCR program, C_p values were determined for all samples using the LightCycler 480 II software.

3.2.2.7. LORD-Q data analysis

LORD-Q data analysis was carried out using experimentally determined C_p values (as calculated with the LightCycler 480 software) and primer pair efficiencies. For all employed primer pairs (and associated probes), E was determined as described above and assumed constant. The respective values are listed in table 3.2.

Table 3.2: Primers and probes employed in ROC analyses.

Method	Fragment	Primer Forward	Primer Reverse	Length bp
LORD-Q	Long	CL5.F	AS2.R	3723
	Short	AS2.F	AS2.R	50
Semi-Long	Long	AL4.F	AS2.R	930
	Short	AS2.F	AS2.R	50

For evaluation of LORD-Q experiments, the following equation was used to calculate lesions per 10 kb:

$$10{,}000 \times \left[\left(\frac{E_L^{Cp_{L(Sample)}} \times E_S^{-Cp_{S(Sample)}}}{[(E_L^{Cp_{L(Ref\,1)}} \times E_S^{-Cp_{S(Ref\,1)}}) \times (E_L^{Cp_{L(Ref\,2)}} \times E_S^{-Cp_{S(Ref\,2)}}) \times \ldots (E_L^{Cp_{L(Ref\,n)}} \times E_S^{-Cp_{S(Ref\,n)}})]^{(1/n)}}\right)^{(1/a)} - 1\right]$$

Cp_L (long fragment) and Cp_S (short fragment) are crossing point values of the respective sample and reference, while E_L and E_S constitute the amplification efficiencies of the long and short fragment. The number of (untreated) reference

samples is n, and a is the length of the corresponding long fragment (in bp), see table 3.1. E, a and n represent constants for any given combination of long probe and short nested fragment, so that exclusively C_p values must be experimentally determined to allow for calculation of the lesion incidence within the respective genomic locus. For each sample and probe, rtPCR was carried out in triplicate.

The LORD-Q formula implies two assumptions. First, detectable lesions are assumed to be randomly (Poisson) distributed, so that the damage incidence is exclusively dependent on the length of the corresponding probe, but not on its sequence. Second, the template sequence is considered as a Bernoulli process, in which every base can be damaged (probability x, $0 < x < 1$) or undamaged (probability 1-x). Only templates with undamaged bases can be amplified:

$$\binom{a}{0}(1-x)^a \cdot x^0 = (1-x)^a$$

In any case, $(1-x)^a$ is between 0 (if each template molecule carries at least one PCR-inhibitory lesion, $x = 1$) and 1 (if $x = 0$ and each template molecule is undamaged). The lesion incidence per 10 kb is therefore $10{,}000 \cdot x$. In the LORD-Q formula, x is expressed as the term in brackets (see above).

3.2.2.8. Receiver Operating Characteristic (ROC) analyses

The sensitivity of LORD-Q was investigated by comparison with a previously published semi-long run rtPCR-based method[105] in a series of Receiver Operating Characteristic analyses[219]. Jurkat cells were incubated with 0, 1, 10, 100 or 2,500 nM bleomycin for 20 min at 37°C (n = 15 per experiment and condition) in serum-free medium. Subsequently, the DNA was isolated and analyzed by both LORD-Q (mitochondrial probe; length 3723 bp) and semi-long run approach (mitochondrial probe; length 974 bp) in 96 well plates. Both methods used the same short internal template (length 67 bp) as reference. All employed primers are listed in Table 3.2. $\Delta C_p = C_p(\text{long}) - C_p(\text{short})$ was determined for each sample. For every bleomycin concentration and evaluation method, ΔC_p values of stimulated (true positives) and control (true negatives) samples were compared by ROC analysis via OriginPro 8 software (OriginLab). Results were expressed as area under the curve (AUC) values.

3.2.2.9. Amplification of modified oligonucleotides and UNG/APE1 digestion

Modified oligonucleotides carrying inserted single modified bases, 1x AGUT motif, 3x AGUT motifs or controls (1x AGCT or 3x AGCT; see section 3.1.6.3) were amplified following the LORD-Q protocol and rtPCR program for short fragments (elongation time 1 s, see section 3.2.2.4). Amplification rates were expressed as relative to respective controls.

For digestion with uracil N-glycosylase (UNG), oligonucleotide template stocks (10 µM) carrying 1x AGUT or 3x AGUT insertions (or respective controls: 1x AGCT or 3x AGCT) were diluted 1:50,000 in 1x Buffer 4 (New England Biolabs). 0.5 µL of UNG (New England Biolabs) and, if applicable, 0.5 µL of apurinic/apyrimidinic endonuclease-1 (APE1; New England Biolabs) were added to 10 µL of diluted template and the reaction mixture was incubated at 37°C for 1 h followed by inactivation of the enzyme(s) at 80°C for 10 min. Digested templates were diluted 1:10 and relative amplification was assayed by LORD-Q as described above.

3.2.3. Expression analysis

3.2.3.1. RNA isolation

RNA was isolated from cultivated cells employing the RNeasy kit (Qiagen) according to the manufacturer's instructions. In the final step, RNA was eluted with 25-50 µL RNase-free water and stored at -80°C until use. RNA concentrations were spectrometrically determined with a Nanodrop-1000 spectrometer and ND-1000 software.

3.2.3.2. Reverse transcription

Per sample, 1 µg of total RNA was reversely transcribed to yield cDNA using the Transcriptor First Strand cDNA Synthesis kit (Roche). Frozen mRNA and cDNA from H1 and H9 hES cells was a kind gift of Dr. Marek Los (Linköping, Sweden). It was assumed that reverse transcription of 1 µg RNA yielded 1 µg cDNA.

3.2.3.3. Real-time PCR-based cDNA quantification

Gene expression analysis was carried out by rtPCR on a LightCycler 480 II system (Roche). Reactions were performed in total volumes of 20 µL per well for 96 well

plates (all volumes and cDNA amounts were halved for 384 well plates), containing 10 µL of 2x SYBR Green master mix (Fermentas), 1 µL (containing 10 pmol) of each forward (sense) and reverse (antisense) primers and 10 ng of template cDNA. The employed PCR program comprised 5 min at 95°C followed by up to 50 amplification cycles (10 s at 95°C, 10 s at 60°C, 10 s at 72°C).
Expression levels were calculated as relative to the cDNA levels of reference genes (glyceraldehyde 3-phosphate dehydrogenase (GAPDH) and/or β-actin (ACTB) and/or δ-aminolevulinate synthetase 1 (ALAS1) as designated in the text) in fibroblasts.

3.2.3.4. Immunostaining for pluripotency markers

Glass coverslips were coated with 0.02% gelatine in PBS and dried. MEF feeders were seeded onto the coverslips and after 2 d iPS cells were seeded and grown on MEF feeder cells. Fixation of the cells was performed by addition of accustain (Sigma) and 30 s of incubation. Cells were washed several times with PBS followed by a combined blocking/permeabilizing step (1 h, 3% FCS and 0.05% saponin in PBS). Primary (rabbit anti-NANOG, rabbit anti-SOX2) and secondary (chicken anti-rabbit Alexa Fluor 594) antibody dilutions (1:150 and 1:1000, respectively, in blocking/permeabilizing solution) were dripped on parafilm and cover slips were headlong put onto the wetted parafilm. Incubation times were 2 h for primary and 1 h for secondary antibody. Prior and post secondary antibody incubation, cover slips were rinsed 5 times with PBS. For staining of nuclei with DAPI, coverslips were headlong incubated for 10 min in the dark employing a 100 ng/mL dilution (in blocking/permeabilizing solution), followed by two washing steps. Coverslips were put on microscope slides and analyzed with ApoTome (Zeiss) and Axio Imager.Z1 software.

3.2.3.5. Alkaline phosphatase staining

Alkaline phosphatase activity was determined employing the Alkaline Phosphatase Detection kit (Millipore). The assay was carried out following the instructions of the manufacturer: On day five after passaging, the medium was aspirated, iPS cells were washed with PBS and fixed with 4% paraformaldehyde for 1-2 min. The fixative was aspirated and the samples were rinsed with TBS/T. Next, the culture dishes were covered with staining solution (Fast Red Violet, Naphthol AS-BI phosphate solution and water mixed in a 2:1:1 ratio) and incubated in the dark for 15 min. Subsequently, the samples were washed with TBS/T and visually analyzed.

3.2.4. Flow cytometry

Flow cytometric analyses were carried out on the LSR II system (BD Biosciences). All data were analyzed by the FACSDiva software (BD Biosciences).

3.2.4.1. Characterization of pluripotent stem cells

Pluripotency of human iPSCs and murine iPSCs and ESCs was monitored using the Human and Mouse Pluripotent Stem Cell Analysis kit (BD Biosciences), comprising mouse anti-OCT4 PerCP-Cy5.5, mouse anti-SSEA-1 PE and mouse anti-SSEA-4 Alexa Fluor 647 as well as corresponding isotype controls. The staining procedure was carried out following the instructions of the manufacturer. Compensation beads (BD Biosciences) were used to compensate the signals of the fluorescent dyes, and cellular debris and cell doublets/multiplets were eliminated by suitable gating.

3.2.4.2. Apoptosis staining

Apoptosis was determined by Annexin V-FITC / propidium iodide co-staining and flow cytometric analysis. After stimulation and harvest by scraping off the plates, the cells were centrifuged (5 min, 300 x g) and singularized by pipetting (Jurkat cells) or enzymatic treatment (accumax: fibroblasts; accutase: pluripotent stem cells) for 10 min at 37°C. Following a second centrifugation step, the supernatant was discarded and the pellet was gently resuspended in staining solution comprising 5 µL Annexin V-FITC (BD Pharmingen), 10 µL of 50 µg/mL propidium iodide solution and 100 µL binding buffer (10 mM HEPES (pH 7.4), 140 mM NaCl, 2.5 mM $CaCl_2$) per sample. Staining occurred during 30 min incubation at RT in the dark. The samples were then transferred to 96 well v-bottom plates and centrifuged for 5 min at 300 x g. After discarding the supernatant, the cells were resuspended in 100 µL binding buffer and analyzed by flow cytometry on a LSR II machine (BD Biosciences) employing a 488 nm excitation laser and the 530/30 and 585/42 emission filters.

3.2.4.3. Determination of intracellular ROS levels

For intracellular ROS level quantification, 1-3 x 10^5 singularized cells were pelletized, resuspended in warm PBS containing 1 µM dihydrorhodamine 123 (DHR123), transferred to a v-bottom 96 well plate and incubated for 15 min at 37°C. Subsequently, cells were stimulated (bleomycin or H_2O_2 as indicated) and centrifuged for 5 min at 300 x g. For UV treatment, 10^6 cells were resuspended in 5 mL PBS, stained with 1 µM DHR123 as described above and irradiated with the

indicated dosages of UV. Cells were then transferred to 15 mL vials and centrifuged for 5 min at 300 x g.
After discarding the supernatants, the pellets were resuspended in FACS buffer (5% FCS in PBS, 100 µL per well) and analyzed by flow cytometry (488 nm excitation laser and 530/30 emission filter).

3.2.5. Protein quantification (BCA assay)

Protein quantification was performed using a bicinchoninic acid (BCA) assay kit (Pierce). Per well, 190 µL of BCA solution (mixture of 50 volumes of kit reagent A and 1 volume of kit reagent B) and 10 µL of sample or protein standard (BSA, 0 - 2 mg/mL) were accomplished in 96-well standard microtiter plates and incubated at 37°C for 20 - 30 min. Readout was performed on a Tecan ELISA reader at 562 nm. Each sample was analyzed in duplicate.

3.2.6. Cellular GSH level determination and manipulation

3.2.6.1. Glutathione depletion & replenishment

For depletion of the cellular glutathione pool, the respective cells were incubated for 1 h at 37°C and 5% CO_2 in the presence of 100 µM dimethyl fumarate (DMF) and 100 µM buthionine sulfoximine (BSO), unless otherwise designated.
Glutathione ethyl ester (GSH-OEt) was applied at concentrations of 1 - 2 mM in parallel to BSO/DMF-mediated depletion to replenish cellular GSH levels.

3.2.6.2. Glutathione assay: Quantification of GSx content

Total glutathione levels c(GSx) = 1 x c(GSH) + 2 x c(GSSG) were determined as originally described by Tietze[220]. Between 10^5 and 10^6 cells per sample were washed with cold PBS twice and centrifuged for 5 min at 300 x g. The supernatants were discarded and the pellets were vigorously resuspended in 500 µL of ice-cold 1% SSA (5-sulfosiacylic acid) each. After 30 min incubation on ice, the samples were centrifuged (10 min, 20,800 x g).
The supernatants were used for GSx quantification, whereas the pellets employed for determination of protein concentrations.
The supernatants were transferred to new reaction tubes and GSx content was determined in as follows: 10 µL of the respective supernatant were pipetted into a

well of a transparent flat bottom 96 well plate and mixed rapidly with 100 µL of reaction solution (containing 400 µM NADPH, 300 µM DTNB and 0.2 µL glutathione reductase in GSH buffer). Subsequently, the absorption at 492 nm was recorded every 60-90 seconds for 10-15 min and the slopes of the curves were determined. A standard (1 - 60 µM GSH in SSA) was used to calculate total GSx concentrations in the samples.

The pellets were resuspended in 500 µL 0.5 M NaOH and centrifuged (10 min, 20,800 x g). Protein concentrations in the supernatants were determined via BCA assay employing a suitable standard curve (0 - 2 mg/ml BSA in 0.5 M NaOH). GSx concentrations were normalized on protein concentrations and expressed as nmol GSx per mg protein. All samples were examined in duplicate (both GSx and protein content).

3.2.7. Chromatin immunoprecipitation

Chromatin immunoprecipitation (ChIP) was carried out as described by Rothfuss *et al*.[221]. Briefly, 10^7 cells were crosslinked by incubation with 1% formaldehyde for 10 min. The reaction was stopped by addition of glycine and the cells were pelletized and washed with PBS twice. The pellets were then lysed at 4°C for 10 min in ChIP cellular lysis buffer (1x protease inhibitor cocktail; Mini Complete, Roche) on a rotating wheel. The suspensions were then centrifuged (3 min, 4°C, 12,000 x g) and the supernatants were discarded. The pelletized nuclei were resuspended in nuclear lysis buffer and incubated for 10 min at 4°C on a rotating wheel.

Subsequently, the lysates were sonicated (Bioruptor, Diagenode) to yield fragments of 300 - 800 bp. The lysates were then centrifuged (5 min, 4°C, 12,000 x g) and resuspended in ChIP dilution buffer. Salmon sperm-blocked protein A agarose beads (Upstate) were added for preclearance. Beads were separated and discarded while the supernatants were diluted (final volume 10 mL per sample) in ChIP dilution buffer. 500 µL per sample were stored at -20°C as “ChIP input”. 5 µg of antibody (anti-acetylated histone H3 K9/K14 antibody, Merck-Millipore) were added per sample and the reaction tubes were spun overnight on a rotation wheel at 4°C.

Immune complexes were collected by addition of 60 µL salmon sperm-blocked protein A agarose beads per sample and incubation on a rotation wheel at 4°C for 3 h. Subsequently, the beads were pelletized and the supernatants were discarded. The beads were resuspended in ChIP dilution buffer and washed three times with ChIP wash buffer 1, 2 and 3, respectively. Next, the beads were washed twice with 1

mL ChIP TE buffer and eluted with 250 µL ChIP elution buffer per sample. The beads were separated by centrifugation and the supernatant was transferred to a fresh tube. Elution from the beads was repeated with another 250 µL elution buffer and the two fractions of elution buffer were combined.

2 µL of proteinase K solution (10µg/µl) were added to the elution fractions and the samples were incubated at 42°C for 1 h. 1 mL phenol/chloroform was added, mixed and centrifuged at 20,000 x g for 2 min. Subsequently the aqueous phase was transferred to a new reaction tube and the phenol/chloroform extraction was repeated.

The aqueous phase was mixed with 1.5 mL isoamyl alcohol and centrifuged again. 1 µl glycogen solution (~20 µg) followed by 2.5 volumes of ethanol/sodium acetate solution were added to the aqueous phase and the samples were stored overnight at -20°C.

The mixtures were centrifuged for 20 min at 4°C and 20,000 x g. Ethanol was decanted and the pellets were rinsed with 70% ethanol twice. The pellets were dried, then carefully resuspended in small volumes of TE buffer (20 µl for samples and 50 µl for input) and dissolved at RT overnight or 55°C for 2 h. DNA concentrations were measured employing a Nanodrop-1000 spectrometer. The DNA was stored at 4°C less than 3 d until rtPCR analysis was carried out.

RtPCR analysis was performed in triplicate employing a 2x SYBR Green rtPCR kit (Ferments; see section 3.2.3.3). Relative enrichment over input control was calculated using the $2^{\Delta\Delta Ct}$ method[222].

3.2.8. Western blot analysis

Cells were harvested by incubation with accumax (iPS cells) or by scraping off the culture dishes (fibroblasts). Cells were spun down by centrifugation (5 min at 500 x g) and stored at -80°C or lysed in 100-200 µL of RIPA lysis buffer including 1x protease inhibitor cocktail (Mini Complete, Roche) and, in case of phospho-CHK2 analysis, 1x phosphatase inhibitor cocktail (PhosSTOP, Roche). Cells were lysed for 30 min on ice, followed by 10 min of centrifugation at 20,000 x g. Protein concentrations of the supernatants were determined via BCA assay. The lysates were diluted to yield identical concentrations throughout the samples, supplemented with 4x Laemmli buffer and heated at 95°C for 5 min. Equal amounts of protein per lane (10 - 50 µg, depending on the experiment) were employed and separated by SDS-PAGE at 40 mA. Spectra Multicolor Broad Range Protein Ladder (Fermentas) served as

marker.

Following electrophoresis, proteins were transferred overnight onto PVDF membranes at 4°C and 25 V.

For protein detection, the SNAP system (Millipore) was used. In accordance to the manufacturer's instructions, membranes were blocked with 0.02% milk powder in TBS/T. Incubation times for primary antibody (diluted between 1:500 and 1:8,000 in TBS/T) and HRP-coupled secondary antibody (1:10,000 in TBS/T) were each 10 min. Between blocking, primary and secondary antibody incubation membranes were washed 3 times with appropriate volumes of TBS/T. Finally, membranes were washed 3 times with TBS/T and wetted by enhanced chemiluminescence (ECL Plus, GE Healthcare) solution. Visualization of bands was carried out using hypersensitive films (Amersham) and an SRX-101 (Konika) tabletop processor.

3.2.9. Statistical analysis

Unless stated otherwise, data were expressed as mean ± standard deviation of at least three independent experiments. P values were determined by unpaired, two-tailed Student's T-Test.

4. RESULTS

4.1. Generation and characterization of hiPS cells

To study DNA damage induction and apoptotic responses, human iPS cells were generated from dermal fibroblasts. Reprogramming was performed following the protocol originally described by Takahashi *et al*.[136] by retroviral transduction of the four transcription factors *Oct4*, *Sox2*, *Klf4* and *c-Myc* (OSKM). After 20 – 30 days, colonies emerged and were further co-cultivated on mitotically arrested MEF feeder cells (Fig. 4.1A).

Before the use of iPS cells in the experiments, it was essential to confirm the pluripotent state of the developing colonies to ensure their stem cell identity. For this purpose, different methods were employed. Staining for alkaline phosphatase activity[1], a hallmark of pluripotent cells, rendered the colonies visible to facilitate colony counting and, accordingly, determination of reprogramming efficiency (Fig. 4.1B). Besides OCT4, SOX2 and NANOG, which are indispensable for maintenance of the pluripotent state[156], markers for pluripotency comprise e.g. telomerase reverse transcriptase (TERT), telomerase RNA component (TERC), REX1, ESG1 and GDF3. Expression levels of these factors were determined in iPS and ES cells relative to levels in primary fibroblasts (Fig. 4.1C). Except TERC, which was moderately elevated in hiPS and hES cells, all examined markers were strongly increased in the pluripotent cells. The presence of OCT4 protein was furthermore confirmed by flow cytometric analysis (Fig. 4.1D). Likewise, the carbohydrate stage-specific embryonic antigen-4 (SSEA-4) was detected on the surface of hiPS cells (Fig. 4.1D), whereas SSEA-1 (also known as CD15; 3-fucosyl-N-acetyl-lactosamine), which constitutes an early differentiation marker in human cells (but a pluripotency marker in murine PSCs), was not expressed (Fig. 4.1D). All flow cytometric signals were normalized on signals of suitable isotype antibody controls. NANOG and SOX2 were additionally visualized by immunostaining (Fig. 4.1E).
To functionally test pluripotency, iPS cells were differentiated in an undirected manner following embryoid body formation. Markers of all the three germ layers – α-fetoprotein (endoderm), β3-tubulin (ectoderm) and smooth muscle actin (mesoderm) – were identified by immunostaining (Fig. 4.1F).

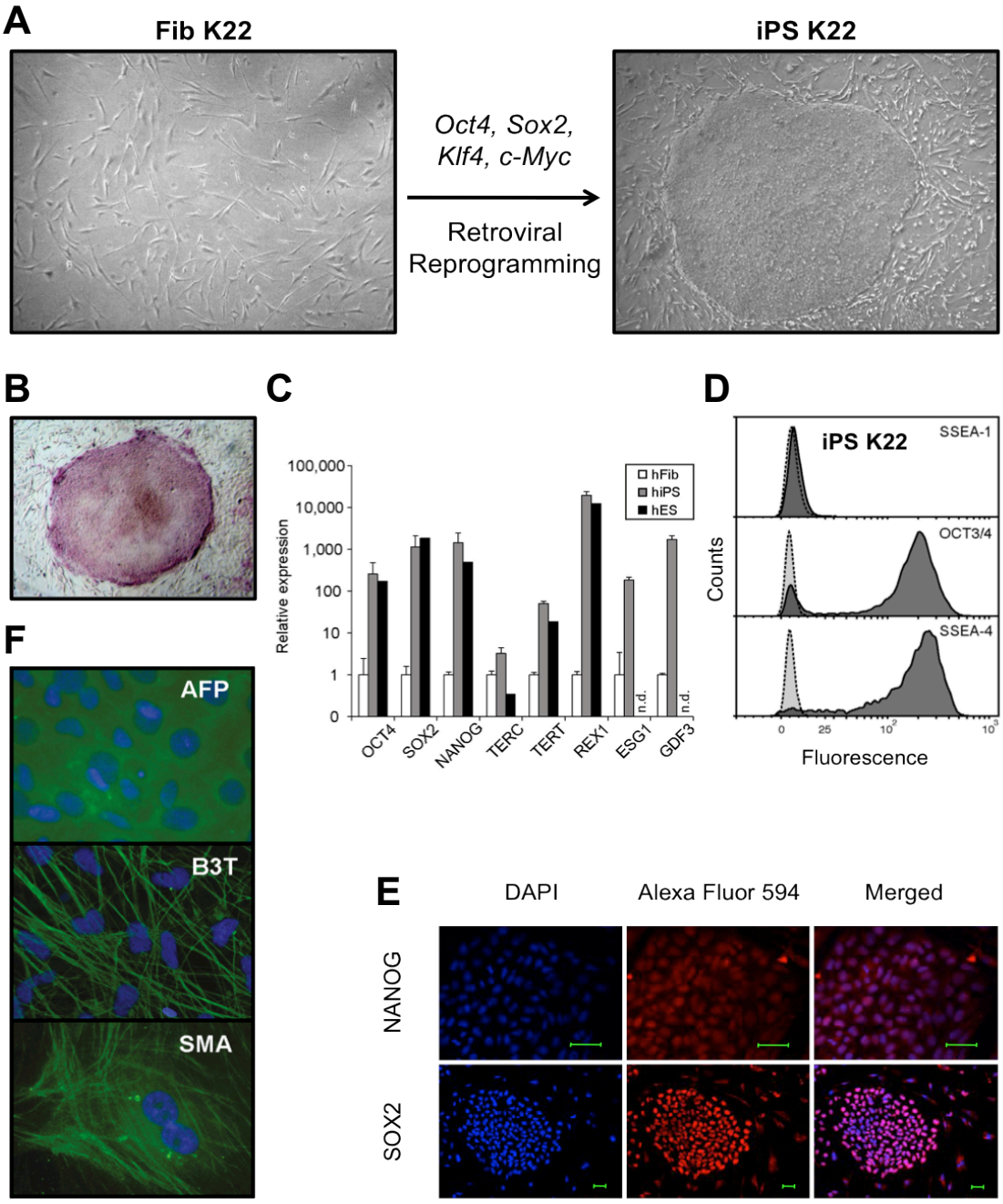

Fig. 4.1: Characterization of human induced pluripotent stem cells.

Representative characterization of the hiPS cell line K22. (**A**) Human dermal K22 fibroblasts, passage 4, were reprogrammed to pluripotency by retroviral transduction of the four Yamanaka factors *Oct4*, *Sox2*, *Klf4* and *c-Myc*. (**B**) Staining for alkaline phosphatase activity (purple). (**C**) mRNA levels of pluripotency factors in K22 hiPS cells and H9 hES cells relative to K22 fibroblasts. (**D**) Flow cytometric analysis of pluripotency factors in hiPS cells. Cells were stained for the mouse-specific factor SSEA-1 and the human factors OCT4 and SSEA-4 (dark grey) and isotype controls (light grey). (**E**) Immunostaining for the pluripotency factors NANOG and SOX2 in hiPS cells. DAPI staining (blue) of nuclei served as control. Scale bars represent 50 µM. (**F**) Immunostaining of markers for all three germ layers in iPS-derived cells. Embryoid bodies were generated from iPS cells and undirectedly differentiated. AFP (α-fetoprotein), endoderm; B3T (βIII tubulin), ectoderm; SMA (smooth muscle actin), mesoderm. Abbreviations: n.d.: not determined.

4.2. Apoptosis in human iPS cells

Apoptosis is a fundamental cellular process which is, for instance, necessary to maintain cellular homeostasis, remove infected or autoreactive cells and superfluous cells during development. Dysregulatad apoptosis has been associated with disorders such as development of malignancy and therapy resistance in tumors or neurodegenerative diseases[48]. Previous publications revealed that human ES and iPS cell are hypersensitive to DNA-damaging stimuli such as ionizing radiation[19,210] (IR). However, a comprehensive characterization of the apoptotic response in human iPS cells upon extrinsic, intrinsic and ER stress-mediated apoptotic signals has not yet been reported. Such global characterization of apoptosis employing iPS cells, fibroblasts and a control cell line (Jurkat T lymphoma cells) is the subject of this chapter. In this context, cellular responses upon different extrinsic, intrinsic and ER-stress-inducing stimuli were examined.

Activation of caspases by limited proteolysis and cleavage of key substrates such as poly(ADP ribose)polymerase-1 (PARP-1) is generally accepted as adequate evidence to detect apoptosis and to exclude other potential forms of cell death. This is exemplified in Fig. 4.2 by induction of apoptosis in Jurkat cells and fibroblasts in consequence of both extrinsic and intrinsic stimulation.

Fig. 4.2A shows the time-dependent proteolytic PARP-1 inactivation and, in parallel, activation of caspase-9 by cleavage of the 49 kDa procaspase form in Jurkat cells upon treatment with staurosporine and Fas ligand (FASL). Staurosporine (STS) is a broad kinase inhibitor and constitutes a strong intrinsic stimulus, while FASL (administered in a chemically crosslinked, highly active form called SuperFasL, see Fig. 4.2A) represents an extrinsic death ligand.

Caspases cleave their substrates within tetrapeptide consensus sequences containing a C-terminal aspartate residue. Specific irreversible caspase inhibitors, which are derivatives of the respective consensus sequences, prevent caspase-mediated autoactivation and substrate cleavage.

As demonstrated by Western blot analysis, the death ligand TRAIL (applied as "SuperKillerTRAIL", representing crosslinked TRAIL) induced caspase-9 activation and PARP-1 cleavage in human fibroblasts (Fig. 4.2B, second lane). Specific inhibitors for caspase-8, -9 and the pancaspase inhibitor Q-VD-OPH suppressed caspase-9 activation (Fig. 4.2B): Following extrinsic apoptotic stimulation, active

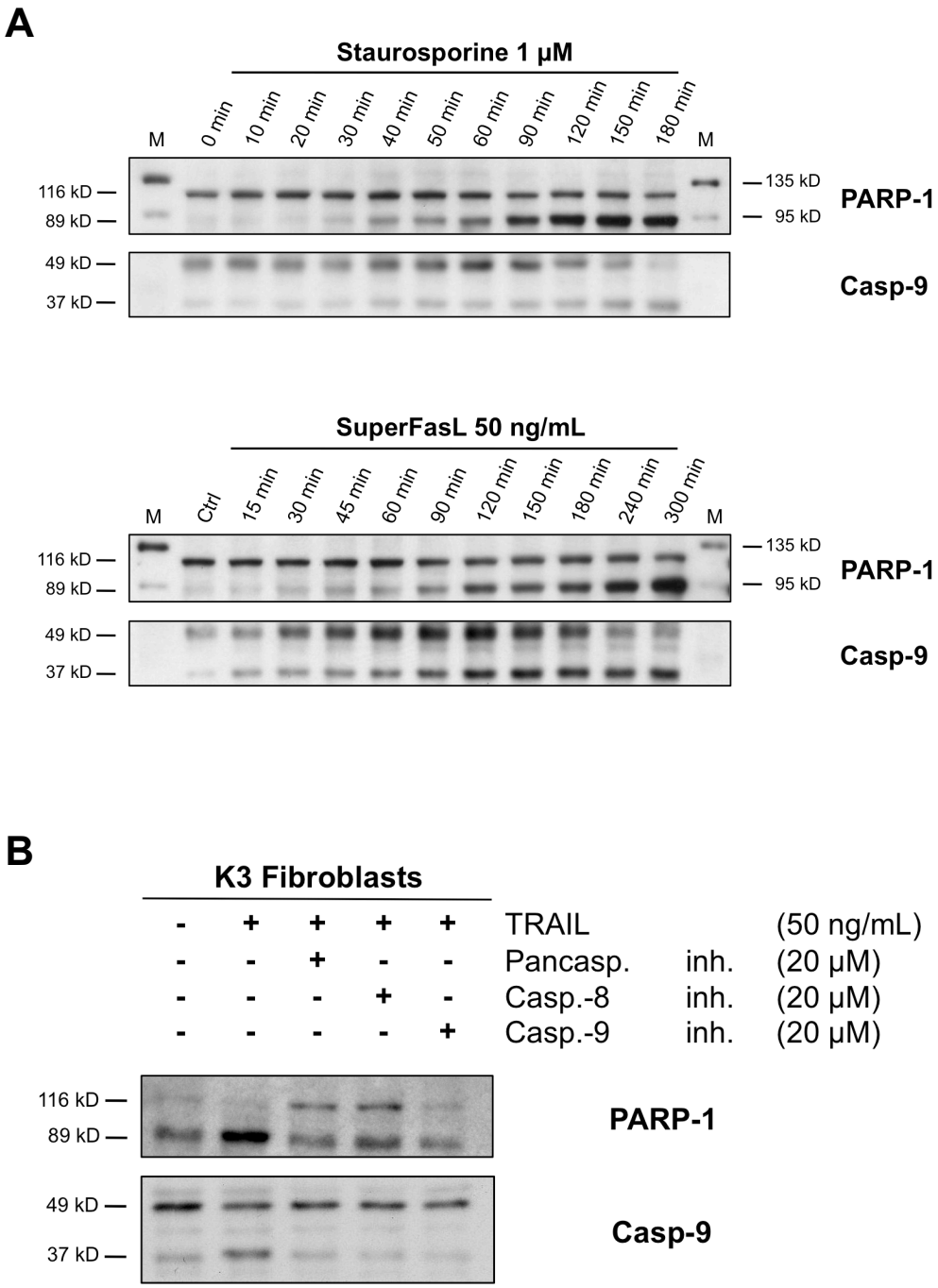

Fig. 4.2: Apoptotic cleavage of initiator caspase-9 and PARP-1 in fibroblasts and Jurkat cells upon extrinsic and intrinsic stimulation.

Western blot analysis of PARP-1 and procaspase-9 cleavage in primary human fibroblasts and Jurkat cells. (**A**) The intrinsic initiator (pro)caspase-9 and the caspase substrate PARP-1 are cleaved upon FASL (SuperFasL)-mediated extrinsic and staurosporine-mediated intrinsic stimulation of apoptosis in Jurkat cells. (**B**) Human K3 fibroblasts were stimulated with 50 ng/mL TRAIL (SuperKiller-TRAIL) for 8 h in the presence or absence of 20 µM caspase inhibitor (pancaspase, caspase-8 or caspase-9 inhibitor). Abbreviations: Casp: caspase; inh.: inhibitor; kD: kDa; M: protein marker.

caspase-8 cleaves BID to tBID (truncated BID), which activates BAX and BAK und leads to MOMP. Consequently, cytochrome c is released to the cytosol and initiates apoptosome formation, resulting in autoactivation of (pro)caspase-9. Thus, inhibition of both caspase-8 and caspase-9 prevent (pro)caspase-9 activation and autoactivation, respectively.

For a global characterization of cell type-specific apoptotic responses, fibroblasts, iPS and Jurkat cells were treated with nine different stimuli to trigger extrinsic, ER stress-mediated and intrinsic apoptosis pathways. Cell death was analyzed by FITC-annexin V / propidium iodide co-staining and flow cytometric analysis.
Apoptotic cells lose plasma membrane asymmetry and externalize phosphatidylserine to the outer leaflet of the membrane bilayer. Annexin V (AnxV) is a phosphatidylserine-binding protein and, consequently, binds to apoptotic cells. The membrane-impermeable DNA dye propidium iodide (PI) cannot enter apoptotic cells (or apoptotic bodies), since membrane integrity is maintained during apoptosis. Necrotic cells appear PI-positive as they lost membrane integrity, allowing PI to diffuse into the cell and to stain the DNA. Summarized, FITC-AnxV/PI co-staining enables to distinguish between vital ($AnxV^-/PI^-$), apoptotic ($AnxV^+/PI^-$) and necrotic (PI^+) cells.

Human primary fibroblasts initiate apoptosis upon extrinsic stimulation

Human primary dermal fibroblasts (hFib) were won from skin punch biopsies of healthy donors (depicted K3 and K22) and cultivated in the presence of basic FGF. Both TRAIL and FASL induced apoptosis, though application of TRAIL initiated programmed cell death faster and more comprehensively (Fig. 4.3A). Staurosporine served as positive control stimulus, since it rapidly initiated apoptosis in all cell lines (Fig. 4.3B, Fig. 4.4B and Fig. 4.5B).
In contrast, fibroblasts proved resistant to ER stress since neither thapsigargin nor brefeldin A significantly induced cell death within 48 h (Fig. 4.3C, left and center chart). Thapsigargin, a sesquiterpene lactone, is an inhibitor of the sarco- or endoplasmic reticulum Ca^{2+}-ATPase (SERCA), while brefeldin A targets COPI (coat protein I) coated vesicle formation. In consequence, brefeldin A causes increased retrograde protein transport from Golgi apparatus to ER, leading to increased ER protein load and unfolded protein response (UPR). Solely tunicamycin, a glycosylation inhibitor, slightly induced cell death after 48 h, even though necrosis was predominantly observed (Fig. 4.3C, right chart).

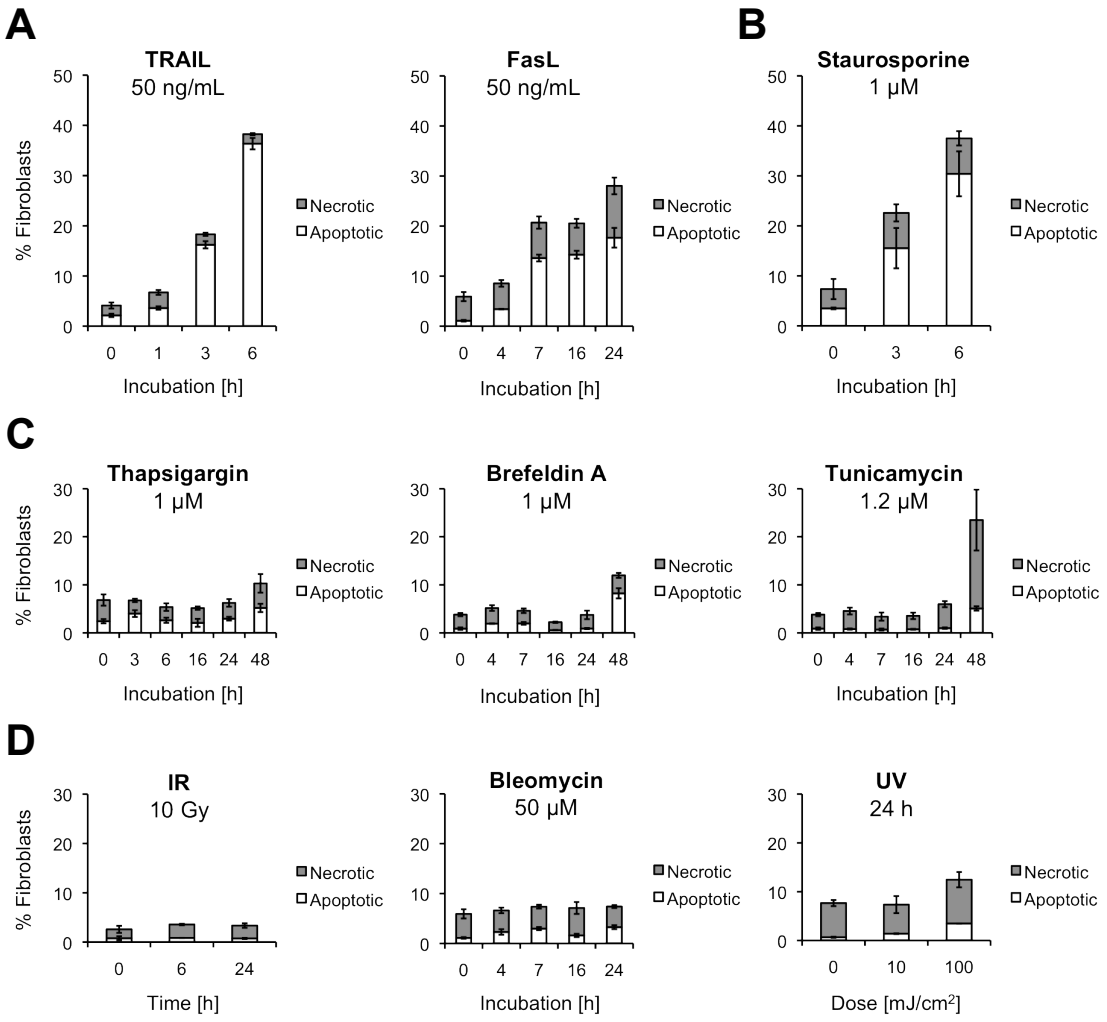

Fig. 4.3: Fibroblasts are resistant to ER stress and DNA damage but are susceptible to extrinsically stimulated apoptosis.

Apoptosis and necrosis rates in human dermal K3 fibroblasts were determined by flow cytometry following FITC-annexin V / propidium iodide (AnxV/PI) staining. n = 3, mean ± s. d. (**A**) Fibroblasts are sensitive to extrinsic stimulation by SuperKillerTRAIL (TRAIL, left graph) and SuperFas ligand (FASL, right graph). Both drugs induced apoptosis during seven hours after stimulation. (**B**) Staurosporine (STS) treatment induced massive apoptosis within six hours after stimulation, confirming STS as a positive control for apoptosis induction in human fibroblasts. (**C**) ER stress applied by thapsigargin, brefeldin A and tunicamycin did not cause apoptosis in fibroblasts. Only after 48 hours, slightly elevated levels of apoptosis (in case of brefeldin A treatment) or necrosis (in case of tunicamycin treatment) were observed. (**D**) Intrinsic stimulation by IR (ionizing radiation), bleomycin and UV (ultraviolet) light did not induce apoptosis in fibroblasts.

Intrinsic DNA damage-inducing stimuli did not initiate apoptosis. Fibroblasts withstood 10 Gray of ionizing radiation (Fig. 4.3D, left chart), 50 µM bleomycin (Fig. 4.3D, center chart) and 100 mJ/cm^2 ultraviolet radiation (Fig. 4.3D, right chart)

without significant increase in cell death rates within 24 h. It can thus be concluded that fibroblasts are susceptible to death ligand-induced extrinsic apoptosis, but resist ER stress- and DNA damage-mediated cell death.

Human iPS cells are resistant to extrinsic stimulation but initiate apoptosis after induction of ER stress and double strand breaks

Unlike fibroblasts, human iPS cells did not undergo apoptosis upon death ligand application. Neither TRAIL nor FASL led to increased cell death during 72 h compared to untreated controls (Fig. 4.4A). Similar results were obtained when higher levels of TRAIL and FASL (up to 250 ng/mL) where applied to the cells (data not shown). Hence, human iPS cells were found to resist extrinsic death stimuli. In contrast, staurosporine caused rapid and extensive apoptosis (Fig. 4.4B).

As human iPS cells undergo continued cell division, interference with protein synthesis ought to constitute a severe stress situation. In accordance with this expectation, ER stress was found to trigger apoptosis in hiPS cells. Brefeldin A and tunicamycin initiated extensive cell death rates at moderate velocity, while thapsigargin provoked apoptosis to a lesser extent (Fig. 4.4C).

Previous studies reported human iPS cells as hypersensitive to DNA damage[19]. The herein outlined results support this notion for DSB-inducing stimuli such as IR and bleomycin, both of which initiated apoptosis in about 50 - 80% of iPS cells after 6 h (Fig. 4.4D, left and center chart). Low dosages, e.g. 0.33 Gy IR and 100 nM bleomycin, were sufficient to trigger programmed cell death in the majority of iPS cells after 6 - 12 h (data not shown).

In contrast, moderate dosages of UVC radiation (1-30 mJ/cm^2, wavelength 254 nm) did not cause cell death in iPS cells (Fig. 4.4D, right chart), thereby contradicting previous reports[19]. UV radiation triggers electrocyclic addition of double bonds in neighbored pyrimidines, resulting in cyclobutane pyrimidine dimer (CPD) or 6-4 photoadduct formation. However, the majority of DNA lesions following UV light exposure is caused by oxidative stress and radicals that are produced when UV quants homolytically cleave chemical bonds. UV therefore mainly causes so-called indirect DNA damage[223] comprising oxidative nucleotide modifications and single strand breaks (which also occur during nucleotide excision repair of modifications), while IR and bleomycin induce significant amounts of DSBs in cells[224,225].

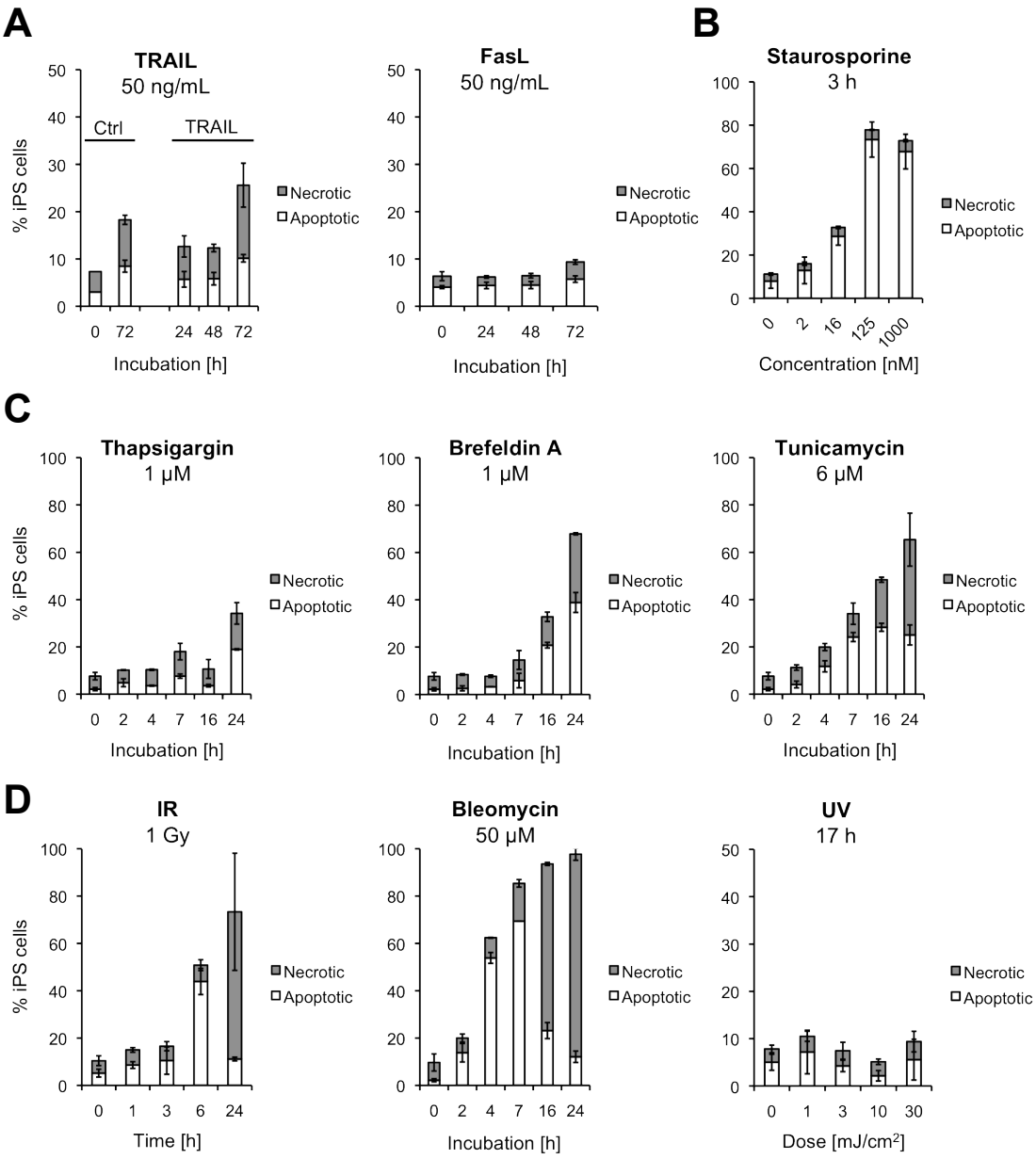

Fig. 4.4: Human iPS cells are resistant to extrinsic stimuli but hypersensitive to DNA damage-induced apoptosis.

Apoptosis and necrosis rates in human K7 iPS cells were determined by AnxV/PI staining and flow cytometry. Cells were singularized by incubation with accutase prior to FACS staining. n = 3, mean ± s. d. (**A**) Incubation of iPS cells in the presence of 50 ng/mL SuperFasL or SuperKillerTRAIL did not induce higher apoptosis rates than in untreated controls. (**B**) Staurosporine induced rapid and massive apoptosis after 3 h in hiPS cells at concentrations of less than 1 µM. (**C**) HiPS cells underwent apoptosis following ER stress induction by thapsigargin, brefeldin A or tunicamycin. However, apoptosis merely occurred in a small fraction of cells within 7 hours after stimulation. (**D**) DSB-inducing stimuli such as IR and bleomycin lead to fast and extensive initiation of apoptosis in hiPS cells. In contrast, UV radiation did not result in enhanced cell death rates.

Previous publications claimed that human ES and iPS cells prove highly resistant to oxidative stress[206], which is in accordance to the herein reported findings. Summarized, iPS cells undergo apoptosis upon treatment with ER-stress mediators and DNA DSB-inducing stimuli, but not following UV irradiation and accompanied application of oxidative stress.

Jurkat T lymphoma cells initiate apoptosis upon extrinsic stimulation, ER-stress and exposure to UV light

Jurkat cells initiate apoptosis upon various extrinsic and intrinsic signals and were therefore employed in numerous studies exploring apoptosis pathways[226,227]. In the current work, Jurkat cells were regarded as "apoptosis-prone" and served as control for the optimization of drug concentrations and incubation times.
Comparable to fibroblasts, Jurkat cells underwent PCD upon extrinsic stimulation by TRAIL and FASL (Fig. 4.5A). Cell death was detectable in >50% of the cells within a few hours in case of both stimuli. Likewise, treatment with 1 µM staurosporine rendered about 80% of the cells AnxV-positive (Fig. 4.5B).
Jurkat T lymphoma cells undergo continued cell division; susceptibility to ER stress was therefore, similar to hiPS cells, expected. All three ER-stress stimuli induced apoptosis, although brefeldin A had the strongest effect (Fig. 4.5C). Within 24 and 48 hours after application of the drugs secondary necrosis prevailed (Fig. 4.5C).
While iPS cells proved sensitive to IR and bleomycin, but not to UV treatment, Jurkat cells exhibited an opposite DNA damage response pattern (Fig. 4.5D). UV radiation induced excessive PCD even at relatively low doses, while bleomycin initiated apoptosis only at high concentrations of > 10 µM and > 16 h incubation time, whereas 1 µM triggered significant induction of apoptosis in iPS cells within 6 h after stimulation (data not shown). Jurkat cells are thus susceptible for extrinsic, ER stress and intrinsic stimulation with exception of IR and bleomycin, which in turn cause apoptosis in iPS cells.

Cell death in hiPS cells triggered by IR is dependent on caspases

In 1998, the group of Rudolf Jaenisch reported that murine ES cells undergo peculiar p53-independent apoptosis following genotoxic exposure[228]. However, based on the current work, this hypothesis could not be supported for human iPS cells. I found that

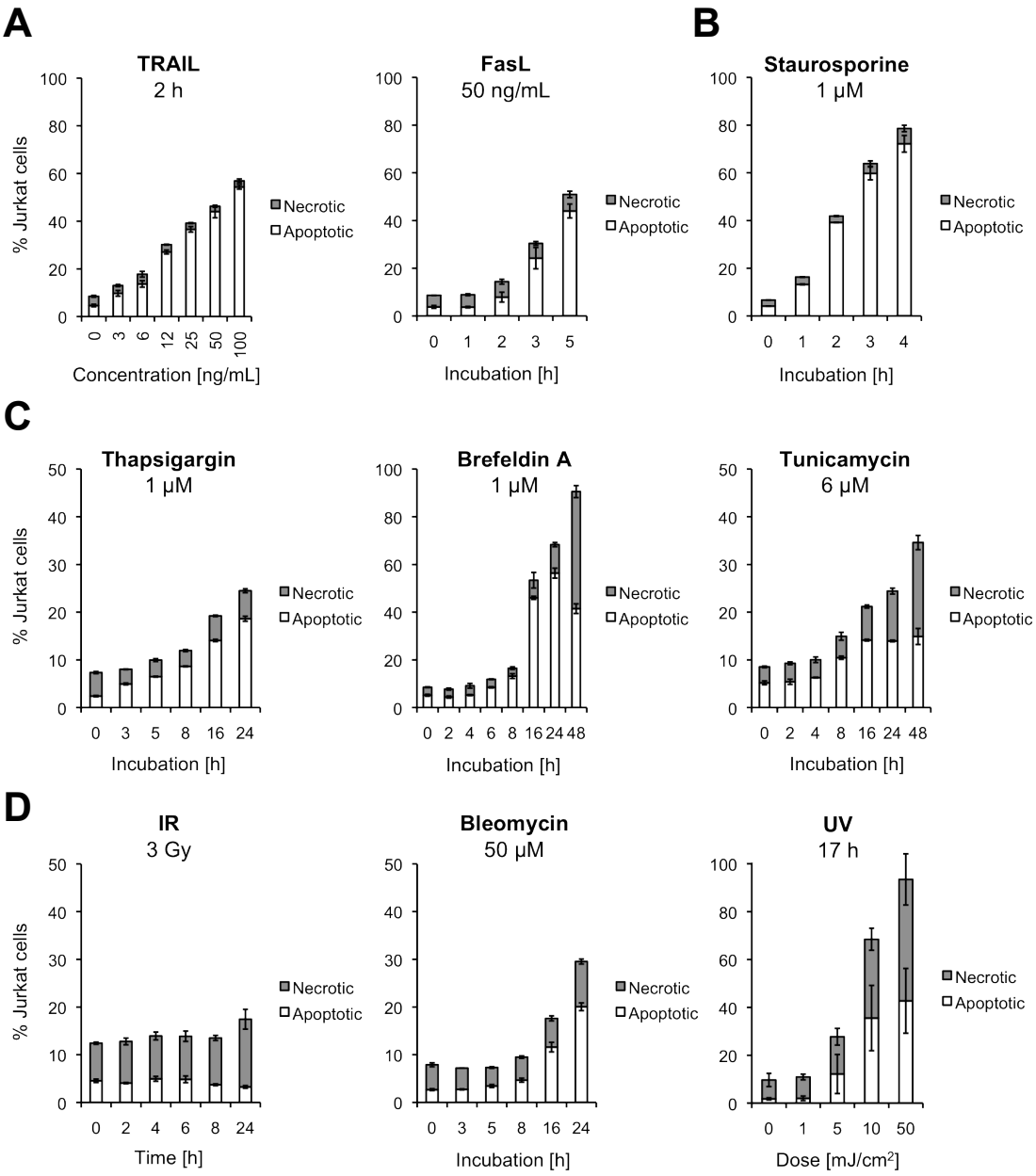

Fig. 4.5: Death ligands, ER stress and UV stimulation trigger apoptosis in Jurkat cells.

Apoptosis and necrosis rates in Jurkat cells were determined by AnxV/PI staining. n = 3, mean ± s. d. (**A**) Jurkat cells are sensitive to extrinsic stimulation by both TRAIL (left chart) and FASL (right chart). Both drugs induced significant apoptosis in less than five hours after stimulation. (**B**) STS induced extensive PCD within four hours after stimulation. (**C**) ER stress induced by thapsigargin and tunicamycin caused moderate apoptosis rates in Jurkat cells (left and right chart, respectively). Brefeldin A initiated extensive cell death. (**D**) Intrinsic stimulation by IR (ionizing radiation, left chart) did not induce apoptosis in Jurkat cells. High dosages of bleomycin led to moderate cell death rates, while Jurkat cells proved highly sensitive to exposure to UV light (right chart).

IR initiated caspase-9 and PARP-1 cleavage in K22 iPS cells and that this limited proteolysis was inhibited in the presence of the pancaspase inhibitor Q-VD-OPH (Fig. 4.6A). Moreover, Q-VD-OPH suppressed phosphatidylserine exposure to the outer leaflet of the plasma membrane ($P<0.001$, Fig. 4.6B), indicating that caspases were essential for the execution of apoptosis in iPS cells. Furthermore, hiPS cells expressed high levels of p53 (see below) and exhibited elevated levels of p21 and phospho-CHK2, both of which represent classical markers of p53 activation, upon IR treatment (Fig. 4.6C). Reverse-transcription PCR analysis of irradiated K22 iPS cells revealed that, at least in part, the increase of p21 protein levels was caused by upregulation of transcription rather than decreased p21 degradation (Fig. 4.6D).
Taken together, these data do not support the predication of p53-independent apoptosis in iPS cells, but suggest a classical p53-dependent execution of PCD. This finding yet provides another hint that results obtained from experiments employing murine ES or iPS cells cannot be transferred to human cellular models.

hiPS cells exhibit downregulated death receptor mRNA expression and altered levels of pro-apoptotic factors

Since iPS cells could not be extrinsically stimulated by FASL, TRAIL (see Fig. 4.4A) or co-incubation with TNF-α and cycloheximide (data not shown), the expression levels of death receptors were examined. As depicted in Fig. 4.7A, both K7 and K22 iPS cell lines exhibited similar expression patterns of death receptors and death ligands. Relative to the transcripts present in K3 fibroblasts, mRNA levels of FAS, TNF receptors R1 and R2 as well as TRAIL R2 and R4 were clearly reduced in iPS cells. Remarkably, TRAIL-R1 expression was slightly increased. Similar to death receptors, mRNA levels of the death ligands TRAIL and TNF-α were lower than in fibroblasts (Fig. 4.7A), whereas FASL expression was neither detectable in iPS cells nor in fibroblasts.

Subsequently, other pro- and anti-apoptotic factors were analyzed. With exception of BAD, all investigated pro-apoptotic proteins exhibited equal (BAX, BIM, PUMA) or increased expression (p53, BAK, BIM, NOXA) in relation to K3 fibroblasts. On the other hand, most examined anti-apoptotic factors featured reduced mRNA levels (XIAP, cIAP1, cIAP2, BCL-2, BCL-X, BCL-W, A1). Exceptions were Survivin and MCL-1, both of which were described to be robustly expressed in hES cells and to play an essential role in human stem cells by controlling self-renewal[216,229].

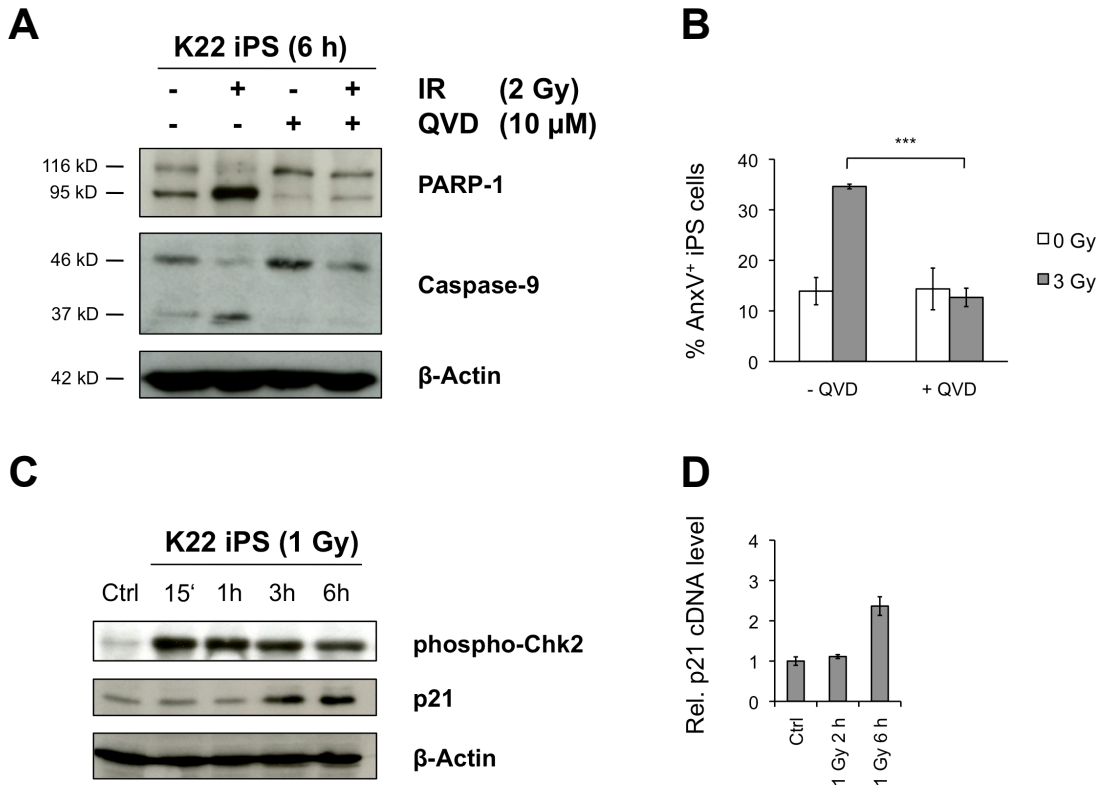

Fig. 4.6: IR induces caspase-dependent cell death in hiPS cells.

(**A**) Western blot analysis of PARP-1 and caspase-9 cleavage. K22 iPS cells were analyzed 6 h post irradiation with 2 Gy. Irradiated cells exhibited PARP-1 and caspase-9 cleavage, both of which were inhibited by addition of the pancaspase inhibitor Q-VD-OPH. (**B**) Caspase inhibition by QVD completely suppressed phosphatidylserine exposure as determined by FITC-annexin V (AnxV) / PI staining and flow cytometric analysis 6 h p.i. n = 3, mean ± s. d. (**C**) CHK2, a p53 kinase, is quickly phosphorylated upon IR exposition. Likewise, p21, a p53 target gene, is detectable at increased levels 3 h after irradiation. (**D**) In accordance with p21 protein, p21 mRNA (or, after reverse transcription, cDNA) amounts were elevated in K22 iPS cells after exposition to 1 Gy of IR. Levels are expressed as relative to Ctrl. n = 3, mean ± s. d. Abbreviations: p.i.: post irradiation; QVD: Q-VD-OPH (pancaspase inhibitor). *** P<0.001.

The expression profile depicted in Fig. 4.7A-C was further confirmed by Western blot experiments that demonstrated upregulation of pro-apoptotic factors 3 h post irradiation compared to untreated iPS cells, while anti-apoptotic proteins were downregulated (data not shown). P53, BAK and BIM levels were significantly elevated in hiPS cells, while BAX and BID amounts were akin to fibroblasts. In contrast to qPCR results, BCL-2 and MCL-1 levels were higher than in fibroblasts.

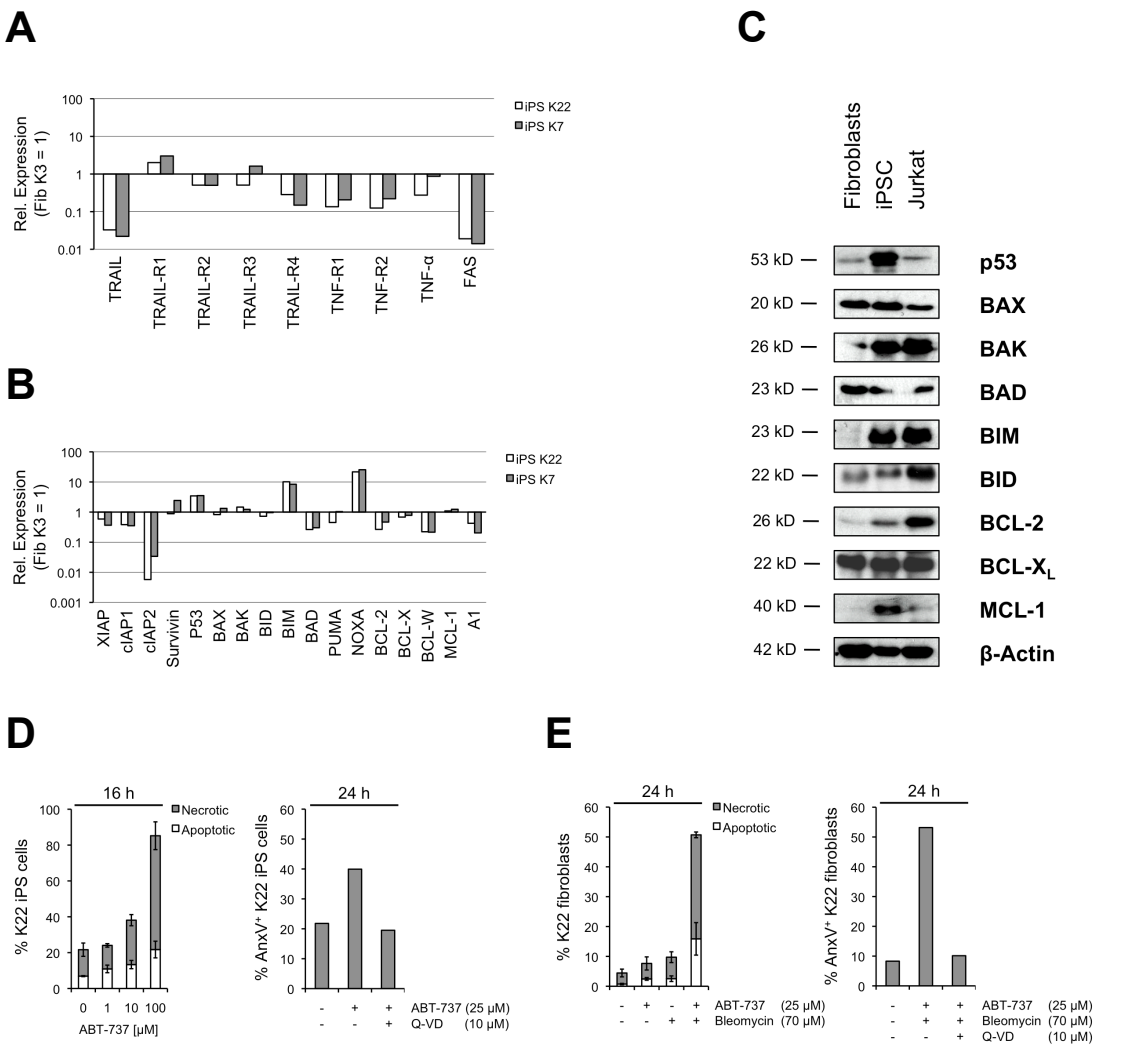

Fig. 4.7: Human iPS cells exhibit altered expression of pro-apoptotic factors and increased susceptibility to ABT-737.

(**A**) Relative mRNA levels of death ligands and death receptors (normalized on K3 fibroblast levels; reference genes: β-actin, GAPDH) in K7 and K22 hiPS cells. A representative analysis is shown. (**B**) Relative mRNA levels of apoptosis-associated factors (normalized on K3 fibroblast levels; reference genes: β-actin, GAPDH) in K7 and K22 hiPS cells. A representative analysis is shown. (**C**) Western blot analysis of apoptosis-associated proteins in K22 fibroblasts, K22 iPS cells and Jurkat cells. β-Actin served as loading control. (**D**) Exposure to ABT-737 dose-dependently induced cell death in iPS cells within 16 h (left, n = 3), while application of pancaspase inhibitor suppressed ABT-737-mediated cell death (right; representative experiment). (**E**) Fibroblasts resisted both ABT-737 and bleomycin exposure in terms of cell death. In contrast, combined application of both drugs induced PCD (left, n = 3), which could be suppressed by addition of pancaspase inhibitor (right; representative experiment). Abbreviations: AnxV: FITC-annexin V; Fib: fibroblasts; Q-VD: Q-VD-OPH (pancaspase inhibitor); Rel.: relative.

ABT-737 reveals iPS cells as "primed for death" and induces apoptosis in bleomycin-treated fibroblasts

Certo *et al*. defined a status named "primed for death" for cells that undergo apoptosis upon treatment with the BAD mimetic ABT-737[31]. Such cells exhibit extensive pro-apoptotic signaling and only survive, under normal culturing conditions, because they express sufficient amounts of anti-apoptotic Bcl-2 proteins (BCL-2, BCL-X_L, BCL-W, MCL-1 and A1). Upon neutralization of these anti-apoptotic factors, cell death occurs. Unprimed cells can be converted into primed cells by death stimuli such as DNA damage. They upregulate the "activators" BID and BIM, which are then sequestered by anti-apoptotic BCL-2 family members. BAD or other "sensitizers" set BID and BIM free, which then activate BAX and BAX, followed by MOMP and apoptosis[31].

In the context of this model, hiPS cells are "primed for death", as ABT-737 dose-dependently initiated PCD (Fig. 4.7D, left chart). Co-incubation with pancaspase inhibitor reversed the death stimulus (Fig. 4.7D, right chart). Following the Certo model, human iPS cells share this property with different tumor cell lines, which, due to failing cell cycle control, suffer from various intrinsic death stimuli and are thus "addicted" to anti-apoptotic Bcl-2 proteins[31]. In wide contrast, human fibroblasts died neither upon ABT-737 nor bleomycin treatment, but co-incubation with both stimuli initiated PCD in the majority of the cells (Fig. 4.7E, left chart). Obviously bleomycin induced DNA damage-mediated pro-apoptotic signaling, thereby rendering the cells "primed for death". Execution of cell death was dependent on caspase activation as confirmed by treatment with a pancaspase inhibitor that suppressed PCD induction. (Fig. 4.7E, left chart). Thus, fibroblasts resemble Certo's "unprimed" somatic cells which do not suffer from intrinsic pro-apoptotic signaling *per se*, while iPS cells parallel the dependence of tumor cells on high levels of anti-apoptotic proteins, such as BCL-2 or MCL-1 (Fig. 4.7C).

The previous results demonstrate that iPS cells are hypersensitive to genotoxic drugs such as IR and bleomycin. This finding raised the question whether the increased vulnerability of iPS cells was due to higher acquisition of DNA lesions or caused by stronger downstream DNA damage or apoptosis responses. In order to match DNA lesion rates to apoptotic outcome, an accurate and high-throughput-compatible DNA damage quantification method was to be developed. This method and possible applications are the subjects of the following chapter.

4.3. Long-run rtPCR-based DNA damage quantification (LORD-Q)

As described in the previous section, human iPS cells exhibited a high vulnerability to apoptosis induction by different DNA-damaging agents. Two different explanations for this phenomenon appeared plausible: On the one hand, hiPS cells may acquire a higher lesion incidence during genotoxic treatment compared to other cell types. On the other, equal amounts of DNA lesions might initiate stronger DNA damage signaling in hiPS cells than e.g. in isogenic fibroblasts and, accompanied, a more vigorous induction of apoptosis.
In order to examine those possibilities, the relation between the frequency of genomic lesions and the following pro- or anti-apoptotic response was investigated.

Disadvantages of current DNA damage analysis methods

So far, most described techniques detect global, but not sequence-specific DNA damage, and are tedious and labor-intense, such as the comet assay, terminal dUTP nick-end labeling (TUNEL) or γH2AX staining. In addition, several techniques require high amounts of DNA (e.g. ELISA-based 8-oxo-dG quantification[104]) or are inaccurate (e.g. qPCR endpoint analysis which requires to match the "linear" fluorescence signal range during template amplification). All of those methods are hardly suitable for high sample numbers since different experimental steps are required, such as determination of DNA concentration, PCR, agarose gel electrophoresis and band densitometry in endpoint qPCR. In addition, sequence specificity is necessary to survey DNA damage incidence in predisposed loci (such as proto-oncogenes), potential hot spots for DNA damage or tumor suppressor genes.
For this purpose, I first developed an accurate and sequence-specific method that enabled high-throughput analyses of DNA damage quantification in microtiter formats of 96- or 384 well plates.

Advantages and restrictions of rtPCR-based DNA damage quantification techniques

Real-time PCR-based DNA damage quantification techniques share considerable methodological advantages compared to the above-mentioned methods. They can be carried out in high-throughput-compatible standard 96 or 384 well plates, allowing automated data evaluation. Moreover, these rtPCR methods are sequence-specific (in principle, every genomic locus can be monitored), comprise few experimental steps and require low labor efforts.

However, the accuracy of the most recent method described by Rothfuss *et al*.[105] is exclusively satisfying in terms of accuracy when abundant mitochondrial genomes are used as template. In whole-cell DNA samples, mtDNA is present in about 10 – 1,000 fold higher copy numbers than nuclear (n)DNA (own observation, data not shown). This leads to C_t or C_p value increase of about 5 to 10 cycles when nDNA instead of mtDNA sequences are investigated for damage levels, thereby potentiating errors of measurement.

The roadblock for rtPCR-based DNA damage quantification in nDNA templates has therefore been the maximal probe length of approximately 1 kb: Longer probes contain – assumed that nucleotide modifications and strand breaks are randomly distributed – statistically more lesions per template molecule. For this reason less template molecules in a genotoxin-treated sample are undamaged, yielding an increased delay in C_t or C_p values as compared to short, undamaged reference sequences. This improves the sensitivity of the assay and may allow for reliable analyses of nuclear DNA damage incidence. In order to achieve successful amplification of long (> 1 kb) probes, restrictions that limit probe length must be overcome.

LORD-Q: A technique for long run rtPCR-based DNA damage quantification

Two critical factors limit the length of the amplified probe and, consequently, the sensitivity of the assay: First, rtPCR relies on dsDNA-specific dyes, which bind to or intercalate into dsDNA, thereby inhibiting the processivity of the employed DNA polymerase. The most commonly used PCR-inhibitory dye is SYBR Green. Second, slow and error-prone polymerases (usually standard *Taq* polymerases) are contained in most commercially available rtPCR master mixes.

In the current approach, an extremely rapid and high-fidelity second generation polymerase (KAPA2G, Peqlab) was used, which possesses a velocity of up to 1 kb/s. This polymerase was combined with ResoLight (Roche), a DNA dye originally developed for endpoint PCR and melting curve analysis. ResoLight exhibits superior brightness and can, for this reason, be applied 20-times less concentrated (own observation) than recommended by the manufacturer, thereby reducing polymerase inhibition by DNA intercalation. The combined utilization of KAPA2G polymerase and ResoLight DNA dye with a refined rtPCR protocol (see Methods section) enabled amplification of fragments of up to 4 kb length.

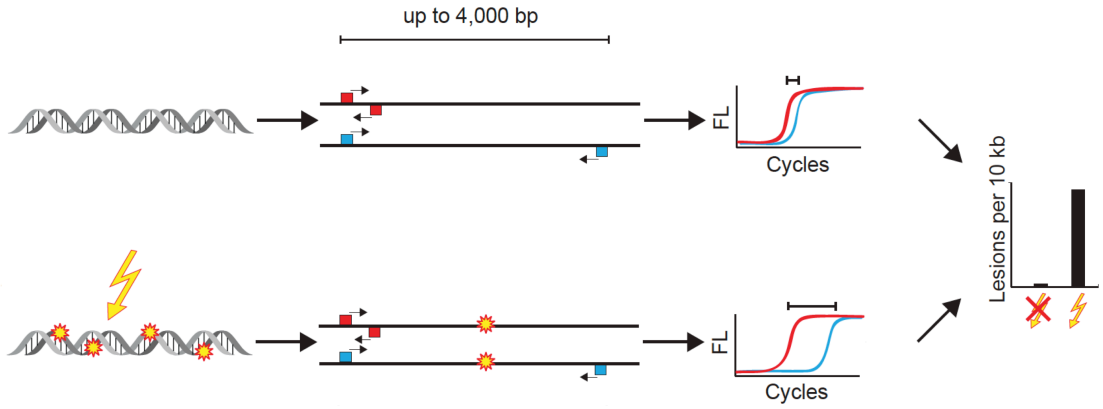

Fig. 4.8: Schematic illustration of the LORD-Q method.

DNA derived from control (top) or genotoxin-exposed cells (bottom) is analyzed by LORD-Q. A short reference fragment of ~50 bp (red) is amplified in a first rtPCR run, yielding readout curves exhibiting early fluorescence increase and, accordingly, low C_p values. The fast fluorescence increase of the short sample is due to high amplification efficiencies (about 100%) and the absence of DNA damage, since only neglectable amounts of polymerase-inhibitory lesions occur in short fragments. A long probe fragment of up to 4 kb (blue) is amplified in a second rtPCR run. Compared to the reference fragments, this probe is amplified less efficiently, as PCR efficiency decreases with product length. Therefore, the increase of fluorescence is slightly delayed (top, blue curve) compared to the small fragment. In contrast, a considerable fraction of template molecules in the genotoxin-treated samples exhibits at least one polymerase-stalling lesion within the probe sequence that cannot be amplified. Thus, the increase of fluorescence for the long probe is notably delayed (blue curve, bottom) as compared to the untreated sample (blue curve, top). As a result, the difference between C_p values of long and short fragment amplification (equal ΔC_p or ΔC_t in conventional rtPCR methods, e.g. for expression analyses) is greater in case of the genotoxically treated sample compared to the untreated sample; equal $\Delta\Delta C_p>0$ or $\Delta\Delta C_t>0$ in conventional rtPCR methods. Finally, the lesion incidence in the genotoxin-treated sample is calculated (right).

Principle of the LORD-Q assay

RtPCR-based methods rely on DNA lesions that interrupt polymerase-driven amplification of a defined PCR product. Only if such lesions lie within the amplified sequence (Fig. 4.8, lower panel), DNA synthesis is inhibited. If less template molecules can be successfully amplified, increase in fluorescence (which is proportional to dsDNA concentration) is delayed (Fig. 4.8, lower panel, blue curve). Accordingly, higher C_t or C_p values are obtained. Given that DNA lesions are randomly distributed among the respective genome, longer amplified sequences exhibit higher probabilities to contain a modification that inhibits polymerase action. This results in less template molecules which exhibit undamaged probes (that can

successfully be amplified). Thus, longer probes yield a higher C_p value compared to an untreated control, thereby increasing the sensitivity of the assay.
A short nested fragment of 45-70 bp length (Fig. 4.8, red fragments and curves) serves as internal control and as measure for the concentration of template DNA. Damage rates within these short reference fragments are neglected since, even at high DNA damage incidence (e.g. 10 lesions per 10 kb), only a minor portion of short fragments within the DNA template molecules is affected.

The new method was named "Long Run rtPCR-based DNA Damage Quantification" (LORD-Q). In comparison to the semi-long run (SLR) method described by Rothfuss *et al.*[105], a theoretical increase in sensitivity of factor 4 was calculated (see Table 4.1). In practice LORD-Q even exceeded this calculated improvement and outclassed the precursor SLR method (see Receiver Operating Characteristic analysis below).

Table 4.1: Correlation between probe length and expected ΔΔCp for commonly used rtPCR methods

Method	Probe Length (bp)	Calculated ΔΔCp
Classical real-time PCR (short template)	50	0.01
Classical real-time PCR (long template)	300	0.04
Semi-Long Run rtPCR	974	0.14
LORD-Q	**3.723**	**0.54**

Commonly used rtPCR methods applied on a hypothetical sample carrying 1 lesion per 10 kb of the template DNA.

LORD-Q enables amplification of probes up to 4 kb length

Following design and testing of various primer pairs, one mtDNA and two nDNA (*Oct4* and *Col1a1* loci) probes of 3438 to 3723 bp length were selected for application in the LORD-Q assay. Agarose gel electrophoretic analysis demonstrated that the probes were successfully amplified using the LORD-Q approach (Fig. 4.9A,

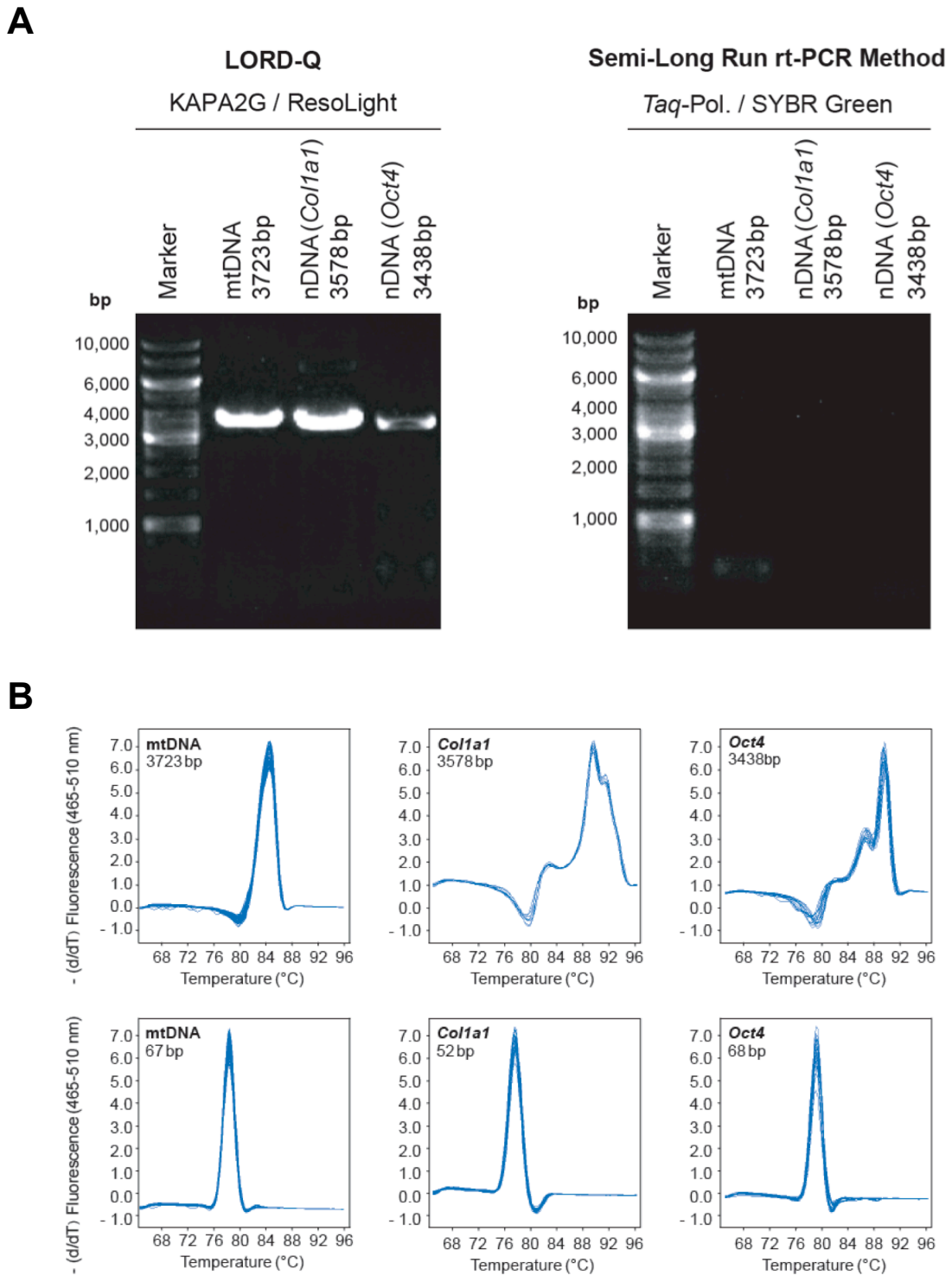

Fig. 4.9: LORD-Q enables amplification of >3 kb rtPCR products.

(**A**) Probes of three distinct loci of the human mitochondrial and nuclear genomes, respectively, were amplified without significant side product generation using the LORD-Q protocol and components as demonstrated by agarose gel electrophoresis (left). Application of a previously published semi-long run rtPCR method[105] did not yield bands of the expected size (right). (**B**) Melting curves of the long and associated short LORD-Q rtPCR products (n = 6 – 10 per fragment).

left), while the SLR method was unable to generate the respective PCR products employing the same primers (Fig. 4.9A, right).
In addition, a LORD-Q probe for the p53 locus (3075 bp) was established (data not shown). Melting curve analyses supported evidence for specific generation of the respective PCR products. The long fragments (Fig. 4.9B, upper charts) displayed elaborated melting profiles, which might be caused by individual melting temperatures of different segments of the PCR product (dependent on the respective GC content). In contrast, the small fragments melted „at once“, yielding a single, sharp melting curve peak (Fig. 4.9B, lower charts).

As these results ensured that the probes could be amplified in a reproducible manner and without significant side product generation, efficiencies of the individual primer pairs were determined by template dilution and regression analysis (see Table 3.1). Employing these experimentally determined efficiencies, relative lesion rates in genotoxin-treated samples could be calculated (see Methods section for the LORD-Q formula).
These results (depicted in Fig. 4.9) demonstrate that, in contrast to the SLR method, not only abundant mitochondrial DNA but also nDNA templates could be successfully amplified using the LORD-Q method.

Quantification of sublethal DNA damage and robustness of the method

Next, I examined whether the method was suitable to monitor the DNA damage incidence applied by exposure of cells to common genotoxins. For this purpose, Jurkat cells were incubated with different doses of bleomycin, UV-irradiated or cultured in the presence of etoposide or cisplatin (Fig. 4.10A-D). Whole-cell DNA was isolated following harvest and snap-freezing of the pellets. Subsequently, LORD-Q analysis was carried out. I found that bleomycin predominantly damages the mitochondrial genome (Fig. 4.10A), while the topoisomerase inhibitor etoposide and the chemotherapeutic drug cisplatin induced higher lesion rates in nDNA than in mtDNA (Fig. 4.10C,D). UV light caused similar damage incidence in both genomes with slightly elevated levels in mtDNA (Fig. 4.10B). These results show that LORD-Q enables both mtDNA and nDNA damage quantification for wide concentration ranges of genotoxic stimuli.
Following this proof of principle, the questions arose whether LORD-Q enabled DNA damage determination at physiologic conditions and whether storage, freezing and

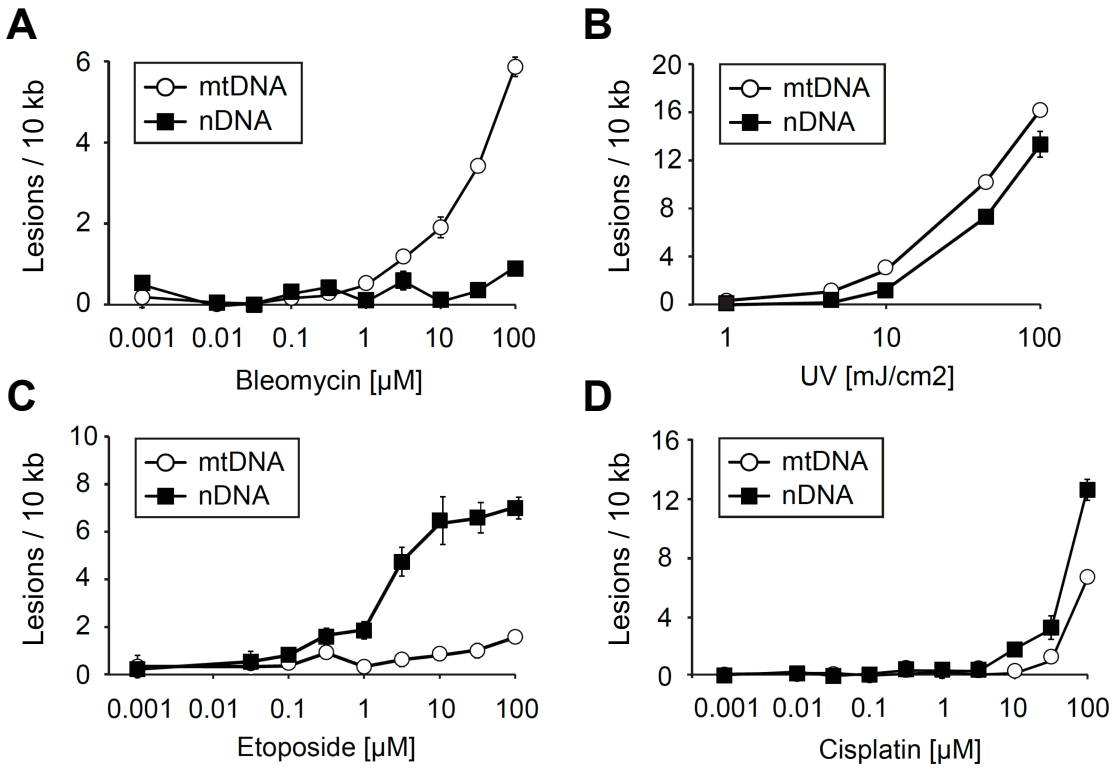

Fig. 4.10: LORD-Q enables accurate DNA damage quantification upon differential stimulation

Dose kinetics of common genotoxic stimuli. Jurkat cells were exposed to 1 nM – 100 µM of the indicated drugs or 1 – 100 mJ/cm^2 UVC radiation. After harvest, whole-cell DNA was isolated and analyzed by LORD-Q employing the *Col1a1* probe for nDNA damage analysis (n = 3, mean ± s.d. for all conditions). (**A**) Jurkat cells were incubated with the indicated doses of bleomycin for 20 min. In this cell type, bleomycin mainly damaged the mitochondrial genome. (**B**) Jurkat cells were exposed to UVC light (254 nm) and immediately harvested after treatment. MtDNA and nDNA proved roughly affected to a similar extent. (**C**) Cells were treated with etoposide and (**D**) cisplatin for 16 h. Both drugs mainly induced nDNA damage.

thawing of DNA samples biased the results of the assay (Fig. 4.11). To address these questions, Jurkat cells were treated with 100 nM to 100 µM bleomycin for 20 min. Then, half of the cells was immediately harvested and the DNA was isolated and analyzed for mtDNA damage by LORD-Q (Fig. 4.11A, filled squares). The remaining cells were kept under standard cell culture conditions for another 6 h, followed by harvest and staining for apoptosis (AnxV/PI co-staining). Flow cytometric analysis revealed that only high bleomycin concentrations decreased cellular viability, while medium doses (0.3 – 10 µM) did not cause cell death (Fig. 4.11A, open circles) but induced evident mtDNA damage.

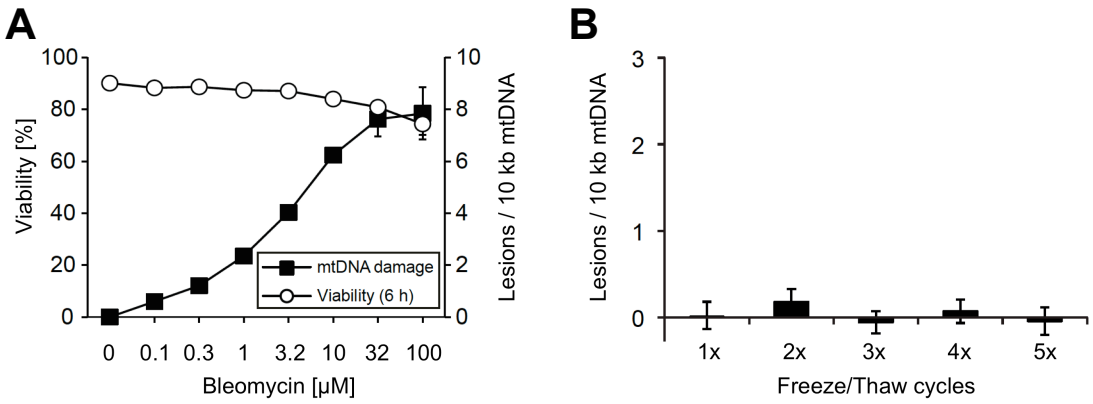

Fig. 4.11: Quantification of sublethal DNA damage and robustness of LORD-Q.

LORD-Q is robust and enables quantification of DNA damage at sublethal conditions. n = 3, mean ± s.d. (**A**) Jurkat cells were incubated with 100 nM – 100 µM bleomycin for 20 min at 37°C. Half of the cells was harvested immediately and mtDNA damage was determined (filled squares). The remaining cells were incubated under cell culture conditions and harvested after 6 h followed by apoptosis staining (FITC-AnxV/PI, open circles). $FITC^-/PI^-$ cells were deemed viable. (**B**) DNA of untreated Jurkat cells was repeatedly frozen and thawed (1x – 5x) before mtDNA damage was determined by LORD-Q.

In a second experiment, freshly isolated DNA derived from untreated Jurkat cells was repeatedly (1 - 5 x) frozen and thawed (F/T) and mtDNA damage was analyzed by LORD-Q. As depicted in Fig. 4.11B, even after several F/T cycles no change in DNA damage levels was observed.

It can thus be stated that LORD-Q enables DNA damage determination at sublethal genotoxic conditions while exhibiting high robustness and reproducibility in terms of freeze/thaw stability of the template DNA.

Determination of assay sensitivity by Receiver Operating Characteristic analyses

The next step for the characterization of LORD-Q was to compare its sensitivity with the SLR precursor technique. The detection limit of a method is reached, when e.g. genotoxically treated ("true positives") and control samples ("true negatives") can barely be distinguished. Receiver Operating Characteristic (ROC) analyses[219] represent a suitable tool to determine the sensitivity of an assay. Fig. 4.12A depicts a typical ROC experiment. In this approach, Jurkat cells were incubated with 100, 10 or 1 nM bleomycin or left untreated (n = 15 per concentration). After 30 min of incubation, the cells were harvested, and whole-cell DNA was isolated and analyzed by LORD-Q employing the long and short mtDNA probe. ΔC_p values (differences

between C_p values of long and short fragment) of true positive samples were plotted against ΔC_p values of true negative samples. Results are expressed as area under the curve (AUC) values, which reach a value of 1 for perfect discrimination and 0.5 if true and false positive or negative events are randomly "recognized" (see black reference line in Fig. 4.12A). As illustrated, LORD-Q perfectly distinguished between treated and untreated cells for samples incubated with 100 nM bleomycin (Fig. 4.12A, red line, AUC = 1.000), while the AUC value for 10 nM bleomycin was lower (green line). In contrast, samples of cells treated with 1 nM bleomycin (blue line) were hardly distinguishable from untreated controls.

In a set of four independent ROC analyses, n = 15 samples per condition and experiment were analyzed both by LORD-Q and semi-long run method. As shown in Fig. 4.12B, both methods failed to discriminate between controls and samples treated with 1 nM bleomycin (AUC = 0.5). In contrast, both assays perfectly distinguished between controls and samples incubated with 2.5 µM of the drug (AUC = 1.0). However, at 100 nM and 10 nM bleomycin, LORD-Q reached AUC values of 1.000 and 0.934, respectively, while the SYBR Green-based semi-long run method scored 0.901 (100 nM) and 0.5 (10 nM; Fig. 4.12B).
Since at a concentration of 10 nM bleomycin LORD-Q reached an AUC value that was higher than the AUC value of the SLR method at 100 nM bleomycin, LORD-Q exhibited a detection limit of 10 nM bleomycin. Furthermore, LORD-Q proved about one order of magnitude more sensitive compared to the semi-long run rtPCR method. Fig. 4.12C displays the calculated lesion rate as determined by LORD-Q. In accordance with Fig. 4.12B, DNA damage levels in samples treated with very low concentrations of bleomycin could be significantly distinguished from untreated controls (P = 1.2E-6 for samples treated with 10 nM bleomycin). Thus, the detection limit of LORD-Q is about 0.3 lesions per 10 kb (Fig. 4.12C).

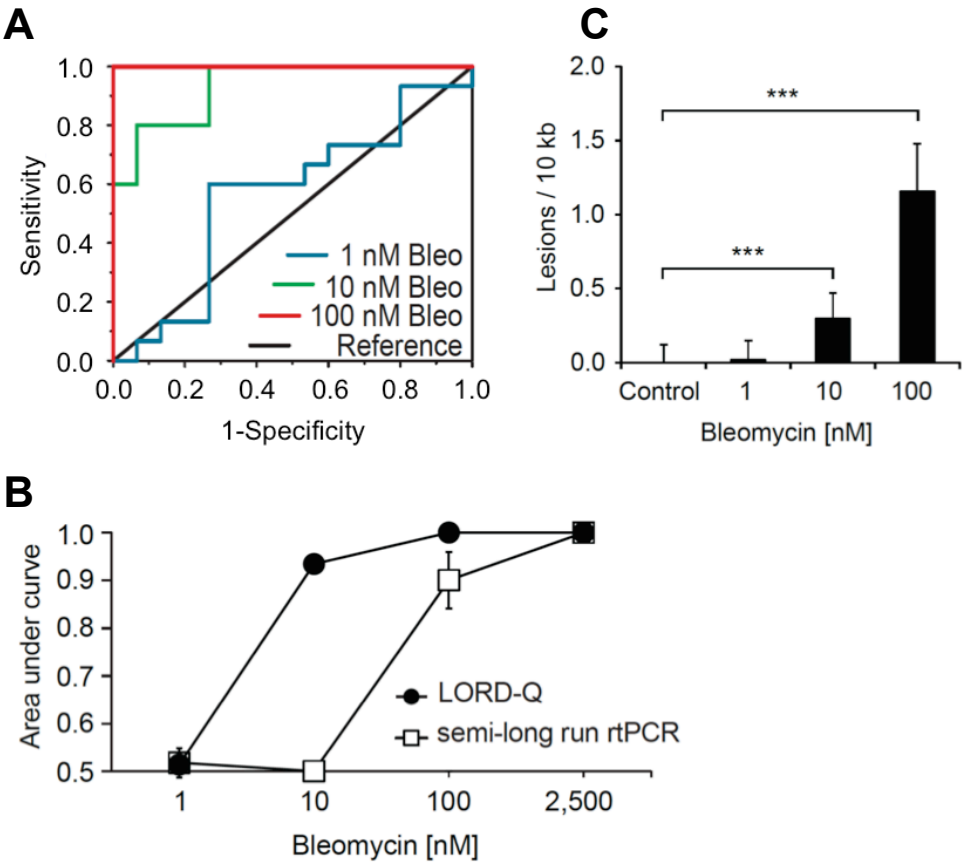

Fig. 4.12: Receiver Operating Characteristic (ROC) analyses of LORD-Q and semi-long run rtPCR method

The sensitivity of LORD-Q was determined by ROC analyses. Jurkat cells were stimulated with 1, 10, 100 or 2,500 nM bleomycin (Bleo) and incubated for 20 min at 37°C (n = 15 per condition and experiment, data are expressed as mean ± s.d.). Subsequently, DNA was isolated and both a long and nested short mtDNA fragment were analyzed by LORD-Q and the semi-long run rtPCR method. The delta between C_p(long fragment) and C_p(short fragment) was used for ROC calculations. Untreated Jurkat DNA served as control. Evaluations were carried out with OriginPro 8 software (OriginLab). (**A**) Representative ROC chart of a single LORD-Q experiment (n = 15 per bleomycin concentration). The black line represents random results (true positives and true negatives cannot be distinguished). (**B**) Averaged areas under the curve (AUC) values of four independent experiments for LORD-Q and semi-long run rtPCR method plotted against bleomycin concentration. (**C**) MtDNA lesion rates according to (A) as determined by LORD-Q analysis. *** $p < 0.001$.

Specificity of LORD-Q

After determination of the assay sensitivity, the question arose which types of lesions were detectable by LORD-Q. Single and double strand breaks disjoint templates, so that (after melting of the DNA) polymerase-mediated synthesis of the

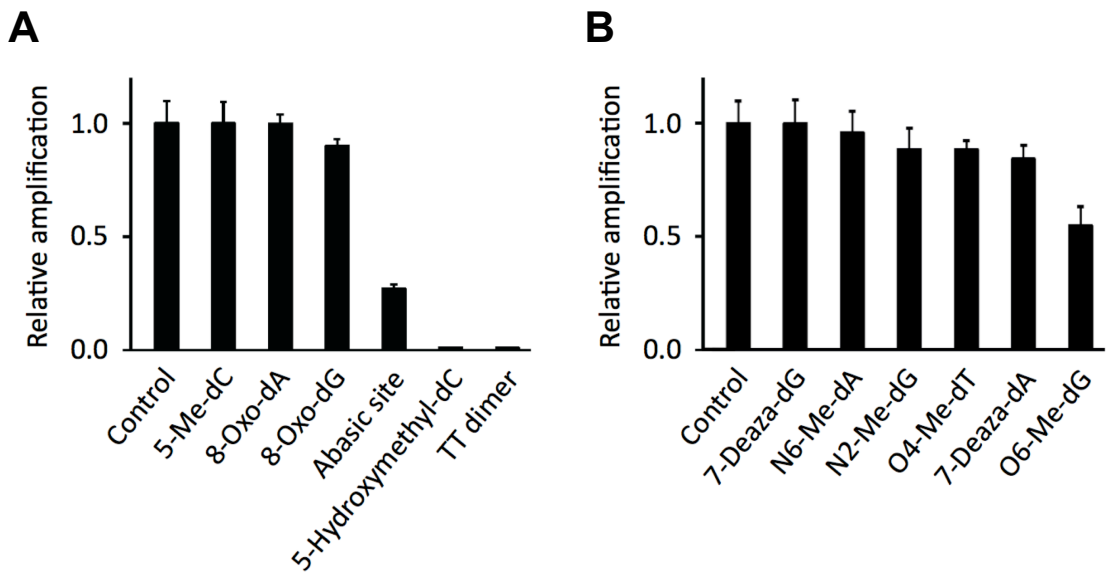

Fig. 4.13: LORD-Q detects abasic sites, thymine dimers and 5-hydroxymethyl-dC

Single modified nucleotides were inserted into synthetic oligonucleotides and their influence on the amplification rate (as determined by LORD-Q) was investigated. n = 3, mean ± s.d. (**A**) Common nucleotide / base modifications were examined by comparison of the amplification rate of the modified oligonucleotide with an unmodified control template. Abasic sites reduced amplification by roughly 75%, whereas 5-hydroxymethyl-dC and thymine dimers completely suppressed template duplication. (**B**) Rare / artificial alterations were investigated. With exception of O6-methyl-dG, none of the investigated modified bases clearly affected template amplification.

complementary strand is abrogated. Besides, several base or nucleotide modifications such as oxidative lesions or abasic sites might inhibit polymerase activity. To identify detectable alterations, synthetic ssDNA oligonucleotides were designed that carried a single modified base or nucleotide. Employing LORD-Q, the relative amplification rates of these oligonucleotides were determined. While 5-methyl-dC, 8-oxo-dG and 8-oxo-dG hardly impaired template amplification, abasic sites reduced relative amplification by 75% (Fig. 4.13A). Thymine dimers as well as the rare natural modification 5-hydroxymethyl-dC (5hmC) fully abrogated polymerase processivity (Fig. 4.13A). Scarce (e.g. N6-methyl-dA) or artificial (such as 7-deaza-dG) modifications did not alter template amplification, with exception of O6-methyl-dG (Fig. 4.13B). Hence, LORD-Q detects strand breaks, abasic sites, thymine dimers and 5hmC. The latter is involved in epigenetics of pluripotent stem cells[230], although its role is yet poorly understood. Thymine dimers are the predominant UV-induced photoadduct of neighbored pyrimidines, while abasic sites occur spontaneously (by hydrolysis of the N-glycosidic bond which connects deoxyribose and base within

nucleotides) or during base excision repair. Except under UV conditions, strand breaks might therefore constitute the sole detected modifications. Defined adaptions of the LORD-Q methodology could, however, extend the repertoire of recognized modifications (see below).

Impact of culturing conditions on DNA damage

Next, it was to be elucidated whether LORD-Q was able to monitor the impact of environmental and culturing conditions on DNA damage. To address this question, Jurkat cells were UV-irradiated in the presence or absence of 400 µM vitamin C (ascorbic acid) either in culture medium or serum-free medium (Fig. 4.14.A). The presence of serum significantly reduced both mitochondrial and nuclear UV-induced DNA damage. Likewise, vitamin C partially protected the cells from UV-induced DNA lesions in a statistically significant manner (Fig. 4.14A). As described above, a substantial part of DNA damage triggered by UV light is caused by an indirect mechanism: UV quants exhibit enough energy to homolytically cleave various chemical bonds, thereby generating ROS and other reactive substances that, in a second reaction, oxidatively alter DNA. As side reactions, single and, to a minor extent, double strand breaks are induced which can then contribute to the lesions detected by LORD-Q. Vitamin C is an antioxidant which is able to scavenge ROS and might, in this way, protect DNA from UV-induced DNA damage.
In non-irradiated cells, however, vitamin C slightly (though significantly) induced DNA damage itself (Fig. 4.14A, left). This surprising finding was confirmed by vitamin C titration studies (Fig. 4.14B). Vitamin C reduced UV-induced DNA damage in both mtDNA and nDNA at concentrations between 100 µM and 1 mM. Anyhow, the same amounts of vitamin C dose-dependently induced DNA damage in non-irradiated Jurkat cells (Fig. 4.14B). Concentrations between 300 µM and 1 mM vitamin C almost completely suppressed UV-induced DNA damage, since the difference of lesion rates between irradiated and non-irradiated cells was marginal but still present. Electrocyclic reactions such as thymine dimer formation can not be suppressed by antioxidants (thymine dimers are detectable by LORD-Q, see Fig. 4.13A). Thus, these results suggest that thymine dimers constitute merely a small fraction of the detected lesions, while most recognized events are strand breaks caused by UV-generated ROS. Further evidence for this hypothesis is provided below, see Fig. 4.14.

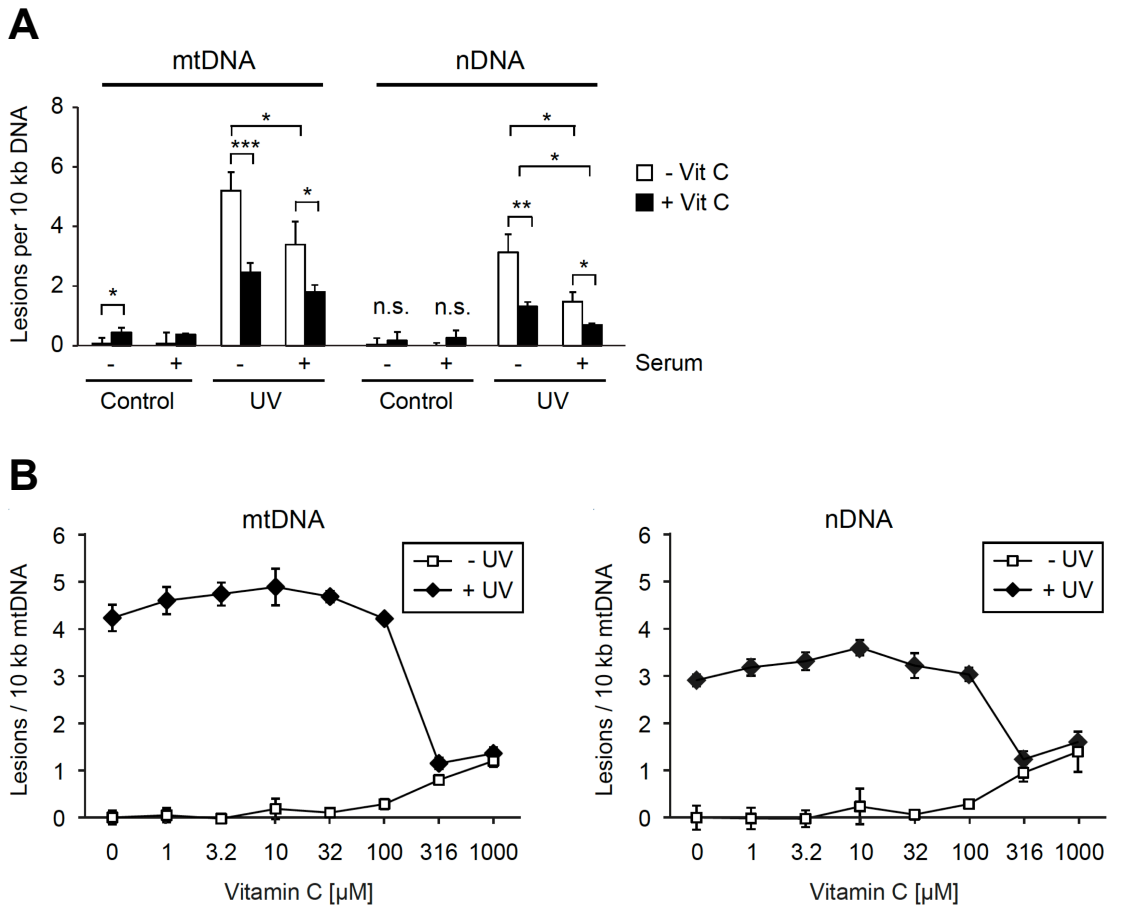

Fig. 4.14: Impact of environmental conditions on DNA damage rates.

Influence of environmental conditions on UV-mediated DNA damage as determined by LORD-Q. n = 3, mean ± s.d. (**A**) Jurkat cells in culturing medium (containing 10% FCS) or in serum-free medium were UV-irradiated (10 mJ/cm^2). In addition, half of the samples was supplemented with 500 µM vitamin C. n = 3. (**B**) Jurkat cells in serum-free medium complemented with different concentrations of vitamin C were UV-irradiated (filled checks) or not exposed to UV (open squares) and both mtDNA (left) and nDNA (right) damage rates were determined by LORD-Q analysis. * $p < 0.05$, ** $p < 0.01$, *** $p < 0.001$.

HiPS cells acquire less DNA damage and remove lesions faster than fibroblasts

After characterizing the LORD-Q method in terms of sensitivity, specificity and applicability at sublethal conditions, potential differences between human iPS cells and fibroblasts concerning DNA damage acquisition (so-called initial damage) and removal of lesions by DNA repair were examined. K7 iPS cells and isogenic fibroblasts were incubated with 10 µM bleomycin or irradiated with 10 mJ/cm^2 UV light in serum-free medium and the DNA was analyzed by LORD-Q. Fibroblasts exhibited significantly higher lesions rates upon exposure to both stimuli in mtDNA and nDNA (Fig. 4.15A). This was surprising, as human iPS cells were shown to be

highly susceptible to bleomycin-induced apoptosis (Fig. 4.4D). Accordingly, such resistance to genotoxic stimuli in terms of DNA damage acquisition was not to be expected. Obviously iPS cells acquire less lesions, but quickly undergo apoptosis upon DSB induction, whereas fibroblasts exhibit high DNA lesion rates after stimulation, but little apoptosis induction.

For comparative examination of DNA repair capacities, iPS cells and fibroblasts were stimulated with bleomycin and UV doses that induced similar lesion frequency in both cell types (Fig. 4.15B, white bars). A second set of samples was allowed to recover after stimulation and was harvested two hours after bleomycin or UV treatment, respectively (Fig. 4.15B, black bars). Following recovery, iPS cells possessed reduced mtDNA damage rates, whereas fibroblasts did not repair DNA damage (in the case of UV stimulation) or repaired lesions to a lesser extent (in the case of bleomycin stimulation) during recovery. These results suggest that human iPS cells remove DNA damage faster than isogenic fibroblasts. This is in accordance with upregulated DNA repair mechanisms in iPS cells as reported by others[19,210].

Transcriptionally active genes are more vulnerable to genotoxic events compared to inactive loci

In contrast to global DNA damage detection methods, LORD-Q is site-specific. In order to exploit this property, gene-specific DNA damage rates were examined. Transcriptionally active loci mostly exhibit an opened euchromatin structure, while permanently silenced genes often lie within tightly packed heterochromatin sequences**.** For this reason, DNA from euchromatin regions was assumed to be more accessible to radicals or genotoxic drugs compared to the sterically shielded heterochromatin DNA sequences. Genes that are active in iPS cells, but inactive in fibroblasts, and vice versa, were chosen in order to test this hypothesis. Collagen I (*Col1a1* locus) is extensively transcribed and translated in fibroblasts, while iPS cells but not fibroblasts express the stem cell marker OCT4. This was approved by relative expression analysis as shown in Fig. 4.16A. An open chromatin state was confirmed employing an anti-acetylated histone H3K9/K14 antibody and ChIP analysis. Q-PCR analysis of the ChIP-enriched loci showed that the *Oct4* locus was predominantly bound to acetylated histone H3 in iPS cells, while the *Col1a1* promoter was enriched in fibroblast samples (Fig. 4.16B). In accordance, bleomycin-treated fibroblasts exhibited a higher lesion incidence in the *Col1a1* than in the *Oct4* probe, yielding *Col1a1*:*Oct4* damage ratios > 1, whereas iPS cells possessed the reversed (*Col1a1*:*Oct4* damage ratios < 1) damage pattern (Fig. 4.16C).

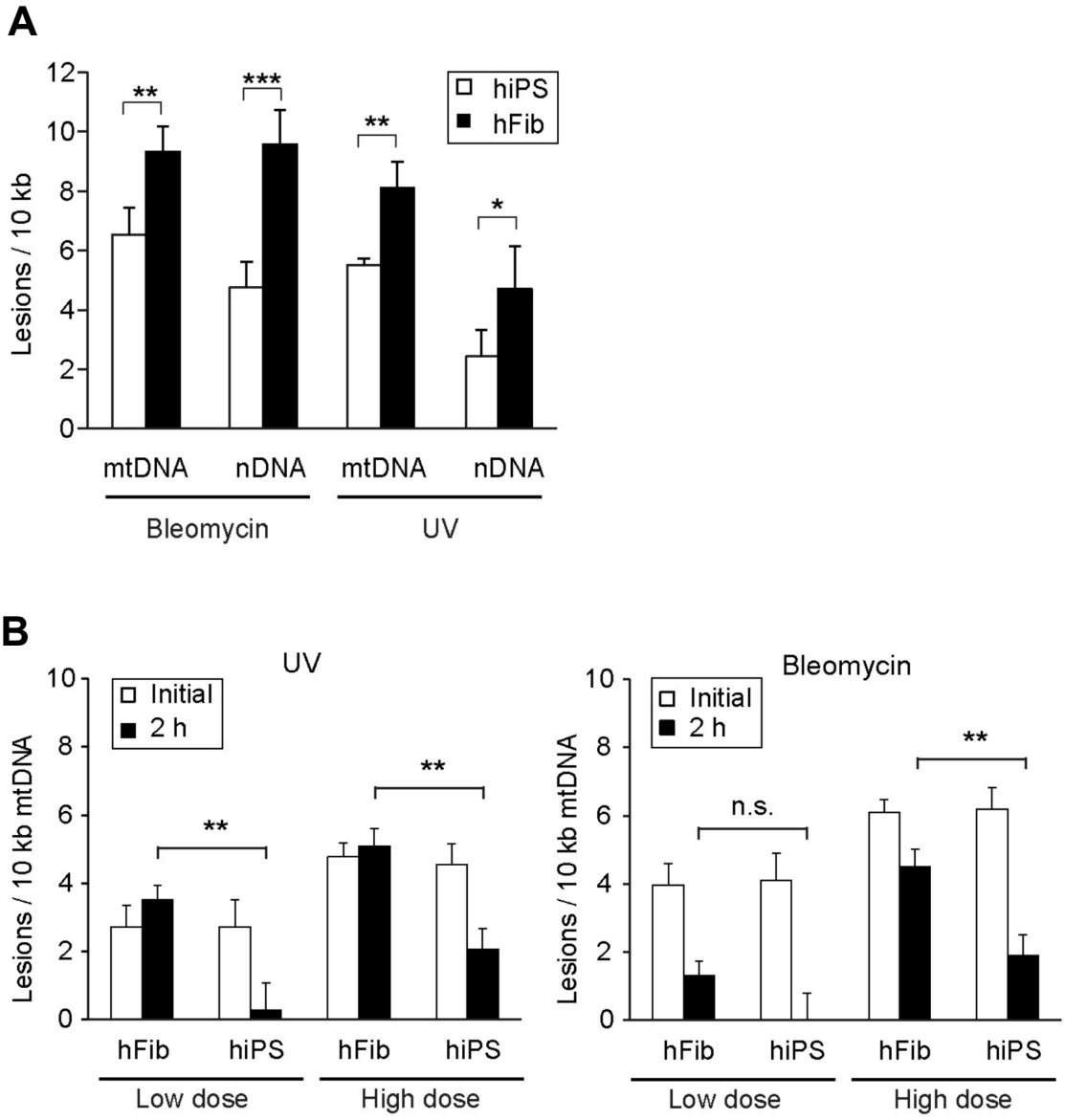

Fig. 4.15: IPS cells acquire lower DNA damage rates upon genotoxic exposure and remove mtDNA lesions faster than fibroblasts.

(**A**) Human K7 iPS cells and K7 fibroblasts were UV-irradiated (10 mJ/cm2) or incubated with bleomycin (10 µM, 20 min at 37°C) in serum-free medium. Following DNA isolation, mtDNA and nDNA damage rates were determined by LORD-Q. n = 3, mean± s.d. (**B**) K7 iPS cells and K7 fibroblasts were treated with different UV and bleomycin dosages that roughly induced similar initial mtDNA damage rates in both cell types (white bars; low dose: fibroblasts 4 mJ/cm^2 and 4 µM; high dose: 8 mJ/cm^2 and 8 µM; iPS cells: low dose 6 mJ/cm^2 and 6 µM; high dose: 10 mJ/cm^2 and 10 µM). Half of the samples was harvested and analyzed immediately after stimulation ("initial"), whereas the other half was allowed to recover (2 h at 37°C) before harvest. Cells were kept in serum-free medium throughout stimulation and in cell culture medium during recovery phase. n = 3, mean± s.d. * $p < 0.05$, ** $p < 0.01$, *** $p < 0.001$.

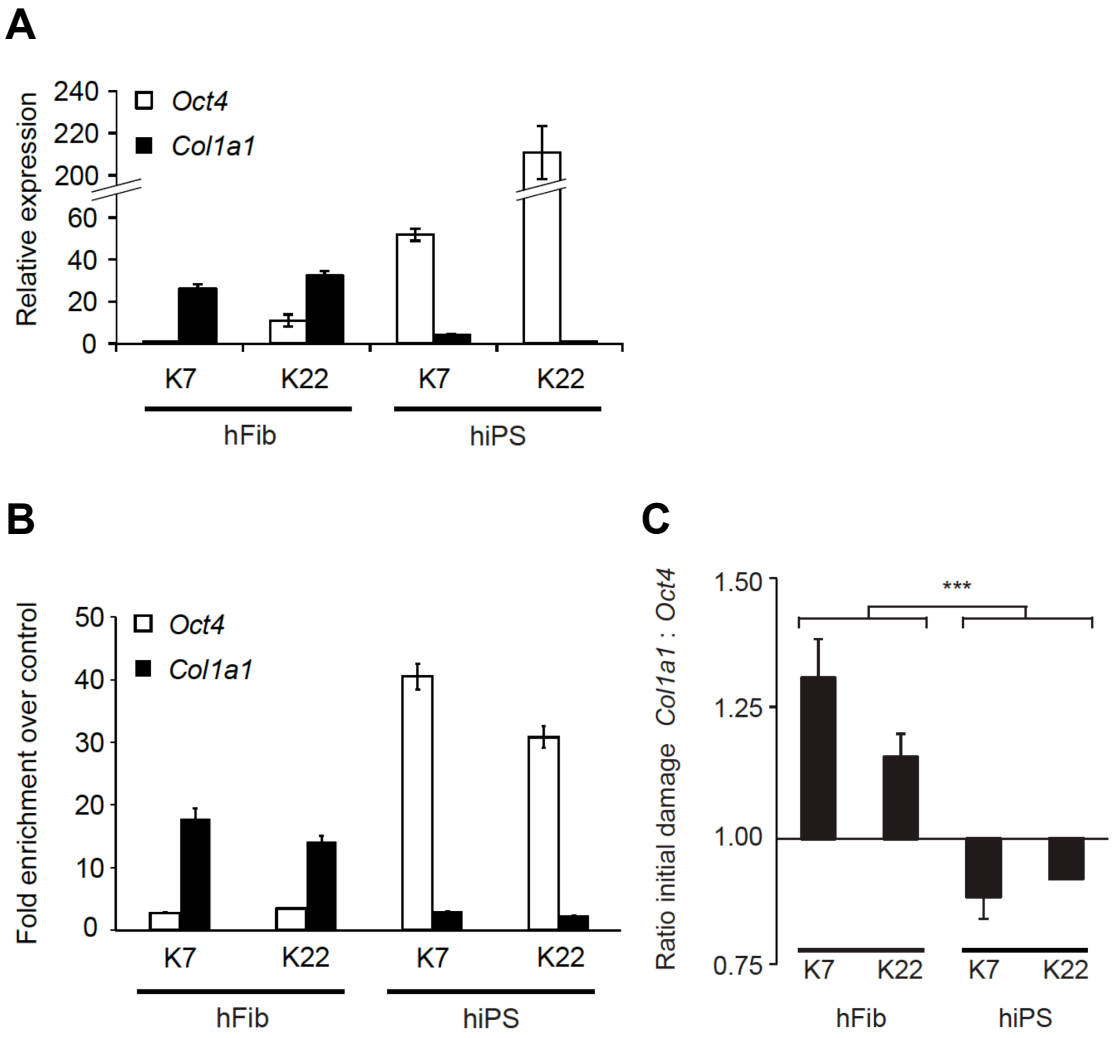

Fig. 4.16: Quantification of locus-specific lesion incidence.

(**A**) Expression analysis (reverse transcription PCR) of Oct4 and Col1a1 genes in K7 and K22 iPS cells and fibroblasts. Fibroblasts express collagen 1 (COL1A1), but not OCT4, while iPS cells possess the reversed transcription pattern. n = 3, mean± s.d. (**B**) Corresponding qPCR analysis of ChIP-enriched Oct4 and Col1a1 promoters employing an anti-acetylated histone H3K9/K14 antibody. Gene transcription as depicted in (A) corresponds to acetylation of the respective promoters in the two cell types. n = 3, mean± s.d. (**C**) DNA damage ratios of Col1a1 and Oct4 loci after stimulation with 10 µM bleomycin (20 min). DNA damage in both loci was determined by LORD-Q. In fibroblasts, Col1a1 exhibited a higher lesion incidence than Oct4, while in iPS cells the damage pattern was reciprocal. n = 6, mean± s.d. * P<0.05, ** P<0.01 and *** P<0.001.

Basal DNA damage in cell lines and extension of the methodology

Cells constantly face spontaneous DNA damage which is normally repaired. As lesions continuously emerge and are removed, the question arises whether a cell

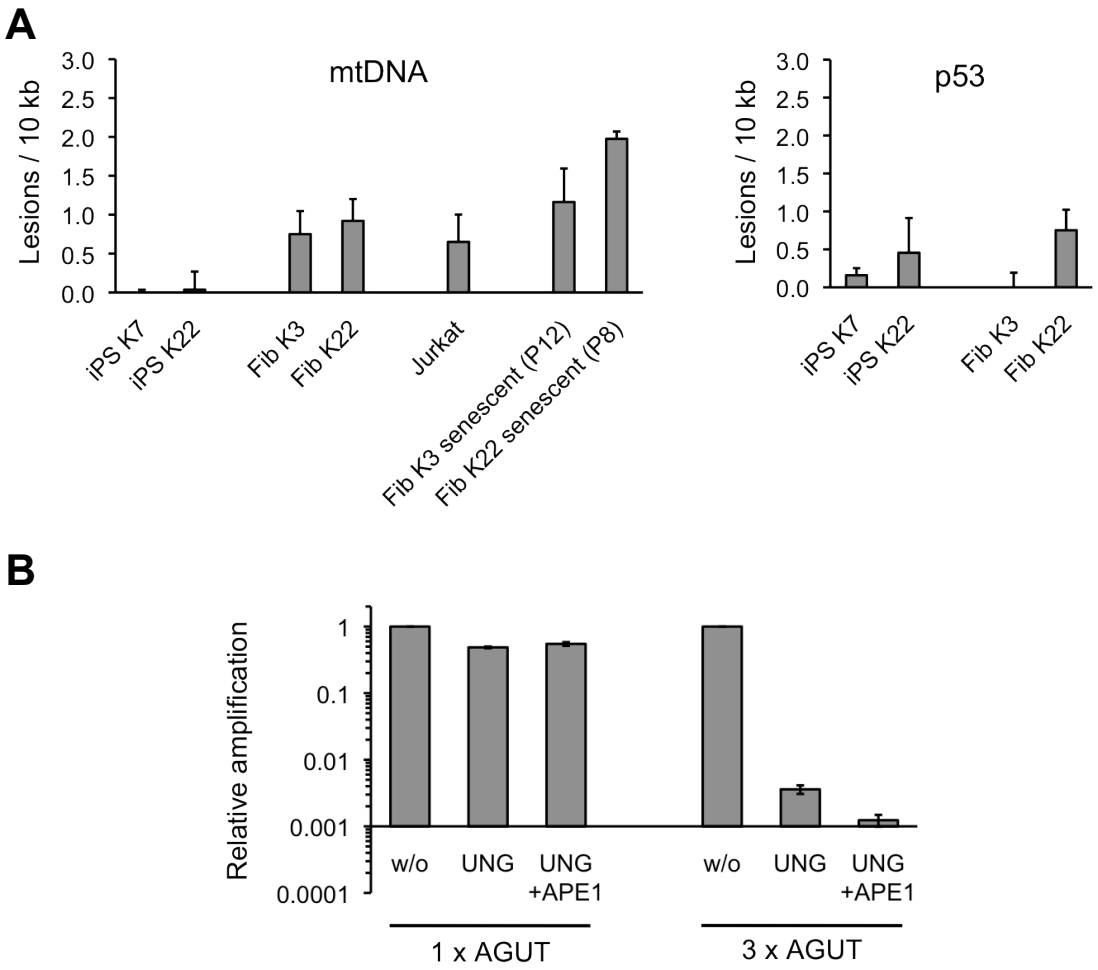

Fig. 4.17: Further applications of LORD-Q: Basal damage determination and extension of the methodology.

(**A**) Untreated iPS cells, fibroblasts (early passage or senescent upon continued cultivation) and Jurkat cells were harvested and compared in terms of basal DNA damage levels. In mtDNA (left), K7 iPS cells exhibited the lowest damage incidence and served as reference, while in nDNA (p53 locus, right) Fib K3 were least damaged and chosen as reference. n = 3, mean± s.d. (**B**) One (left) or three (right) uracil-containing tetranucleotide motifs (AGUT) were inserted into synthetic oligonucleotides. Uracil does not interfere with KAPA2G (as confirmed by insertion of one and three AGCT motifs, data not shown), but digestion of the templates with uracil N-glycosylase (UNG) and apurinic/apyrimidinic endonuclease 1 (APE1) strongly reduced the amplification of the template. n = 4, mean± s.d.

type-specific "basal damage" rate could be determined which mirrors a steady-state equilibrium of DNA damage acquisition and removal. To examine such basal damage rates, untreated human iPS cells, Jurkat cells and either dividing or senescent fibroblasts were harvested and analyzed by LORD-Q. As pointed out in Fig. 4.17A, iPS cells exhibited the lowest mtDNA damage rates, followed by dividing fibroblasts

and Jurkat cells, whereas for senescent fibroblasts the highest lesion frequency was detected. In nDNA (*p53* locus), however, DNA damage rates in fibroblasts did not exceed that in hiPS cells, pointing to especially low damage rates in iPS cell mtDNA (Fig. 4.17A). Obviously, LORD-Q can be employed to characterize basal DNA damage levels in primary cells and cell lines. This is important as malignancy and senescence are often linked to elevated DNA damage and chromosomal aberration incidence. This association may be further examined employing LORD-Q.

The specificity of LORD-Q is, as described above, restricted to strand breaks and recognition of certain nucleotide modifications. However, indirect oxidative lesions such as 8-oxo-dG constitute a major part of modifications that are acquired upon exposure to different genotoxic stimuli (e.g. UV radiation and hydrogen peroxide). LORD-Q proved incapable to detect such lesions. This is, for most applications, not disadvantageous since strand breaks occur as side products of most genotoxic treatments in a dose-dependent manner and can subsequently be analyzed. Nonetheless, if an individual scientific problem demands the quantification of a specific modification, the LORD-Q methodology might be appropriately extended.
One example of such extension is the detection of uracil. In somatic hypermutation[61] and class switch recombination[60] activation-induced deaminase deaminates cytosines to uracil which finally leads to mutations, thereby e.g. enlarging antibody diversity or enabling class switch. Uracil does not interfere with KAPA2G, but abasic sites reduce the relative amplification of the respective template (see Fig. 4.13A). Excision of uracil by uracil N-glycosylase (UNG), which is followed by backbone hydrolysis carried out by apurinic/apyrimidinic endonuclease-1 (APE1), enables recognition of the former uracil site by LORD-Q (Fig. 4.17B). In the experimental setup, one or three AGUT motifs were introduced into the control oligonucleotide, followed by digestion with UNG alone or UNG plus APE1 in combination. Relative amplification was reduced to about 50% for one inserted AGUT motif. In the case of 3 x AGUT, UNG digestion reduced the amplification rate to roughly 0.4%, while APE1 co-digestion further lowered the remaining amount of intact template (Fig. 4.17B).
Equal procedures may be carried out for other glycosylases that specifically excise modified bases, e.g. OGG1 (which removes 8-oxo-dG). LORD-Q can therefore serve as a platform for individual adaptions dependent on the specific scientific or experimental demand.

In order to generate a suitable tool for DNA damage analysis applicable to various conditions, high sample numbers and different cell types, LORD-Q was developed

and extensively characterized. LORD-Q is suitable for high-throughput analyses, accurate and specific for defined nucleotide modifications. Application of LORD-Q revealed increased resistance of hiPS cells to DNA damage acquisition and rapid removal of mtDNA lesions compared to fibroblasts.

While several publications previously reported elevated DNA repair capacities in human PSCs[19,210], there is only scarce information about DNA-protective mechanisms in hiPS cells. The last section of the current chapter thus describes the efforts to identify such mechanisms.

4.4. DNA damage prevention in human iPS cells

Following exposure to DSB-inducing agents or radiation, human iPS cells proved hypersensitive and rapidly underwent apoptosis (see section 4.2). This finding led to the suggestion that iPS cells, which are continuously dividing, metabolically active cells, are vulnerable to genotoxic insults by acquisition of increased DNA lesion incidence. Astonishingly, employing a newly developed method to quantify DNA lesions, significantly reduced nDNA and mtDNA damage rates were detected in hiPS cells as compared to isogenic fibroblasts (Fig. 4.15A) and Jurkat cells. Besides, hiPS cells repaired DNA damage faster than fibroblasts (Fig. 4.15B).
Since iPS cells were immediately harvested after UV irradiation by scraping off the culture dishes and snap-freezing in liquid nitrogen, DNA repair could be discarded as explanation for low initial damage rates. Thus, the reason for damage resistance might be the presence of DNA-protective mechanisms in iPS cells.
A likely candidate for such protection was glutathione (GSH), which is the most important small molecule antioxidant in the cell. Dozens of enzymes (e.g. GSH-specific peroxidases, transferases and reductases) are involved in the GSH defense network. Besides, several antioxidative enzymes such as catalase, superoxide dismutases, peroxiredoxins and the thioredoxin system are involved in cellular defense against ROS and concomitant DNA damage.

I evaluated a microarray data set published by Liu *et al.*[231] to initially examine expression levels of genes involved in glutathione metabolism, "non-GSH" antioxidative defense mechanisms and factors associated with DNA repair. Fig. 4.18 shows a heat map that mirrors the relative expression levels of these three gene clusters in hES H1 cells (left column), differentiated hES H1 cells (middle column) and human dermal fibroblasts (named "ATCC feeder"). Among the GSH-related genes, GSH peroxidase GPX2, glutathione transferases (GST) class alpha, glutamate-cysteine ligase catalytic subunit (GCLC) and GSH reductase (GSR) exhibited high expression levels compared to fibroblasts. Examining the cluster of other antioxidative factors, I found that iPS cells express high levels of peroxiredoxins 1 and 3. Moreover, some members of the thioredoxin protein family displayed higher expression levels than fibroblasts (Fig. 4.18). Surprisingly, among the top 50 hits of most upregulated genes in hiPS cells (compared to fibroblasts), apolipoproteins E and A-II (APOE and APOA2) were on positions 6 and 22, respectively. Both proteins have been associated with oxidative stress and neurodegenerative disorders in patients with defects in these apolipoproteins[232,233].

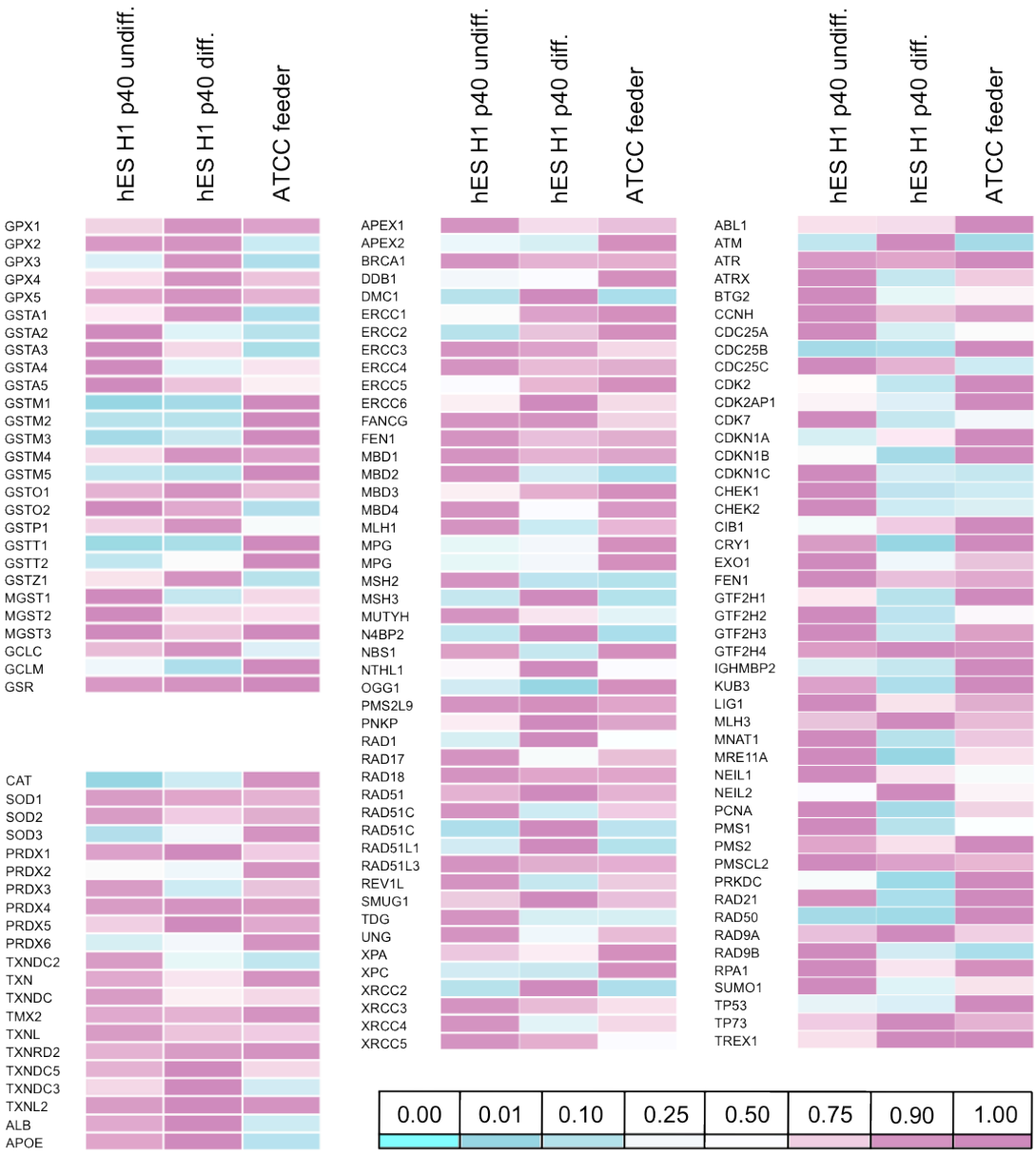

Fig. 4.18: Expression of DNA-protective factors in PSCs and fibroblasts.

Heat map (microarray data from Liu *et al.*[231]) of enzymes involved in glutathione metabolism (upper left panel), other factors of cellular antioxidative defense mechanisms (lower left panel) and factors involved in DNA damage signaling and repair (center and right panel). Relative expression in hES H1 cells (passage 40), differentiated hES H1 cells (passage 40) and human feeder fibroblasts (depicted ATCC feeder) is shown. Data are normalized on the highest expression level per gene. Abbreviations: diff.: differentiated; undiff.: undifferentiated.

Several antipoxidative factors and apolipoproteins are highly expressed in hiPS cells

In order to verify these *in silico* findings, expression analysis via RT-PCR was performed employing K3 and K22 fibroblasts and K7 and K22 iPS cells. Fig. 4.19

displays expression levels as relative to the geometric mean values of the reference genes β-actin (ACTB), GAPDH and δ-aminolevulinate synthase-1 (ALAS1) of the respective cells. Averaged levels of K7 and K22 hiPS cells are displayed, while averaged levels of K3 and K22 fibroblasts served as reference. With exception of GPX1, iPS cells expressed increased levels of all glutathione peroxidases compared to fibroblasts (Fig. 4.19A). GPX4 exhibited (besides GPX1) the highest absolute expression (data not shown), whereas GPX2 mRNA was hardly detectable in fibroblasts (Fig. 4.19A). Among GSTs, GSTA1 and GSTA2 were strongly expressed in iPS cells, but virtually not present in fibroblasts (Fig. 4.19B). Moreover, GSTO2, GSTZ1 and MGST2 were found to be elevated in iPS cells, while expression of GSTM2 and GSTM5 was decreased (Fig. 4.19B).

Astonishingly, all analyzed apolipoproteins exhibited high mRNA levels in hiPS cells, but were hardly detectable in fibroblasts (Fig. 4.19C). Similarly, most investigated apolipoprotein receptors (LDLR, VLDLR, LRP2 and the APOE receptor LRP8) were clearly increased in iPS cells (Fig. 4.19D). Finally, all peroxiredoxins were found to be clearly stronger expressed in iPS cells than in fibroblasts. PRDX1 was the only gene of the data set that, exclusively in iPS cells, exhibited an mRNA level that exceeded the averaged mRNA level of the reference genes (data not shown). This finding hints at extensive translation of this important peroxide-detoxifying enzyme. In contrast, secretory superoxide dismutase-3 (SOD3) and catalase (CAT) were significantly downregulated in iPS cells compared to fibroblasts (Fig. 4.19E).

HiPS cells exhibit high GSH levels which can be chemically depleted

GSH is involved in a well-understood network of antioxidative defense factors and its cellular levels can be determined and manipulated by previously published methods. It has been implicated in DNA damage prevention in numerous studies[97,234]. Therefore, the correlation between GSH concentrations, levels of GSH-converting enzymes and DNA damage was examined.

In a first approach total cellular glutathione (GSx) concentrations comprising reduced GSH and its oxidized form, glutathione disulfide (GSSG), were determined. For this purpose, a colorimetric assay originally described by Tietze[220] was carried out to investigate GSx levels in cell lysates. The resulting concentrations were normalized on cellular protein content as determined by BCA assay (see Methods section for details). As depicted in Fig. 4.20A, iPS cells featured significantly higher GSx levels than fibroblasts ($P<0.001$), even though clonal differences were observed. The

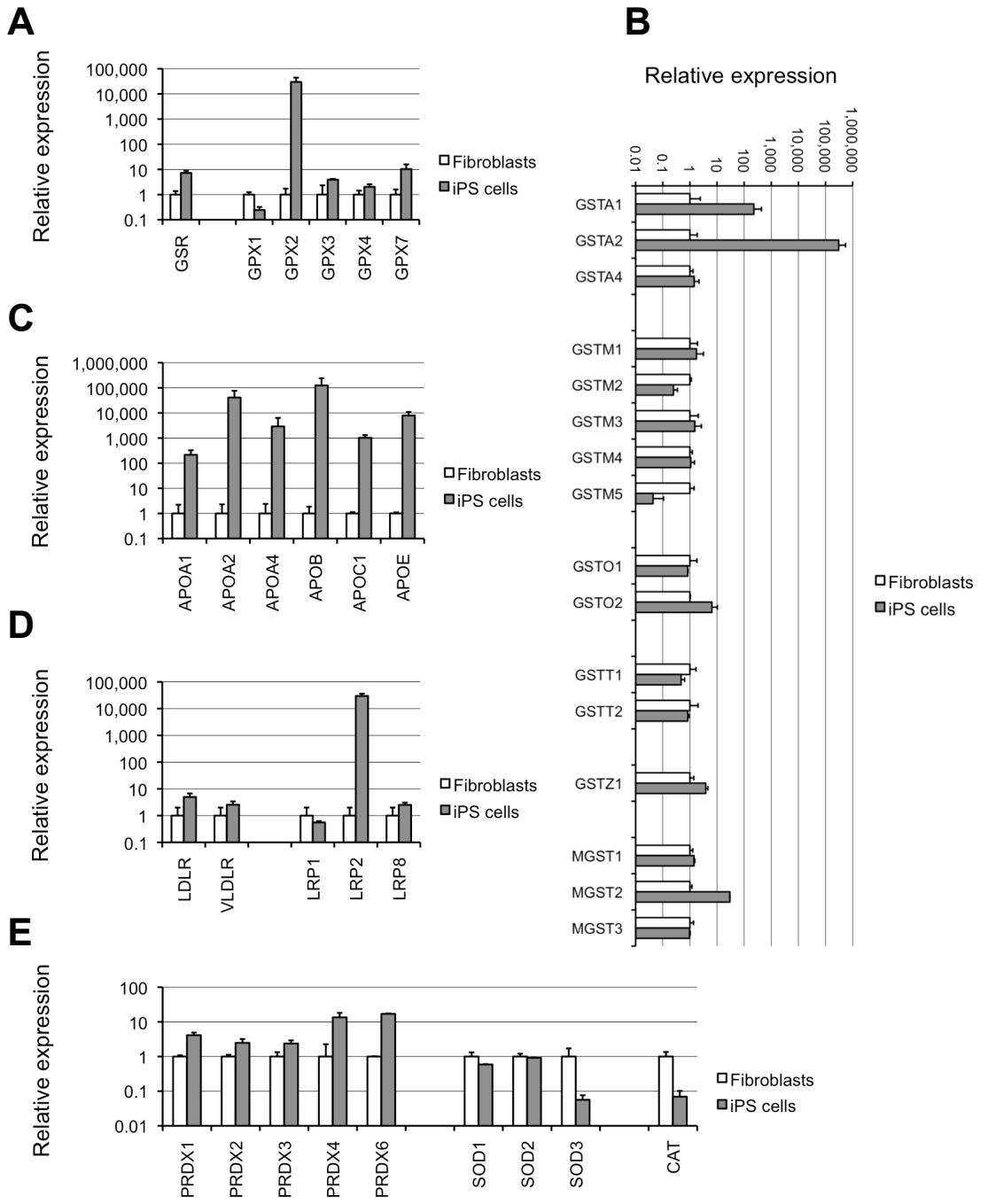

Fig. 4.19: Representative expression analysis of genes involved in antioxidative defense.

Data are displayed as relative to geometrical mean of ACTB, ALAS1 and GAPDH mRNA levels. Depicted values are means of K7 and K22 hiPS cells or means of K3 and K22 fibroblasts (± s.d.). A representative set of data is shown. (**A**) Expression of GSH reductase (GSR) and GSH peroxidases (GPXs). GPX2 is expressed in iPS cells, but only marginally present in fibroblasts. (**B**) mRNA levels of GSH transferases (GSTs) demonstrate that GSTA2 is exclusively expressed in iPS cells. (**C**) Apolipoproteins and (**D**) apolipoprotein receptors are predominantly expressed in iPS cells. (**E**) Expression of peroxiredoxins (PRDXs), superoxide dismutases (SODs) and catalase (CAT). PRDXs exhibit elevated expression in hiPS cells, while fibroblasts display higher levels of SOD1, SOD3 and CAT.

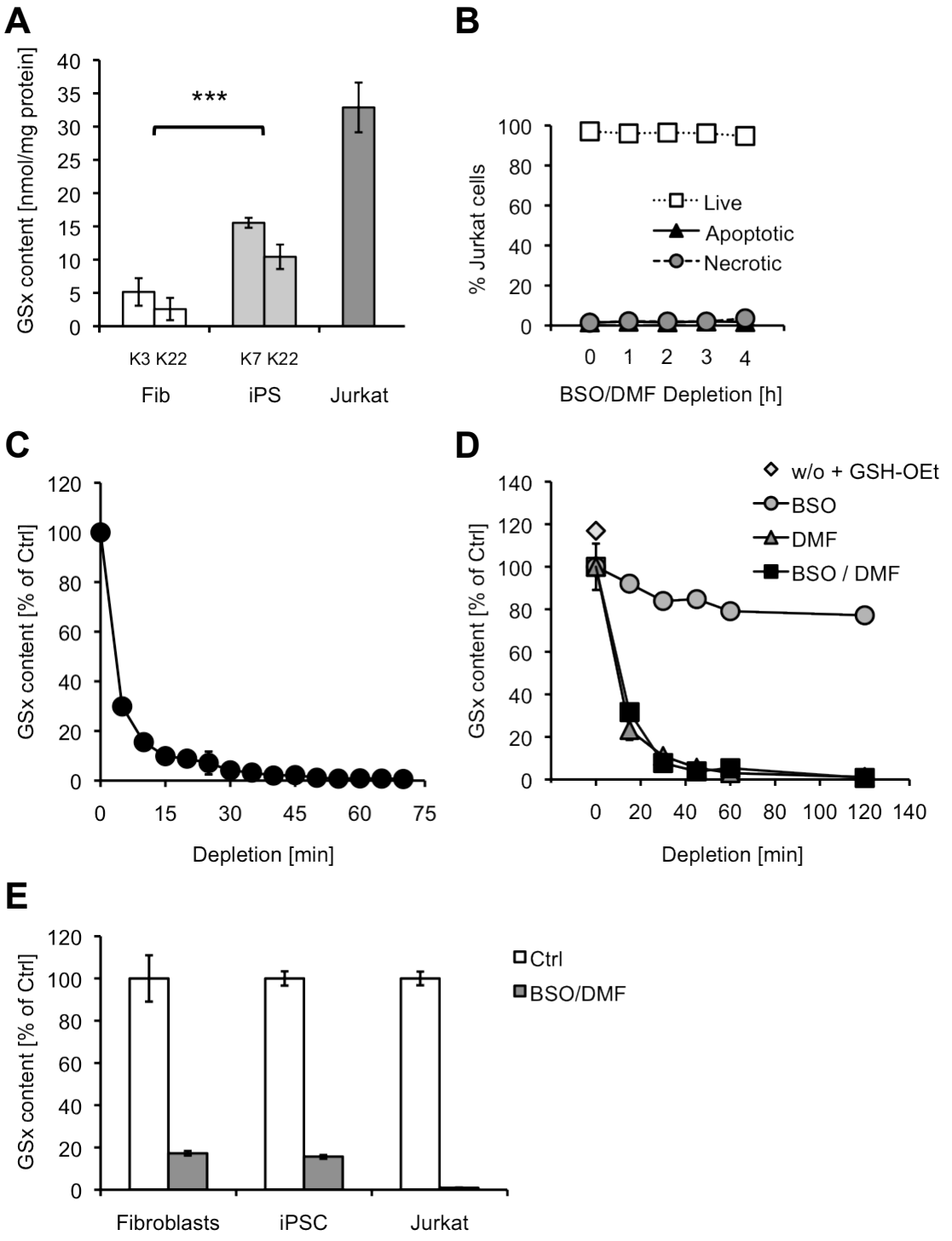

Fig. 4.20: GSx levels and glutathione depletion in human fibroblasts, iPS and Jurkat cells.

(**A**) Total glutathione (c(GSx) = c(GSH) + 2 x c(GSSG)) content in human iPS cell lines, primary fibroblasts and Jurkat cells n = 3 – 8, mean ± s.d. (**B**) Analysis of apoptosis and necrosis in Jurkat cells upon GSH depletion. Cells were depleted 0 – 4 h by incubation with 100 µM BSO and 100 µM DMF, followed by FITC-annexin V / propidium iodide co-staining and FACS analysis. A representative experiment is depicted. (**C**) Virtually complete GSH depletion of Jurkat cells upon BSO/DMF treatment occurred within 60 min of incubation with BSO/DMF. A representative experiment (samples in triplicate) is shown. (**D**) Comparative

depletion approaches employing treatment of Jurkat cells with 100 µM BSO alone, 100 µM DMF alone or BSO/DMF (each 100 µM) co-incubation revealed that depletion is dependent on the presence of DMF, whereas BSO alone only slightly decreased cellular GSx levels. A representative experiment is shown. (**E**) Human iPS cells (K7, K22; averaged values), fibroblasts (K3, K22; averaged values) and Jurkat cells displayed less than 20% of initial cellular GSx levels after 60 min of depletion with 100 µM BSO/DMF. n = 3, mean ± s.d. Abbreviations: BSO: buthionine sulfoximine; DMF: dimethyl fumarate; GSH-OEt: glutathione O-ethyl ester. *** P<0.001.

control Jurkat lymphoma cell line exhibited extraordinary high GSx levels (Fig. 4.20A). This is in accordance with previous reports suggesting very high GSx levels in several tumor cell lines[235].

To investigate whether GSx levels correlated with DNA damage, a previously published depletion method was employed. Cells were treated with a final concentration of 100 µM buthionine sulfoximine (BSO) and 100 µM dimethyl fumarate (DMF). BSO specifically suppresses GSH synthesis by inhibition of glutamate-cysteine ligase (GCL)[236], which constitutes the rate-limiting enzyme of GSH synthesis[90]. Cells excrete DMF by nucleophilic addition of GSH and secretion of the adduct, thereby depleting the intracellular GSH pool[237]. However, BSO/DMF-mediated GSH depletion has been referred to as cytotoxic[236]. For this reason, Jurkat cells were depleted up to 4 h employing BSO/DMF and cell death was determined by FITC-annexin V / propidium iodide staining and flow cytometric analysis. Within 4 h, no increase in cell death was detectable (Fig. 4.20B).

The original protocol suggested that GSx depletion occurred during 4 h[236]. However, GSx levels in Jurkat cells were roughly reduced by 99% already within 60 min (Fig. 4.20C). Surprisingly, DMF alone was able to induce depletion, while BSO alone only slightly decreased intracellular GSx levels (Fig. 4.20D). The cell-permeable GSH analog glutathione O-ethyl ester (GSH-OEt) proved capable to enhance intracellular GSH level in untreated cells (Fig. 4.20D) and to partially rescue BSO/DMF-mediated depletion (30-70% GSx compared to untreated cells after 60 min of GSH/BSO+GSH-OEt co-incubation; data not shown). Fig. 4.20E demonstrates that, similar to Jurkat cells, fibroblasts and iPS cells could be GSx-depleted to less than 20% of initial levels by BSO/DMF treatment (100 µM each, 60 min).

GSH depletion increases DNA lesion incidence in genotoxin-exposed fibroblasts and Jurkat cells, but not in hiPS cells

Nevertheless, GSx-depleted iPS cells failed to exhibit a higher DNA lesion incidence

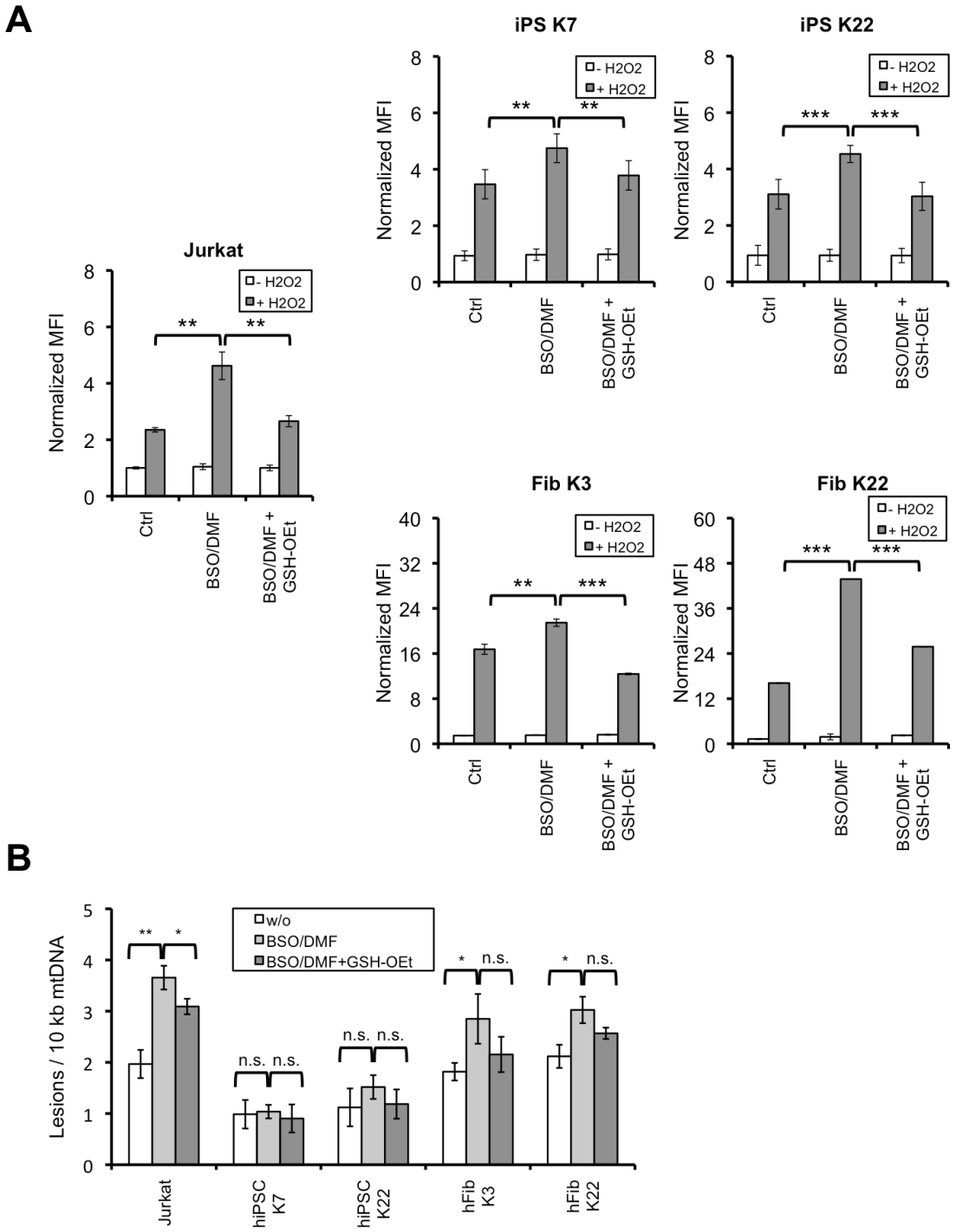

Fig. 4.21: Correlation between cellular GSH depletion, ROS generation and DNA damage acquisition in Jurkat cells, fibroblasts and iPS cells.

Jurkat cells, fibroblasts and iPS cells were GSH-depleted by 100 µM BSO / 100 µM DMF (±2 mM GSH-OEt) co-incubation for 60 min, stained with DHR123 and subsequently treated with 5 mM H_2O_2 for 5 min. at 37°C. Samples were split for ROS level and DNA damage analysis. n = 3, mean ± s. d. (**A**) Flow cytometric analysis of ROS levels in DHR123-stained cells prior and after treatment with of H_2O_2 . All cell types exhibited clearly increased fluorescence upon H_2O_2 treatment whereas GSH-depletion itself did not increase MFI values. This effect was significantly amplified in GSH-depleted samples and reversed by GSH-OEt co-incubation

during depletion. MFI values were normalized on untreated control samples of the respective cell type. (**B**) Corresponding mtDNA lesion rates in Jurkat cells, hiPS cells and fibroblasts as determined by LORD-Q. GSH-depleted Jurkat and fibroblast samples exhibited significantly increased mtDNA damage rates while GSH-OEt was able to partially rescue this phenotype. However, in iPS cells only marginal changes in mtDNA damage rates were observed upon depletion and/or rescue by GSH-OE. * P<0.05, ** P<0.01 and *** P<0.001. Abbreviations: Ctrl: control, n.s.: not significant, MFI: median of fluorescence intensity.

following UV irradiation (data not shown). This result posed the question whether genotoxic stimulation would, at least, induce similar intracellular stress (or ROS) levels in the different cell types. For instance, H_2O_2 itself exhibits moderate reactivity but it can give rise to formation of highly genotoxic ROS such as hydroxyl radicals during Fenton's reaction, which thereupon may cause DNA lesions[89].

A suitable method to quantify internal ROS levels is dihydrorhodamine 123 (DHR123) staining. ROS oxidize DHR123 to rhodamine 123 (R123)[238], which can be quantified in flow cytometric analyses. Jurkat, iPS cells and fibroblasts were left untreated, depleted by BSO/DMF treatment or rescued by parallel incubation with BSO/DMF and GSH-OEt. Subsequently, cells were stained with DHR123 and stimulated by application of H_2O_2 (5 mM, 5 min). As shown in Fig. 4.21A, both GSH depletion and rescue significantly elevated and decreased intracellular median of fluorescence intensity (MFI) levels. Both iPS and Jurkat cells exhibited a 2- to 5-fold MFI increase upon hydrogen peroxide stimulation. Contrariwise, fibroblasts featured a roughly 12- to 40-fold increase (depending on the GSx content), indicating a generally higher susceptibility to oxidative stress (Fig. 4.21A).

However, on the DNA damage level Jurkat and fibroblasts exhibited a similar and significant increase of H_2O_2-induced mtDNA damage following GSx depletion, which was partially reversed by GSH-OEt co-incubation (Fig. 4.21B). This finding supports the assumption that GSH protects cells from ROS-induced DNA damage. Nonetheless GSx-depleted hiPS cells resisted H_2O_2 and exhibited merely marginal increase in DNA damage rates (Fig. 4.21B).

Analogous results were obtained if the cells were stimulated by UV irradiation instead of H_2O_2 (data not shown). Summarized, these results indicate that, besides elevated GSx concentrations and increased levels of GSH-converting enzymes, iPS cells possess further mechanisms that prevent ROS-induced DNA damage upon genotoxic stimulation.

5. DISCUSSION

Human iPS cells represent a promising new cell type for future cell and tissue replacement therapies. Similar to other PSCs, however, iPSCs exhibit significant tumorigenic potential, which is a major roadblock for proximate practical applications. A second drawback for therapeutic use of iPS cells is provided by incomplete epigenetic reprogramming during their generation. For this reason, iPS cells constitute merely "ES-like" cells that retain an epigenetic memory of origin. Consequently, iPS cell lines are heterogeneous, and processing of external stimuli and regulation of signaling pathways in these cells is yet difficult to predict. However, such predictability of cellular "behavior" is a fundamental prerequisite for any therapeutic application.

The current project has shed some light on the cellular regulation of survival and apoptosis in iPS cells. A high sensitivity to genotoxic, and more precisely to DSB-inducing treatment was demonstrated. In order to link induction of apoptosis to preceding DNA lesion incidence in iPS cells, a simple and accurate high-throughput-compatible new method for DNA damage quantification (LORD-Q) was developed and characterized in terms of practical applicability, sensitivity and specificity. Application of this method for genotoxicity testing in various cell types revealed enhanced resistance of iPS cells to ROS-mediated DNA stress. Both mtDNA and nDNA lesion incidences were significantly lower in hiPS cells compared to isogenic fibroblasts and Jurkat cells. In addition, this resistance turned out to be independent of cellular glutathione levels, thus implicating the existence of additional DNA-protective mechanisms in hiPS cells.

This section discusses the current findings in detail and suggests a model that integrates the properties of hiPS cells and fibroblasts in terms of DNA damage prevention, DNA damage acquisition and the balance between apoptosis induction and survival.

5.1. Apoptosis in human iPS cells

HiPSCs are predominantly equipped with pro-apoptotic factors

It has previously been reported that hiPS cells prove hypersensitive to ionizing radiation-induced apoptosis[19]. However, a global analysis of the apoptotic response in hiPS cells upon treatment with intrinsic, extrinsic and ER stress pathway-stimulating agents was yet lacking.

Analysis of the overall expression of pro- and anti-apoptotic factors (see Fig. 4.7) implied a pro-apoptotic basic state of iPS cells. Thus, the mRNA levels of inhibitor of apoptosis proteins (IAPs) and anti-apoptotic Bcl-2 family members were found to be downregulated (with exception of survivin and MCL-1), while most pro-apoptotic factors (such as p53, BAK and BIM) exhibited increased expression in iPS cells. These results were largely confirmed on the protein level by clearly increased amounts of p53, BAK and BIM compared to the expression detected in isogenic fibroblasts. Therefore, a predominant "pro-apoptotic hegemony" of apoptosis-regulating factors was found in iPS cells.

ER stress induces apoptosis in hiPS cells

In accordance to the high expression levels of pro-apoptotic factors, most employed stimuli (except extrinsic death ligands, see below) provoked apoptosis in iPS cells (Fig. 4.4). Tunicamycin[42], which inhibits glycosylation of proteins, brefeldin A[43], which induces degradation of the Golgi apparatus and blocks protein sorting, and the SERCA inhibitor thapsigargin[42] are known ER-stress mediators. All these agents proved capable to induce potent apoptosis in iPS cells. This finding might be explained by the fact that human PSCs are considered immortal and undergo continuous cell division and, thus, require steady protein synthesis. If unfolded proteins accumulate or protein sorting is stalled, UPR pathways are activated and apoptosis occurs[36]. Accordingly, rapidly dividing Jurkat cells initiated massive apoptosis following incubation with ER stress inducers, whereas fibroblasts, which display moderate cell division rates and can transiently or permanently exit the cell cycle upon metabolic stress[239], revealed only moderate apoptosis rates upon ER stress induction.

HiPSCs do not initiate apoptosis if stimulated by extrinsic death ligands

In contrast to ER stress inducers, iPS cells proved resistant to extrinsic apoptotic stimuli such as FASL and TRAIL. This is notable, since fibroblasts, which resist most

other apoptotic stimuli, as well as Jurkat cells underwent apoptosis upon application of both death ligands. Consistent with this finding, the mRNA levels for FAS and most other death receptors were found to be remarkably decreased in iPS cells compared to fibroblasts. IPS cells might therefore resist extrinsic stimulation by immune cells that are a major source of death ligands. It might be speculated that this property of PSCs, which constitute the inner cell mass of the blastocyst-stage embryo[159], is associated with the immune privilege of the placenta and fetus[240]. Immune-privileged sites, comprising eye, brain, testes and uterus/fetus, suppress immune reactions and concomitant inflammation, which would otherwise lead to organ failure or abort of pregnancy. In this context, resistance of embryonic cells to apoptotic stimulation by death ligands expressed on the surface of immune cells appears consistent with prevention of cell death and potential immune responses.

The low or even absent presence of death receptors on hiPS cells should be explored in detail in future experiments. Likewise, restoration of susceptibility to extrinsic stimuli (e.g. by retroviral transduction with genes encoding death receptors) might provide deeper insights into the compromised functionality of the extrinsic apoptosis pathway in human PSCs. Yet, it cannot be excluded that additional factors of the respective pathway are dysfunctional or absent in PSCs.

Curiously, the data obtained from experiments using murine ESCs or iPSCs cannot be transferred to human PSCs. Murine ESCs, unlike human iPSCs, do express Fas and can be extrinsically stimulated[241]. For this reason, MEF-derived knockout miPSCs will hardly support elucidation of apoptotic pathways in human PSCs.

DNA damage signaling factors are highly expressed in hiPS cells

In accordance with an "apoptosis-prone" cellular status, DNA damage applied by bleomycin or IR turned out to be a strong apoptosis inducer in iPS cells, but not in Jurkat cells or fibroblasts. Both stimuli cause DSBs which in turn activate ATM/ATR, followed by activation of the kinases CHK1/2. An important target of CHK1/2 is p53, which is phosphorylated on Ser20 and thereby stabilized against MDM2-dependent degradation. As shown in Fig. 4.7C, hiPS cells contain high p53 levels compared to fibroblasts and Jurkat cells. In addition, as illustrated in the heatmap depicted in Fig. 4.18, both CHK1 and CHK2 (see CHEK1 and CHEK2) were clearly upregulated in H9 hESCs compared to differentiated H9 hESC-derived cells and ATCC feeder fibroblasts. Likewise, BRCA1, CDC25A and MRE11 exhibited elevated mRNA levels, all of which are involved in the DNA damage response.

Following stimulation, CHK2 was phosphorylated within 15 min and expression of the

p53 target gene *p21* was increased within a few hours. Likewise, mRNA levels of the pro-apoptotic target genes *Bak*, *Noxa* and *Puma* were found to be 4- and 2-fold elevated 3 h post irradiation with 3 Gy. Under the same conditions, *Bcl-2*, *Bcl-w* and *Mcl-1* mRNA levels were about 50% reduced (data not shown). Previous publications stated that other anti-apoptotic proteins such as IAPs are similarly downregulated following IR[86].

Taken together, IR led to the rapid activation of the p53 kinase CHK2, which is highly expressed in human PSCs, and p53 targets were upregulated within 3 h after IR. These gene-regulatory events were followed by massive induction of apoptosis within 3 and 6 h post-irradiation. The high expression levels of active p53, CHK1 and CHK2 suggest that hPSCs are hypersensitive to classical p53-dependent intrinsic apoptosis signaling, which is in contrast to the largely p53-independent apoptosis of murine ESCs as previously reported by the group of Rudolf Jaenisch[228]. The differential dependence on p53 provides additional evidence for the intriguing difference of apoptosis signaling in human and murine PSCs. In addition to p53 dependency, apoptosis in human iPS cells was shown to be caspase-dependent, since application of pan-caspase inhibitor prevented execution of cell death (Fig 4.6).

P21 is expressed at low levels in hiPS cells and fails to induce cell cycle arrest upon exposure to IR

Following exposure to DSB-inducing agents such as IR, upregulation of p21 leads to cell cycle arrest in G1 phase in most cell lines[87]. However, basal p21 mRNA levels in iPS cells were less than 10% of the basal levels determined in fibroblasts (data not shown). Following exposure to 1 Gy of IR, p21 mRNA level was roughly doubled 6 h p.i. and protein levels were elevated 3 to 6 hours p.i. (Fig. 4.6C,D), whereas 3 Gy induced a ten-fold p21 mRNA induction within 90 minutes (data not shown).

Nevertheless, a G1 arrest could not be observed in hiPS cells. Even ten-fold elevated p21 mRNA levels were slightly lower than those detectable in untreated primary fibroblasts undergoing regular cell division. The mechanisms by which hPSCs maintain low basal p21 levels and whether other factors besides p21 are involved in abrogation of a G1 arrest yet remain to be determined.

Other groups similarly reported that human iPS cells exhibited low basal p21 protein levels and that upregulation of p21 upon acquisition of DNA damage was insufficient to induce a G1/S arrest[242]. Abrogation of a functional G1 arrest in hiPS cells could therefore be simply explained by a dose-dependent effect caused by low p21 expression.

High MCL-1 levels do not rescue hiPS cells from ABT-737-induced apoptosis

As shown in Fig. 4.7C, iPS cells contain higher levels of the anti-apoptotic Bcl-2 family protein MCL-1 than fibroblasts or Jurkat cells. This is of notice since MCL-1 cannot be bound and neutralized by the BH3-only protein BAD[31]. MCL-1 has, moreover, been implicated in the control of the human stem cell hierarchy and in regulation of self-renewal capacities[229]. However, treatment of hiPS cells with the BAD mimetic ABT-737[31] led to apoptosis in hiPS cells, revealing that hiPS cells are "primed for death" (similar to diverse tumor cell lines[243]) and that the presence of MCL-1 was unable to rescue the cells. A possible reason for this unexpected finding is the high expression level of NOXA (Fig. 4.7B), which constitutes an MCL-1 antagonist, in hiPS cells. Following this hypothesis, changes in NOXA levels might adjudicate on the question whether forced expression of BAD alone is sufficient to induce apoptosis in iPS cells.

In contrast to iPSCs, MCL-1 was barely present in Jurkat cells and fibroblasts. Thus, both cell types depend on anti-apoptotic factors that can be neutralized by ABT-737, such as BCL-2, BCL-X and BCL-W. Accordingly, treatment with ABT-737 induced potent apoptosis in Jurkat cells (data not shown). However, neither the single application of bleomycin nor ABT-737 initiated apoptosis, whereas the combined treatment with both agents led to massive cell death of fibroblasts (Fig. 4.7E). As Fig. 4.7C shows, fibroblasts contain only low levels of the "activator"[32] BH3-only proteins BID and BIM. Both IR and bleomycin treatment induced expression of *Bid* mRNA (data not shown), implying that elevated levels of such “activator” BH3-only proteins are sufficient for apoptosis induction in fibroblasts, provided that BCL-2, BCL-X and BCL-W are neutralized by ABT-737.

Apoptosis in hiPS cells is induced by a peculiar, rapid mechanism

An intriguing finding was the strikingly rapid course of apoptosis induction in hiPS cells. Whereas apoptosis induction by ER stress and intrinsic stimuli required about 16 h in Jurkat cells, iPS cells became annexin V-positive already within 3-6 h after application of ER stress or intrinsic stimuli (Fig. 4.4C,D).

In order to address this differential phenotype, it was investigated whether mitochondria of iPS cells were especially susceptible to pro-apoptotic BH3-only proteins. To this end, mitochondria from human iPS cells, primary fibroblasts and Jurkat cells were isolated and treated with synthetic peptides of BH3 domains (as described by Letai *et al*.[32]), followed by the measurement of cytochrome c release. Unexpectedly, both Jurkat and hiPS cells exhibited a similar extent of cytochrome c

release upon stimulation with the BH3 peptides of BID and BIM, although mitochondria of fibroblasts released less cytochrome c under identical conditions (data not shown).

Interestingly, Deshmukh and colleagues recently reported a peculiar mechanism that might explain the rapid apoptosis induction in hiPS cells[218]. Employing an activation-specific antibody, Dumitru *et al*. found that activated BAX colocalized with the trans-Golgi marker TGN46. The authors demonstrated that pre-activated BAX resides at the Golgi apparatus and, upon pro-apoptotic stimulation, quickly translocated to the mitochondrial outer membrane and initiated MOMP[218]. However, the molecular details underlying the regulation of BAX pre-activation, its sequestration at the Golgi and translocation to the mitochondrial outer membrane remain to be elucidated.

Summarized, a broad characterization of apoptotic response in human iPS cells and fibroblasts was demonstrated in terms of susceptibility to different stimuli which initiate the three main apoptosis signaling pathways. In addition, DNA damage signaling components such as CHK2, p53 and p21 were examined in terms of expression, induction and phosphorylation. BH3 factor profiling[243] was carried out to provide an explanation for differential responses to equal stimuli among the investigated cell types, revealing a “primed for death” status[31] in hiPS cells.

5.2. An assay for long-run rtPCR-based DNA damage quantification

As pointed out in sections 4.2 and 5.1, human iPS cells proved hypersensitive to apoptosis induction following exposure to low dosages of IR and bleomycin. In contrast, equal conditions caused a minor or even no apoptotic response in Jurkat cells and fibroblasts. In order to correlate DNA damage rates to the extent of apoptosis in the particular cell types, an accurate and simple long-run rtPCR-based method for DNA damage quantification (LORD-Q) was developed.

DNA damage rates in both mtDNA and nDNA were detected and quantified following cellular exposure to bleomycin, UV radiation, etoposide and cisplatin or hydrogen peroxide. Similarly, protective effects of medium additives such as serum and vitamin C were quantified.

LORD-Q analyses revealed that initiation of apoptosis was apparently independent from DNA repair in iPS cells, since bleomycin-stimulated iPS cells underwent apoptosis (roughly 30% $AnxV^+$ cells 6 h after stimulation, data not shown) even though mtDNA lesions were completely removed 2 h after treatment (Fig. 4.15B).

LORD-Q is not suitable for DNA damage quantification upon IR exposure

In contrast to DNA damage induced by the above-mentioned stimuli, IR-mediated DNA damage proved not to be quantifiable by LORD-Q. As previously reported, 1 Gy of gamma-radiation causes about 50 DSBs per cell[244]. Another group determined merely 20-40 DSBs per cell following exposure to 1 Gy, correlating to an incidence of 5.4×10^{-3}/Mbp per Gy[245]. In wide contrast, a detection limit of LORD-Q of some 0.3 lesions per 10 kb (equal to 300 lesions / Mbp) was estimated (Fig. 4.12C), which exceeds physiological incidences of DSBs by roughly four to five orders of magnitude. Even if the entire composition of cellular DNA modifications caused by 1 Gy of IR is factored – estimated 1000–2000 base modifications, 800–1600 backbone modifications, 500–1000 SSBs, 150 DNA-protein crosslinks and 50 DSBs[244], the calculated DNA damage rate is 0.65 / Mbp or 0.0065 / 10 kb. Assumed that all modifications were detectable by LORD-Q, the detection limit of the method would still exceed the calculated lesion incidence (caused by 1 Gy) by a factor of 50.

Thus, in accordance with experimental results (data not shown), LORD-Q is unable to detect IR-mediated DNA damage at physiologically relevant dosages (roughly 1-20 Gy). Therefore, alternative methods, such as counting of γH2AX foci or a pulsed-field gel electrophoresis[246], might be employed to monitor DSB acquisition and repair.

SSB repair can be successfully traced by LORD-Q

LORD-Q was successfully employed to investigate mtDNA repair capacities in different cell types upon differential genotoxic treatment (Fig. 4.15B). The main lesions detectable by LORD-Q are abasic sites and SSBs, whereas DSBs account for merely a minor portion of modifications and 8-oxo-dG(/dA) was not recognized. This may bias repair kinetics, since UV or H_2O_2 mainly cause ROS-mediated oxidative DNA damage[247] (e.g. 8-oxo-dG and 8-oxo-dA). 8-Oxo-dG repair and SSB repair might differ in terms of velocity and capacity among the different cell lines. In other words, LORD-Q-mediated monitoring of SSB repair does not necessarily parallel repair of oxidative DNA damage. Likewise, the detected damage rates do not imperatively mirror the entirety of genomic lesions: First, different loci were differentially affected by genotoxic stimuli (Fig. 4.16) and second, frequency of SSBs, which constitute the predominantly recognized DNA modifications, may not be proportional to other types of DNA damage. This topic is further discussed in section 5.4.

The LORD-Q methodology can be extended in a modular way

Nonetheless, LORD-Q constitutes a simple, accurate and reliable analytical tool. Besides DNA damage, another useful application of LORD-Q is represented by the following finding. Pastor *et al*. reported that 5-hydroxymethylation of cytosines (5hmC) is an important epigenetic modification particularly found in embryonic stem cells[230]. As reported by Booth *et al*. in 2012, several genomic regions that were suggested to "undergo epigenetic reprogramming in ES cells"[248] displayed between 0.2 and 18.5% of 5-hydroxymethylated CpG islands[248]. LORD-Q allows for the detection of 5hmC as shown in Fig. 4.13A. It can be applied to survey any specific region of up to 4 kb length for 5hmC content if suitable primer pairs are employed. In this context, different genomic regions of choice may be simultaneously monitored during embryonic development and differentiation of PSCs. LORD-Q allows for both monitoring of single CpG islands (if primers and PCR conditions similar to the above-mentioned analysis of modified oligonucleotides are employed, see Fig. 4.13) within highly hydroxymethylated genomic regions or surveillance of long sections to measure 5hmC frequency in less hydroxymethylated regions.

A second possible extension of the LORD-Q methodology is represented by the supervision of cytosine deamination, e.g. during activation-induced deaminase (AID)-dependent somatic hypermutation or class switch recombination. Faili *et al*. have described an *in vitro* method for induction of somatic hypermutation. In this assay,

BL2 Burkitt's Lymphoma cells are incubated in the presence of a cocktail composed of three antibodies that stimulate AID initiation within 90 min[61]. Deamination sites might then be converted into abasic sites by digestion with uracil N-glycosylase (UNG) and quantified by LORD-Q (see Fig. 4.17B).
This excision-mediated recognition of base modifications can likewise be extended to oxidative lesions, for instance if 8-oxo-deoxyguanine glycosylase 1 (OGG1) or other specific DNA glycosylases are used. By this means, LORD-Q might allow for detection of oxidative lesions: Exemplarily, undigested and OGG1-digested DNA derived from UV-irradiated and control cells could be compared by LORD-Q analysis. This might reveal the ratio between SSBs and oxidative lesions for any given stimulus.
Likewise, DNA derived from UV-irradiated cells could be repaired using an *in vitro* nucleotide excision repair (NER) assay to examine the extent of cyclobutane pyrimidine dimers (CPDs). In contrast to the above-mentioned DNA glycosylases which generate abasic sites in the first step of base excision repair, NER decreases the DNA damage rate by removal of CPDs. LORD-Q analysis prior and following NER may thus reveal the extent of photoadducts within the respective DNA probe.

The above-mentioned technical modifications were successfully tested in a first series of experiments (data not shown), thereby basically confirming the feasibility of such extensions of the methodology. Summarized, LORD-Q provides a suitable platform for SSB detection which can be extended in a modular way.

5.3. DNA damage prevention in human iPS cells

In accordance with previously published results[19], hiPS cells were found to acquire less DNA lesions than fibroblasts and Jurkat cells during exposure to genotoxic stimuli (Fig. 4.15A, Fig. 4.21B). It can thus be suggested that hiPS cells possess pronounced DNA damage-preventing defense mechanisms. All PSCs need to minimize DNA damage to avoid accumulation of mutations which would otherwise be passed down generations. However, to date no publications have yet elucidated such distinct DNA-protective mechanisms.

Several possible reasons could explain the reduced DNA damage incidence in hiPS cells. First of all, pluripotent cells might keep endogenous stress levels low. One strategy to assure this is the restriction of oxygen consumption. Oxygen is *de facto* a diradical which can oxidize cellular components such as proteins and lipids. Many cell types are extremely sensitive to lipid peroxidation[249]. Embryonic tissues exist under hypoxic conditions *per se*, therefore oxygen levels in hES cells are inherently low. In addition, oxygen consumption in hPSCs is yet limited by metabolic reasons. Compared to primary fibroblasts, hPSCs possess a significantly lower number of mitochondria and, consequently, mtDNA copies. While fibroblasts exhibited between 100 and 1000 copies, merely 10 to 100 copies were found in iPS cells as determined by LORD-Q (data not shown), suggesting a minor role of the respiratory energy metabolism in iPS cells. Accordingly, iPS cells were described to consume high amounts of glucose and to depend rather on glycolysis than on oxidative phosphorylation in terms of ATP generation[250]. Therefore, hiPS cells exhibit low oxygen turnover, accompanied by little ROS generation compared to e.g. fibroblasts. In this way, iPS cells maintain minimal endogenous stress levels and marginal endogenously provoked DNA damage[84]. However, since glucose represents an aldehyde of moderate reactivity, high glucose uptake and consumption due to metabolic dependency on glycolysis may lead to glycosylation of proteins or even DNA. Moreover, continued cell division causes high replicative stress in hPSCs. Thus, iPS cells minimize metabolic generation of ROS, but exhibit enhanced stress levels caused by rapid cell division and elevated glucose consumption.

HiPS cells display minimal basal mtDNA damage

Investigation of basal DNA damage levels, which reflect a steady-state equilibrium between spontaneously occurring DNA lesions (10^5 to 10^6 estimated events per cell and day[45]) and DNA repair, showed that hiPS cells exhibit lower basal mtDNA damage levels than fibroblasts and Jurkat cells, while senescent fibroblasts featured

the highest damage incidence. In contrast, nDNA levels in both hiPS cells and fibroblasts were similar to each other. These data would be consistent with the suggested existence of low mtDNA stress in hiPS cells.

However, "initial damage" rates as depicted in Fig. 4.15A display lesion rates after subtraction of basal DNA damage. Thus, high endogenous stress and/or basal DNA damage levels do not account for low initial damage rates in hiPS cells. Since predominantly SSBs are recognized by LORD-Q and cells cannot avoid direct radiation-mediated strand breaks (such as SSBs and DSBs provoked by direct absorption of high-energy photons or UV-induced electrocyclic photoadduct formation), common cellular antioxidative defense systems were investigated.

First, the role of GSH was elucidated. GSH levels were found to be significantly elevated in iPS cells compared to fibroblasts. In addition, glutathione reductase, two GSH peroxidases (GPX2, GPX7) and several GSH transferases (GST class alpha and microsomal GSTs) were expressed to a higher level in iPS cells than in fibroblasts. Employing a GSH depletion assay, cellular GSH levels were reduced by more than 80% in all cell lines examined. Both application of H_2O_2 and UVR (data not shown) to fibroblasts, Jurkat cells and iPS cells significantly induced ROS formation within the respective cells, as determined by staining with the ROS-sensitive dye dihydrorhodamine 123. However, this increase in internal stress levels exclusively corresponded to increased DNA damage levels in Jurkat cells and fibroblasts, while iPS cells remained widely unaffected (Fig. 4.21B).

Apolipoproteins might protect hiPSCs from oxidative damage or regulate cholesterol homeostasis in embryonic tissues

It was concluded that, besides GSH and GSH-depending enzymes which reduced ROS-mediated DNA lesions in Jurkat cells and fibroblast, other mechanisms protect hiPS cells from DNA damage.

A noteworthy observation was the finding that hiPS cells exhibited highly upregulated apolipoprotein expression (see Fig. 4.19). For instance, apolipoprotein E was more than 1,000 fold higher expressed in iPS cells than in fibroblasts. Similarly, mRNA levels of other apolipoproteins, the APOE receptor LRP8, LDL and VLDL receptors (LDLR and VLDLR) were strongly expressed in hiPS cells. It is generally accepted that different APOE genotypes correlate with age of onset and severity of Alzheimer's disease[232]. In addition, APOE has been shown to play an important role in prevention of lipid peroxidation and oxidative damage in neurons[98]. Thus, apolipoproteins may constitute important contributors to the antioxidative defense in hiPS cells.

Another explanation for the high apolipoprotein expression in hiPS cells comes yet from parallels between uterus and brain: Both organs are isolated from the bloodstream by blood-brain and blood-placenta barriers (BBB and BPB), respectively. In brain, supply with lipoproteins that contain cholesterol (e.g. needed for axon synthesis) from the bloodstream is inhibited by the BBB. For this reason, a "self-sufficient" lipoprotein system exists in the brain[251]. A similar system could likewise be present in embryonic tissues in the uterus (or iPS cells *in vitro*), since fetal cells rapidly divide and thus require large amounts of cholesterol, fatty acids and phospholipids for membrane synthesis. This speculation is supported by microarray data which revealed that several genes involved in cholesterol synthesis are 3-10 fold upregulated in H9 hES cells compared to ATCC feeder fibroblasts[231]. These genes comprise HMG-CoA reductase, the rate-limiting enzyme in cholesterol biosynthesis, HMG-CoA synthase 1 and 2, isopentenyl-diphosphate delta isomerase 1 and farnesyl-diphosphate farnesyl transferase 1. Taken together, the role of apoplipoproteins in both antioxidative defense in hiPS cells and an independent embryonic cholesterol/lipoprotein metabolism appears plausible but remains to be elucidated.

Additional candidates for DNA damage prevention in hiPS cells

Another promising candidate for DNA damage prevention in hiPS cells is the peroxiredoxin family, which was found to be throughout highly upregulated in hiPS cells compared to fibroblasts. These proteins, together with SODs, CAT, thioredoxin peroxidases and GSH peroxidases, represent "a first line" of antioxidant defense and convert ROS into less noxious compounds (Hayes *et al*.[97]). Peroxiredoxins have been shown to be of prime importance to detoxify peroxides and can, by reduction of the ROS load, even inhibit apoptosis in cells treated with genotoxins[89,252]. In the current project, fibroblasts upregulated antioxidative factors upon stimulation with UV and hydrogen peroxide (data not shown), thereby “closing the gap” between expression levels of peroxiredoxins, apolipoproteins and GSTs in hiPS cells and fibroblasts. However, future studies will have to clarify to which extent peroxiredoxins effectively contribute to iPS cell-specific DNA damage prevention. Besides, potential biophysical barriers, e.g. differences between hiPS cells and fibroblasts concerning architecture of the nuclear envelope or chromatin organization, may be addressed.
The below-mentioned model (Fig. 5.1) summarizes the findings concerning DNA damage prevention, DNA damage signaling and apoptotic response in hiPS cells and fibroblasts. It combines increased DNA damage prevention in hiPS cells and strong

DNA damage response signaling, which leads to apoptosis induction even at low DNA lesion frequencies.

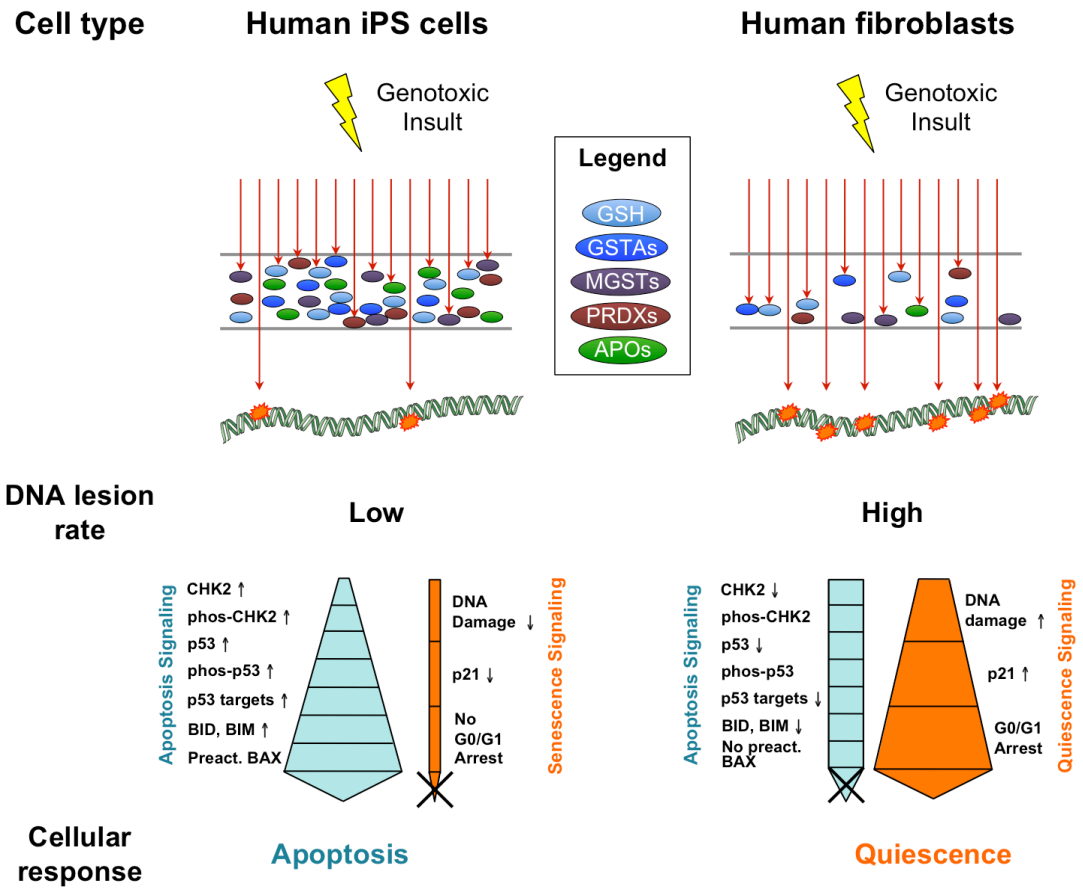

Fig. 5.1: Model for DNA damage acquisition and apoptosis signaling in hiPS cells and primary human fibroblasts.

Human iPS cells and fibroblasts display differential DNA damage incidence and DNA damage response upon genotoxic treatment. A genotoxic insult, e.g. exposure to bleomycin, generates ROS which have to pass several „filters“ of antioxidant defense before DNA damage can occur (red arrows). In hiPS cells, GSH, GSTA, MGST, PRDX and apolipoprotein levels are strikingly increased compared to fibroblasts, resulting in a reduced DNA lesion incidence (upper part). In fibroblasts, high DNA damage rates combined with high p21 levels provide a strong stimulus for induction of senescence or quiescence (orange pathway/arrow). In contrast, low DNA damage frequency and low p21 levels, accompanied by absence of a G0/G1 arrest abrogate quiescence in hiPS cells. Apoptotic signaling, however, is enforced by increased expression levels of pro-apoptotic factors (CHK1/2, p53, BID, BIM) and pre-activated BAX^{218} in hiPS cells (cyan pathway/arrow). Fibroblasts, contrariwise, display low levels of DNA damage signaling factors, thereby petering out pro-apoptotic signals. Abbreviations: APO: apolipoprotein; GSH: glutathione; GSTA: glutathione S-transferase class alpha; MGST: microsomal glutathione S-transferase; phos: phosphorylated; PRDX: peroxiredoxin; Preact.: pre-activated. Figure was produced using Servier Medical Art.

5.4. Outlook

In the current study, hiPS cells were shown to be especially sensitive to DSB-inducing agents. Upon stimulation with IR or bleomycin, common DBS inducers, hiPS cells initiated rapid and massive apoptosis. Several components of the p53 pathways were found at markedly increased levels in hiPS cells as compared to isogenic fibroblasts.

P53 is activated via phosphorylation of upstream DSB response factors. However, p53 is not exclusively activated by phospho-CHK1/2 at Ser20. In addition to CHK1/2, AMT/ATR can directly activate p53 via phosphorylation at Ser15[85]. Future studies may clarify whether direct activation by ATM/ATR or phospho-CHK1/2-mediated activation of p53 predominates in human PSCs.

Further investigations might likewise address the vulnerability of iPS cells to UV radiation. In this study, hiPS cells proved to be resistant to moderate dosages of UVR, while other groups reported apoptosis induction by UVR treatment in these cells. However, the DNA damage pattern caused by UVR depends on the employed wavelength. In the current study, UVC (254 nm) radiation was used, whereas thymine dimers are predominantly generated by UVA and UVB radiation[63]. Thus, comparative analyses of the effect of UVA, UVB and UVC radiation on hiPS cells and fibroblasts should be performed.

In addition, oxidative lesions (predominantly 8-oxo-dG) might be excised and, thus, recognized by LORD-Q. This might help to unveil the differential compositions of DNA lesions following exposure of UVA, UVB and UVC radiation. The differences between the current findings and the results of other studies concerning induction of apoptosis in hiPS cells by UVR might be explained in this way.

Since hiPS cells are hypersensitive to IR-mediated apoptosis, but LORD-Q failed to detect DNA lesions following exposure of cells to IR (see section 5.2), other methods may be employed to determine DSB incidence in hiPS cells following IR treatment. In this context, it might be examined whether iPS cells acquire less lesions than fibroblasts or Jurkat cells during exposure to IR, thereby paralleling DNA damage acquisition during exposure to bleomycin, UVR and H_2O_2.

A suitable method to investigate DSB frequencies was described by Löbrich *et al*.[246]. In this approach, NotI-digested whole-cell DNA is separated by size via pulsed-field gel electrophoresis. In a second step, a radioactively labeled probe is added that recognizes a specific 3.2 Mbp fragment by Southern blot analysis. With increasing number of DSBs, a smear below the original band occurs which can in turn be used

for DSB quantification. Alternatively, counting of immunostained γH2AX foci might be employed to determine DSB frequencies.

Mitochondria exhibit several copies of mtDNA per organelle. Unlike nuclear DNA, highly damaged mtDNA molecules can be degraded prior, during or following duplication of undamaged mtDNA copies. In addition, mitochondria can undergo fusion or fission to reduce their load of damaged DNA. Finally, mitochondria bearing severely damaged DNA can be removed by mitophagy, a subtype of autophagy[84]. If all safety mechanisms comprising repair pathways, duplication of undamaged DNA and degradation of severely damaged mtDNA copies or even whole organelles fail, the mitochondrial membrane potential is lost and apoptosis ensues. In future studies, LORD-Q might be applied to reveal specific mtDNA damage response in hiPS cells, namely mtDNA repair, mtDNA degradation or replication of mtDNA copies. Similarly, repair kinetics of nDNA lesions, e.g. employing different inhibitors of factors involved in nDNA damage signaling and repair (such as the ATM/ATR inhibitor caffeine), might be carried out.
In addition, DNA protection in hiPS cells remains to be more precisely examined. Further studies might clarify the roles of GSH peroxidases and transferases, SODs, peroxiredoxins or apolipoproteins within the antioxidative defense of this peculiar cell type. In this respect, localization and function of apolipoproteins in hiPS cells might be revealed. It is yet unknown whether e.g. APOE is secreted and to which extent it contributes to protect lipids from oxidative modifications such as peroxidation. Likewise, the correlation between lipid peroxidation and apoptotic response in hiPS cells remains to be illuminated.

In summary, the above-mentioned steps might help to better characterize intricate antioxidative defense, DNA damage prevention, DNA repair and apoptosis signaling in human pluripotent stem cells. In this way, this study contributes to the knowledge that is necessary to monitor and control cellular fate of hiPS cells in order to make stem cells safe for future therapeutic applications.

6. SUMMARY

Unlike any other discovery in life sciences throughout the past years, human induced pluripotent stem (iPS) cells have raised the hope for personalized medical therapies. IPS cells represent embryonic stem (ES)-like cells, are immortal and can, in principle, infinitely give rise to all somatic cells and their precursors. Since they are generated from patient-derived cells (e.g. fibroblasts), they enable isogenic replacement of defective tissues or cells such as cardiomyocytes after cardiac infarction or dopaminergic neurons in Parkinson's disease. In addition, during iPS cell generation no human embryos are destroyed, thereby circumventing several ethical issues that accompany scientific or medical applications employing ES cells. However, iPS cells do not exhibit all features of ES cells. At least in part, iPS cells keep the epigenetic "memory" of their cells of origin. Likewise, genomic instability, chromosomal aberrations and mutations can hardly be removed during or after reprogramming. This is of prime importance as pluripotent cells generally exhibit increased tumorigenic potential compared to terminally differentiated cells. A detailed understanding of survival and apoptosis pathways is, hence, essential for the development of safe stem cell therapies.

In the first part, this thesis elucidates apoptotic responses in iPS cells, fibroblasts and a control cell line (Jurkat) upon extrinsic, intrinsic and ER stress stimulation. It is demonstrated that iPS cells prove hypersensitive to DNA double-strand breaks(DSB)-inducing treatment, but resist extrinsic death ligands, while fibroblasts show a reversed pattern of susceptibility.

In order to link the extent of cellular DNA damage to the induction of apoptosis, an accurate and sequence-specific real-time PCR-based method for DNA damage quantification was developed. The characterization and specification of the method and different applications are subject of the second section of this work. It is shown that, although being highly sensitive to DSBs in terms of apoptosis, iPS cells acquire lower DNA lesion rates than fibroblasts and Jurkat cells, indicating elevated protection mechanisms in iPS cells.

The last part of this thesis discusses the examination of such DNA damage prevention mechanisms. It is demonstrated that the level of the most important cellular small molecule antioxidant, glutathione (GSH), is elevated in iPS cells compared to fibroblasts. In addition, fibroblasts and Jurkat cells exhibited significantly increased DNA damage upon genotoxic treatment after GSH depletion. However, in iPS cells, GSH depletion had no effect on DNA damage frequency. Finally, increased

expression of various genes coding for proteins or enzymes involved in antioxidative defense was found in iPS cells.

The current work provides new insights into the apoptotic response, the relation between DNA damage and apoptosis and cellular DNA damage prevention mechanisms in human pluripotent cells, which might prove useful for a more detailed understanding of physiological properties of this promising new cell type.

7. ZUSAMMENFASSUNG

Wie kaum eine andere wissenschaftliche Entdeckung haben humane induzierte pluripotente Stammzellen (iPS-Zellen) die Hoffnung auf personalisierte Therapien belebt. Sie sind embryonalen Stammzellen (ES-Zellen) ähnlich, immortal und können alle somatischen Zelltypen und deren Vorläufer in prinzipiell unbegrenzter Anzahl hervorbringen. Da sie aus Fibroblasten oder anderen Zelltypen patienten-spezifisch erzeugt werden können, eröffnen sie die Möglichkeit, mit körpereigenen Ersatzgeweben ohne Abstoßungsreaktion defekte oder abgestorbene Zellen zu ersetzen, z.B. Herzmuskelzellen nach einem Herzinfarkt oder dopaminerge Neuronen bei Parkinson-Patienten. Zugleich werden zu ihrer Herstellung keine menschlichen Embryonen zerstört, weswegen die ethische Problematik, welche bei Verwendung von ES-Zellen besteht, weitgehend entfällt.
Dennoch sind iPS-Zellen und ES-Zellen nicht identisch. So behalten iPS-Zellen teilweise das epigenetische "Gedächtnis" ihrer Herkunftszellen bei. Auch mögliche genomische Instabilität, chromosomale Aberrationen und Mutationen des Erbguts der Ausgangszellen können nur teilweise wieder rückgängig gemacht werden. Dies ist von besonderer Brisanz, da pluripotente Zellen generell ein erhöhtes Potential zur Erzeugung von Tumoren besitzen. Das Verständnis der Regulation von Überlebens- und Apoptose-Signalen in iPS-Zellen ist daher von zentraler Bedeutung für die zukünftige Entwicklung sicherer Stammzelltherapien.

Die vorliegende Dissertation behandelt im ersten Teil die umfassende vergleichende Charakterisierung von zellulären Reaktionen auf extrinsische, intrinsische und ER-Stress-vermittelte Apoptose-Signale in humanen iPS-Zellen, Fibroblasten und einer Kontroll-Zelllinie (Jurkat). Es wird gezeigt, dass iPS-Zellen hochsensitiv auf DNA-Doppelstrangbruch(DSB)-induzierende Behandlung reagieren, jedoch Signalen durch extrinsische Todesliganden widerstehen. In Fibroblasten wird das umgekehrte Sensitivitätsprofil demonstriert.
Um den Zusammenhang zwischen dem Ausmaß des induzierten DNA-Schadens und dem Eintritt von Apoptose zu untersuchen, wurde eine akkurate und sequenzspezifische Methode zur Real-time PCR-basierten DNA-Schadens-quantifizierung entwickelt. Diese Methodenentwicklung und deren Anwendung auf DNA-Schadensbestimmung in Fibroblasten, iPS- und Jurkat-Zellen werden im zweiten Abschnitt erläutert. Es wird gezeigt, dass iPS-Zellen trotz hoher Empfindlichkeit gegenüber DSBs geringere Schadensraten als Fibroblasten und Jurkat-Zellen aufweisen, was auf erhöhte zelluläre Schutzmechanismen in iPS-Zellen

schließen lässt.
Der letzte Abschnitt behandelt die Untersuchung dieser Schutzmechanismen. Es wird gezeigt, dass das wichtigste zelluläre Molekül zur Verteidigung gegen oxidative Schäden, Glutathion, in iPS-Zellen in erhöhten Spiegeln vorhanden ist. Die Depletion von Glutathion kann die DNA-Schädigung in Fibroblasten und Jurkat-Zellen deutlich verstärken, nicht jedoch in iPS-Zellen. Weiterhin werden zahlreiche Gene antioxidativer Proteine und Enzyme identifiziert, deren Expression in humanen iPS-Zellen gegenüber Fibroblasten erhöht ist.

Die vorliegende Arbeit liefert Einblicke in die Zelltod-Regulation, den Zusammenhang von DNA-Schaden und Apoptose sowie die DNA-Schadensprävention in humanen iPS-Zellen. Sie leistet daher einen Beitrag zum besseren Verständnis der Eigenschaften dieses neuen, vielversprechenden Zelltyps.

8. REFERENCES

1 Takahashi, K. & Yamanaka, S. (2006). Induction of pluripotent stem cells from mouse embryonic and adult fibroblast cultures by defined factors. *Cell* **126** (4): 663-676.

2 Kerr, J. F., Wyllie, A. H. & Currie, A. R. (1972). Apoptosis: a basic biological phenomenon with wide-ranging implications in tissue kinetics. *Br J Cancer* **26** (4): 239-257.

3 Crespi, B. & Springer, S. (2003). Ecology. Social slime molds meet their match. *Science* **299** (5603): 56-57.

4 Rathmell, J. C. & Thompson, C. B. (2002). Pathways of apoptosis in lymphocyte development, homeostasis, and disease. *Cell* **109 Suppl**: S97-107.

5 Meier, P., Finch, A. & Evan, G. (2000). Apoptosis in development. *Nature* **407** (6805): 796-801.

6 Aitken, R. J., Findlay, J. K., Hutt, K. J. & Kerr, J. B. (2011). Apoptosis in the germ line. *Reproduction* **141** (2): 139-150.

7 Pender, M. P. (1998). Genetically determined failure of activation-induced apoptosis of autoreactive T cells as a cause of multiple sclerosis. *Lancet* **351** (9107): 978-981.

8 Muller, P. A. & Vousden, K. H. (2013). p53 mutations in cancer. *Nat Cell Biol* **15** (1): 2-8.

9 Fuchs, Y. & Steller, H. (2011). Programmed cell death in animal development and disease. *Cell* **147** (4): 742-758.

10 Kurokawa, M. & Kornbluth, S. (2009). Caspases and kinases in a death grip. *Cell* **138** (5): 838-854.

11 Enari, M. *et al.* (1998). A caspase-activated DNase that degrades DNA during apoptosis, and its inhibitor ICAD. *Nature* **391** (6662): 43-50.

12 Nagata, S., Nagase, H., Kawane, K., Mukae, N. & Fukuyama, H. (2003). Degradation of chromosomal DNA during apoptosis. *Cell Death Differ* **10** (1): 108-116.

13 Lauber, K. *et al.* (2003). Apoptotic cells induce migration of phagocytes via caspase-3-mediated release of a lipid attraction signal. *Cell* **113** (6): 717-730.

14 Lauber, K., Blumenthal, S. G., Waibel, M. & Wesselborg, S. (2004). Clearance of apoptotic cells: getting rid of the corpses. *Mol Cell* **14** (3): 277-287.

15 Fadok, V. A. *et al.* (1992). Exposure of phosphatidylserine on the surface of apoptotic lymphocytes triggers specific recognition and removal by macrophages. *J Immunol* **148** (7): 2207-2216.

16 Sebbagh, M. *et al.* (2001). Caspase-3-mediated cleavage of ROCK I induces MLC phosphorylation and apoptotic membrane blebbing. *Nat Cell Biol* **3** (4): 346-352.

17 Rothstein, T. L. (2000). Inducible resistance to Fas-mediated apoptosis in B cells. *Cell Res* **10** (4): 245-266.

18 Musgrove, R. E., King, A. E. & Dickson, T. C. (2013). alpha-Synuclein Protects Neurons from Apoptosis Downstream of Free-Radical Production Through Modulation of the MAPK Signalling Pathway. *Neurotox Res* **23** (4): 358-369.

19 Luo, L. Z. *et al.* (2012). DNA repair in human pluripotent stem cells is distinct from that in non-pluripotent human cells. *PloS one* **7** (3): e30541.

20 Krammer, P. H. (2000). CD95's deadly mission in the immune system. *Nature* **407** (6805): 789-795.

21 Ashkenazi, A. & Dixit, V. M. (1998). Death receptors: signaling and modulation. *Science* **281** (5381): 1305-1308.

22 Los, M., Wesselborg, S. & Schulze-Osthoff, K. (1999). The role of caspases in development, immunity, and apoptotic signal transduction: lessons from knockout mice. *Immunity* **10** (6): 629-639.

23 Siegel, R. M. (2006). Caspases at the crossroads of immune-cell life and death. *Nat Rev Immunol* **6** (4): 308-317.

24 Dutton, A., Young, L. S. & Murray, P. G. (2006). The role of cellular FLICE inhibitory protein (c-FLIP) in the pathogenesis and treatment of cancer. *Expert Opin Ther Targets* **10** (1): 27-35.

25 Meinl, E., Fickenscher, H., Thome, M., Tschopp, J. & Fleckenstein, B. (1998). Anti-apoptotic strategies of lymphotropic viruses. *Immunol Today* **19** (10): 474-479.

26 Schimmer, A. D. (2004). Inhibitor of apoptosis proteins: translating basic knowledge into clinical practice. *Cancer Res* **64** (20): 7183-7190.

27 Brenner, D. & Mak, T. W. (2009). Mitochondrial cell death effectors. *Curr Opin Cell Biol* **21** (6): 871-877.

28 Vousden, K. H. & Lu, X. (2002). Live or let die: the cell's response to p53. *Nat Rev Cancer* **2** (8): 594-604.

29 Reed, J. C. (1997). Double identity for proteins of the Bcl-2 family. *Nature* **387** (6635): 773-776.

30 Adams, J. M. & Cory, S. (1998). The Bcl-2 protein family: arbiters of cell survival. *Science* **281** (5381): 1322-1326.

31 Certo, M. *et al.* (2006). Mitochondria primed by death signals determine cellular addiction to antiapoptotic BCL-2 family members. *Cancer cell* **9** (5): 351-365.

32 Letai, A. *et al.* (2002). Distinct BH3 domains either sensitize or activate mitochondrial apoptosis, serving as prototype cancer therapeutics. *Cancer cell* **2** (3): 183-192.

33 Chen, L. *et al.* (2005). Differential targeting of prosurvival Bcl-2 proteins by their BH3-only ligands allows complementary apoptotic function. *Mol Cell* **17** (3): 393-403.

34 Kuwana, T. *et al.* (2002). Bid, Bax, and lipids cooperate to form supramolecular openings in the outer mitochondrial membrane. *Cell* **111** (3): 331-342.

35 Annis, M. G. *et al.* (2005). Bax forms multispanning monomers that oligomerize to permeabilize membranes during apoptosis. *EMBO J* **24** (12): 2096-2103.

36 Tabas, I. & Ron, D. (2011). Integrating the mechanisms of apoptosis induced by endoplasmic reticulum stress. *Nat Cell Biol* **13** (3): 184-190.

37 Ron, D. & Hubbard, S. R. (2008). How IRE1 reacts to ER stress. *Cell* **132** (1): 24-26.

38 Zhang, K. & Kaufman, R. J. (2004). Signaling the unfolded protein response from the endoplasmic reticulum. *J Biol Chem* **279** (25): 25935-25938.

39 Ma, Y. & Hendershot, L. M. (2003). Delineation of a negative feedback regulatory loop that controls protein translation during endoplasmic reticulum stress. *J Biol Chem* **278** (37): 34864-34873.

40 Liu, G., Zhao, J., Chang, Z. & Guo, G. (2013). CaMKII Activates ASK1 to Induce Apoptosis of Spinal Astrocytes Under Oxygen-Glucose Deprivation. *Cell Mol Neurobiol* **33** (4): 543-549.

41 Oyadomari, S. & Mori, M. (2004). Roles of CHOP/GADD153 in endoplasmic reticulum stress. *Cell Death Differ* **11** (4): 381-389.

42 Chung, H., Chung, H. Y., Bae, C. W., Kim, C. J. & Park, S. (2011). Ghrelin suppresses tunicamycin- or thapsigargin-triggered endoplasmic reticulum stress-mediated apoptosis in primary cultured rat cortical neuronal cells. *Endocr J* **58** (5): 409-420.

43 Pelham, H. R. (1991). Multiple targets for brefeldin A. *Cell* **67** (3): 449-451.

44 Chardin, P. & McCormick, F. (1999). Brefeldin A: the advantage of being uncompetitive. *Cell* **97** (2): 153-155.

45 Ciccia, A. & Elledge, S. J. (2010). The DNA damage response: making it safe to play with knives. *Mol Cell* **40** (2): 179-204.

46 Tamir, S., Burney, S. & Tannenbaum, S. R. (1996). DNA damage by nitric oxide. *Chem Res Toxicol* **9** (5): 821-827.

47 Lombard, D. B. *et al.* (2005). DNA repair, genome stability, and aging. *Cell* **120** (4): 497-512.

48 Fischer, U. & Schulze-Osthoff, K. (2005). New approaches and therapeutics targeting apoptosis in disease. *Pharmacol Rev* **57** (2): 187-215.

49 Gorgoulis, V. G. *et al.* (2005). Activation of the DNA damage checkpoint and genomic instability in human precancerous lesions. *Nature* **434** (7035): 907-913.

50 Lovell, M. A. & Markesbery, W. R. (2007). Oxidative DNA damage in mild cognitive impairment and late-stage Alzheimer's disease. *Nucleic Acids Res* **35** (22): 7497-7504.

51 Bender, A. *et al.* (2006). High levels of mitochondrial DNA deletions in substantia nigra neurons in aging and Parkinson disease. *Nat Genet* **38** (5): 515-517.

52 Fato, R., Bergamini, C., Leoni, S., Strocchi, P. & Lenaz, G. (2008). Generation of reactive oxygen species by mitochondrial complex I: implications in neurodegeneration. *Neurochem Res* **33** (12): 2487-2501.

53 Song, N., Wang, J., Jiang, H. & Xie, J. (2010). Ferroportin 1 but not hephaestin contributes to iron accumulation in a cell model of Parkinson's disease. *Free Radic Biol Med* **48** (2): 332-341.

54 Kirkwood, T. B. & Holliday, R. (1979). The evolution of ageing and longevity. *Proc R Soc Lond B Biol Sci* **205** (1161): 531-546.

55 Kuilman, T., Michaloglou, C., Mooi, W. J. & Peeper, D. S. (2010). The essence of senescence. *Genes Dev* **24** (22): 2463-2479.

56 Hildebrand, D. G. *et al.* (2013). alpha-Fucosidase as a novel convenient biomarker for cellular senescence. *Cell cycle* **12** (12):

57 Hoare, M., Das, T. & Alexander, G. (2010). Ageing, telomeres, senescence, and liver injury. *J Hepatol* **53** (5): 950-961.

58 Sies, H. (1997). Oxidative stress: oxidants and antioxidants. *Exp Physiol* **82** (2): 291-295.

59 Cooke, M. S., Evans, M. D., Dizdaroglu, M. & Lunec, J. (2003). Oxidative DNA damage: mechanisms, mutation, and disease. *FASEB J* **17** (10): 1195-1214.

60 Chaudhuri, J. & Alt, F. W. (2004). Class-switch recombination: interplay of transcription, DNA deamination and DNA repair. *Nat Rev Immunol* **4** (7): 541-552.

61 Faili, A. *et al.* (2002). AID-dependent somatic hypermutation occurs as a DNA single-strand event in the BL2 cell line. *Nat Immunol* **3** (9): 815-821.

62 Garinis, G. A. *et al.* (2005). Transcriptome analysis reveals cyclobutane pyrimidine dimers as a major source of UV-induced DNA breaks. *EMBO J* **24** (22): 3952-3962.

63 Mouret, S. *et al.* (2006). Cyclobutane pyrimidine dimers are predominant DNA lesions in whole human skin exposed to UVA radiation. *Proc Natl Acad Sci U S A* **103** (37): 13765-13770.

64 Borosky, G. L. (2008). Quantum chemical studies on ultimate carcinogenic metabolites from polycyclic aromatic hydrocarbons. *Curr Med Chem* **15** (28): 2901-2920.

65 Ferguson, L. R. & Denny, W. A. (1991). The genetic toxicology of acridines. *Mutat Res* **258** (2): 123-160.

66 Krejci, L., Altmannova, V., Spirek, M. & Zhao, X. (2012). Homologous recombination and its regulation. *Nucleic Acids Res* **40** (13): 5795-5818.

67 Muslimovic, A., Nystrom, S., Gao, Y. & Hammarsten, O. (2009). Numerical analysis of etoposide induced DNA breaks. *PloS one* **4** (6): e5859.

68 French, S. L. *et al.* (2011). Distinguishing the roles of Topoisomerases I and II in relief of transcription-induced torsional stress in yeast rRNA genes. *Mol Cell Biol* **31** (3): 482-494.

69 Povirk, L. F., Wubter, W., Kohnlein, W. & Hutchinson, F. (1977). DNA double-strand breaks and alkali-labile bonds produced by bleomycin. *Nucleic Acids Res* **4** (10): 3573-3580.

70 Blanpain, C., Mohrin, M., Sotiropoulou, P. A. & Passegue, E. (2011). DNA-damage response in tissue-specific and cancer stem cells. *Cell stem cell* **8** (1): 16-29.

71 Memisoglu, A. & Samson, L. (2000). Base excision repair in yeast and mammals. *Mutat Res* **451** (1-2): 39-51.

72 Kelley, M. R., Kow, Y. W. & Wilson, D. M., 3rd (2003). Disparity between DNA base excision repair in yeast and mammals: translational implications. *Cancer Res* **63** (3): 549-554.

73 Kamileri, I., Karakasilioti, I. & Garinis, G. A. (2012). Nucleotide excision repair: new tricks with old bricks. *Trends Genet* **28** (11): 566-573.

74 Larrea, A. A., Lujan, S. A. & Kunkel, T. A. (2010). SnapShot: DNA mismatch repair. *Cell* **141** (4): 730 e731.

75 Pluciennik, A. *et al.* (2010). PCNA function in the activation and strand direction of MutLalpha endonuclease in mismatch repair. *Proc Natl Acad Sci U S A* **107** (37): 16066-16071.

76 Iyer, R. R., Pluciennik, A., Burdett, V. & Modrich, P. L. (2006). DNA mismatch repair: functions and mechanisms. *Chem Rev* **106** (2): 302-323.

77 Moore, J. K. & Haber, J. E. (1996). Cell cycle and genetic requirements of two pathways of nonhomologous end-joining repair of double-strand breaks in Saccharomyces cerevisiae. *Mol Cell Biol* **16** (5): 2164-2173.

78 van Gent, D. C. & van der Burg, M. (2007). Non-homologous end-joining, a sticky affair. *Oncogene* **26** (56): 7731-7740.

79 Yano, K. *et al.* (2008). Ku recruits XLF to DNA double-strand breaks. *EMBO Rep* **9** (1): 91-96.

80 Paques, F. & Haber, J. E. (1999). Multiple pathways of recombination induced by double-strand breaks in Saccharomyces cerevisiae. *Microbiol Mol Biol Rev* **63** (2): 349-404.

81 Szostak, J. W., Orr-Weaver, T. L., Rothstein, R. J. & Stahl, F. W. (1983). The double-strand-break repair model for recombination. *Cell* **33** (1): 25-35.

82 Fung-Leung, W. P. & Mak, T. W. (1992). Embryonic stem cells and homologous recombination. *Curr Opin Immunol* **4** (2): 189-194.

83 Slupianek, A. *et al.* (2011). Targeting RAD51 phosphotyrosine-315 to prevent unfaithful recombination repair in BCR-ABL1 leukemia. *Blood* **118** (4): 1062-1068.

84 Kazak, L., Reyes, A. & Holt, I. J. (2012). Minimizing the damage: repair pathways keep mitochondrial DNA intact. *Nat Rev Mol Cell Biol* **13** (10): 659-671.

85 Bitomsky, N. & Hofmann, T. G. (2009). Apoptosis and autophagy: Regulation of apoptosis by DNA damage signalling - roles of p53, p73 and HIPK2. *FEBS J* **276** (21): 6074-6083.

86 Kannan, K. *et al.* (2001). DNA microarrays identification of primary and secondary target genes regulated by p53. *Oncogene* **20** (18): 2225-2234.

87 Abbas, T. & Dutta, A. (2009). p21 in cancer: intricate networks and multiple activities. *Nat Rev Cancer* **9** (6): 400-414.

88 Lin, T. *et al.* (2005). p53 induces differentiation of mouse embryonic stem cells by suppressing Nanog expression. *Nat Cell Biol* **7** (2): 165-171.

89 Nordberg, J. & Arner, E. S. (2001). Reactive oxygen species, antioxidants, and the mammalian thioredoxin system. *Free Radic Biol Med* **31** (11): 1287-1312.

90 Lu, S. C. (2009). Regulation of glutathione synthesis. *Mol Aspects Med* **30** (1-2): 42-59.

91 Sun, X. *et al.* (2006). Two-photon imaging of glutathione levels in intact brain indicates enhanced redox buffering in developing neurons and cells at the cerebrospinal fluid and blood-brain interface. *J Biol Chem* **281** (25): 17420-17431.

92 Balendiran, G. K., Dabur, R. & Fraser, D. (2004). The role of glutathione in cancer. *Cell Biochem Funct* **22** (6): 343-352.

93 Dringen, R. & Hamprecht, B. (1996). Glutathione content as an indicator for the presence of metabolic pathways of amino acids in astroglial cultures. *J Neurochem* **67** (4): 1375-1382.

94 Rhee, S. G., Chae, H. Z. & Kim, K. (2005). Peroxiredoxins: a historical overview and speculative preview of novel mechanisms and emerging concepts in cell signaling. *Free Radic Biol Med* **38** (12): 1543-1552.

95 Neumann, C. A. *et al.* (2003). Essential role for the peroxiredoxin Prdx1 in erythrocyte antioxidant defence and tumour suppression. *Nature* **424** (6948): 561-565.

96 Van De Straat, R., De Vries, J., Kulkens, T., Debets, A. J. & Vermeulen, N. P. (1986). Paracetamol, 3-monoalkyl- and 3,5-dialkyl derivatives. Comparison of their microsomal cytochrome P-450 dependent oxidation and toxicity in freshly isolated hepatocytes. *Biochem Pharmacol* **35** (21): 3693-3699.

97 Hayes, J. D. & McLellan, L. I. (1999). Glutathione and glutathione-dependent enzymes represent a co-ordinately regulated defence against oxidative stress. *Free Radic Res* **31** (4): 273-300.

98 Ramassamy, C. *et al.* (1999). Oxidative damage and protection by antioxidants in the frontal cortex of Alzheimer's disease is related to the apolipoprotein E genotype. *Free Radic Biol Med* **27** (5-6): 544-553.

99 Rogakou, E. P., Boon, C., Redon, C. & Bonner, W. M. (1999). Megabase chromatin domains involved in DNA double-strand breaks in vivo. *J Cell Biol* **146** (5): 905-916.

100 McKelvey-Martin, V. J. *et al.* (1993). The single cell gel electrophoresis assay (comet assay): a European review. *Mutat Res* **288** (1): 47-63.

101 Lesko, S. A. *et al.* (1989). Quantitative immunofluorescence assay for cyclobutyldithymidine dimers in individual mammalian cells. *Carcinogenesis* **10** (4): 641-646.

102 Evans, M. D. *et al.* (2008). Analysis of urinary 8-oxo-7,8-dihydro-purine-2'-deoxyribonucleosides by LC-MS/MS and improved ELISA. *Free Radic Res* **42** (10): 831-840.

103 Santos, J. H., Meyer, J. N., Mandavilli, B. S. & Van Houten, B. (2006). Quantitative PCR-based measurement of nuclear and mitochondrial DNA damage and repair in mammalian cells. *Methods Mol Biol* **314**:183-199.

104 Singh, B. & Bhat, H. K. (2012). Superoxide dismutase 3 is induced by antioxidants, inhibits oxidative DNA damage and is associated with inhibition of estrogen-induced breast cancer. *Carcinogenesis* **33** (12): 2601-2610.

105 Rothfuss, O., Gasser, T. & Patenge, N. (2010). Analysis of differential DNA damage in the mitochondrial genome employing a semi-long run real-time PCR approach. *Nucleic Acids Res* **38** (4): e24.

106 Hayflick, L. & Moorhead, P. S. (1961). The serial cultivation of human diploid cell strains. *Exp Cell Res* **25**: 585-621.

107 Goldstein, S. (1990). Replicative senescence: the human fibroblast comes of age. *Science* **249** (4973): 1129-1133.

108 Zeng, X. (2007). Human embryonic stem cells: mechanisms to escape replicative senescence? *Stem Cell Rev* **3** (4): 270-279.

109 Chambers, I. *et al.* (2003). Functional expression cloning of Nanog, a pluripotency sustaining factor in embryonic stem cells. *Cell* **113** (5): 643-655.

110 Wang, J. *et al.* (2006). A protein interaction network for pluripotency of embryonic stem cells. *Nature* **444** (7117): 364-368.

111 Tonge, P. D. & Andrews, P. W. (2010). Retinoic acid directs neuronal differentiation of human pluripotent stem cell lines in a non-cell-autonomous manner. *Differentiation* **80** (1): 20-30.

112 Chen, Y. F. *et al.* (2012). Rapid generation of mature hepatocyte-like cells from human induced pluripotent stem cells by an efficient three-step protocol. *Hepatology* **55** (4): 1193-1203.

113 Zhu, Z. & Huangfu, D. (2013). Human pluripotent stem cells: an emerging model in developmental biology. *Development* **140** (4): 705-717.

114 Guguen-Guillouzo, C., Corlu, A. & Guillouzo, A. (2010). Stem cell-derived hepatocytes and their use in toxicology. *Toxicology* **270** (1): 3-9.

115 Vojnits, K. & Bremer, S. (2010). Challenges of using pluripotent stem cells for safety assessments of substances. *Toxicology* **270** (1): 10-17.

116 Robinton, D. A. & Daley, G. Q. (2012). The promise of induced pluripotent stem cells in research and therapy. *Nature* **481** (7381): 295-305.

117 Bellin, M., Marchetto, M. C., Gage, F. H. & Mummery, C. L. (2012). Induced pluripotent stem cells: the new patient? *Nat Rev Mol Cell Biol* **13** (11): 713-726.

118 Roy, N. S. *et al.* (2006). Functional engraftment of human ES cell-derived dopaminergic neurons enriched by coculture with telomerase-immortalized midbrain astrocytes. *Nat Med* **12** (11): 1259-1268.

119 Ganat, Y. M. *et al.* (2012). Identification of embryonic stem cell-derived midbrain dopaminergic neurons for engraftment. *J Clin Invest* **122** (8): 2928-2939.

120 Laflamme, M. A. *et al.* (2007). Cardiomyocytes derived from human embryonic stem cells in pro-survival factors enhance function of infarcted rat hearts. *Nat Biotechnol* **25** (9): 1015-1024.

121 Shiba, Y. *et al.* (2012). Human ES-cell-derived cardiomyocytes electrically couple and suppress arrhythmias in injured hearts. *Nature* **489** (7415): 322-325.

122 Rashid, S. T. *et al.* (2010). Modeling inherited metabolic disorders of the liver using human induced pluripotent stem cells. *J Clin Invest* **120** (9): 3127-3136.

123 Ghodsizadeh, A. *et al.* (2010). Generation of liver disease-specific induced pluripotent stem cells along with efficient differentiation to functional hepatocyte-like cells. *Stem Cell Rev* **6** (4): 622-632.

124 Alipio, Z. *et al.* (2010). Reversal of hyperglycemia in diabetic mouse models using induced-pluripotent stem (iPS)-derived pancreatic beta-like cells. *Proc Natl Acad Sci U S A* **107** (30): 13426-13431.

125 Maehr, R. *et al.* (2009). Generation of pluripotent stem cells from patients with type 1 diabetes. *Proc Natl Acad Sci U S A* **106** (37): 15768-15773.

126 Dimos, J. T. *et al.* (2008). Induced pluripotent stem cells generated from patients with ALS can be differentiated into motor neurons. *Science* **321** (5893): 1218-1221.

127 Han, S. S., Williams, L. A. & Eggan, K. C. (2011). Constructing and deconstructing stem cell models of neurological disease. *Neuron* **70** (4): 626-644.

128 Kondo, T. *et al.* (2013). Modeling Alzheimer's Disease with iPSCs Reveals Stress Phenotypes Associated with Intracellular Abeta and Differential Drug Responsiveness. *Cell stem cell* **12** (4): 487-496.

129 Ben-Porath, I. *et al.* (2008). An embryonic stem cell-like gene expression signature in poorly differentiated aggressive human tumors. *Nat Genet* **40** (5): 499-507.

130 Li, Y. *et al.* (2011). c-Met signaling induces a reprogramming network and supports the glioblastoma stem-like phenotype. *Proc Natl Acad Sci U S A* **108** (24): 9951-9956.

131 Leis, O. *et al.* (2012). Sox2 expression in breast tumours and activation in breast cancer stem cells. *Oncogene* **31** (11): 1354-1365.

132 Pelengaris, S., Khan, M. & Evan, G. (2002). c-MYC: more than just a matter of life and death. *Nat Rev Cancer* **2** (10): 764-776.

133 Kregel, S. *et al.* (2013). Sox2 is an androgen receptor-repressed gene that promotes castration-resistant prostate cancer. *PloS one* **8** (1): e53701.

134 Schrock, A. *et al.* (2013). Sex Determining Region Y-Box 2 (SOX2) Amplification Is an Independent Indicator of Disease Recurrence in Sinonasal Cancer. *PloS one* **8** (3): e59201.

135 Baccelli, I. & Trumpp, A. (2012). The evolving concept of cancer and metastasis stem cells. *J Cell Biol* **198** (3): 281-293.

136 Takahashi, K. *et al.* (2007). Induction of pluripotent stem cells from adult human fibroblasts by defined factors. *Cell* **131** (5): 861-872.

137 Tapia, N. & Scholer, H. R. (2010). p53 connects tumorigenesis and reprogramming to pluripotency. *J Exp Med* **207** (10): 2045-2048.

138 Warren, L. *et al.* (2010). Highly efficient reprogramming to pluripotency and directed differentiation of human cells with synthetic modified mRNA. *Cell stem cell* **7** (5): 618-630.

139 Zhou, H. *et al.* (2009). Generation of induced pluripotent stem cells using recombinant proteins. *Cell stem cell* **4** (5): 381-384.

140 Sancho-Bru, P. *et al.* (2011). Directed differentiation of murine-induced pluripotent stem cells to functional hepatocyte-like cells. *J Hepatol* **54** (1): 98-107.

141 Banito, A. & Gil, J. (2010). Induced pluripotent stem cells and senescence: learning the biology to improve the technology. *EMBO Rep* **11** (5): 353-359.

142 Muller, R. & Lengerke, C. (2009). Patient-specific pluripotent stem cells: promises and challenges. *Nat Rev Endocrinol* **5** (4): 195-203.

143 Yamanaka, S. & Blau, H. M. (2010). Nuclear reprogramming to a pluripotent state by three approaches. *Nature* **465** (7299): 704-712.

144 Tachibana, M. *et al.* (2013). Human Embryonic Stem Cells Derived by Somatic Cell Nuclear Transfer. *Cell* : Epub ahead of print.

145 Soza-Ried, J. & Fisher, A. G. (2012). Reprogramming somatic cells towards pluripotency by cellular fusion. *Curr Opin Genet Dev* **22** (5): 459-465.

146 Takahashi, K., Okita, K., Nakagawa, M. & Yamanaka, S. (2007). Induction of pluripotent stem cells from fibroblast cultures. *Nat Protoc* **2** (12): 3081-3089.

147 Liu, H., Ye, Z., Kim, Y., Sharkis, S. & Jang, Y. Y. (2010). Generation of endoderm-derived human induced pluripotent stem cells from primary hepatocytes. *Hepatology* **51** (5): 1810-1819.

148 Seki, T. *et al.* (2010). Generation of induced pluripotent stem cells from human terminally differentiated circulating T cells. *Cell stem cell* **7** (1): 11-14.

149 Zhou, T. *et al.* (2012). Generation of human induced pluripotent stem cells from urine samples. *Nat Protoc* **7** (12): 2080-2089.

150 Liao, J. *et al.* (2009). Generation of induced pluripotent stem cell lines from adult rat cells. *Cell stem cell* **4** (1): 11-15.

151 Liu, H. *et al.* (2008). Generation of induced pluripotent stem cells from adult rhesus monkey fibroblasts. *Cell stem cell* **3** (6): 587-590.

152 Nakagawa, M. *et al.* (2008). Generation of induced pluripotent stem cells without Myc from mouse and human fibroblasts. *Nat Biotechnol* **26** (1): 101-106.

153 Kim, J. B. *et al.* (2008). Pluripotent stem cells induced from adult neural stem cells by reprogramming with two factors. *Nature* **454** (7204): 646-650.

154 Giorgetti, A. *et al.* (2009). Generation of induced pluripotent stem cells from human cord blood using OCT4 and SOX2. *Cell stem cell* **5** (4): 353-357.

155 Kim, J. B. *et al.* (2009). Oct4-induced pluripotency in adult neural stem cells. *Cell* **136** (3): 411-419.

156 Sterneckert, J., Hoing, S. & Scholer, H. R. (2012). Concise review: Oct4 and more: the reprogramming expressway. *Stem cells* **30** (1): 15-21.

157 Efe, J. A. *et al.* (2011). Conversion of mouse fibroblasts into cardiomyocytes using a direct reprogramming strategy. *Nat Cell Biol* **13** (3): 215-222.

158 Sancho-Martinez, I., Baek, S. H. & Izpisua Belmonte, J. C. (2012). Lineage conversion methodologies meet the reprogramming toolbox. *Nat Cell Biol* **14** (9): 892-899.

159 Ohgushi, M. & Sasai, Y. (2011). Lonely death dance of human pluripotent stem cells: ROCKing between metastable cell states. *Trends Cell Biol* **21** (5): 274-282.

160 Ohgushi, M. *et al.* (2010). Molecular pathway and cell state responsible for dissociation-induced apoptosis in human pluripotent stem cells. *Cell stem cell* **7** (2): 225-239.

161 Krtolica, A. *et al.* (2007). Disruption of apical-basal polarity of human embryonic stem cells enhances hematoendothelial differentiation. *Stem cells* **25** (9): 2215-2223.

162 Hanna, J. *et al.* (2010). Human embryonic stem cells with biological and epigenetic characteristics similar to those of mouse ESCs. *Proc Natl Acad Sci U S A* **107** (20): 9222-9227.

163 Buecker, C. *et al.* (2010). A murine ESC-like state facilitates transgenesis and homologous recombination in human pluripotent stem cells. *Cell stem cell* **6** (6): 535-546.

164 Miura, K. *et al.* (2009). Variation in the safety of induced pluripotent stem cell lines. *Nat Biotechnol* **27** (8): 743-745.

165 Mostoslavsky, G. (2012). Concise review: The magic act of generating induced pluripotent stem cells: many rabbits in the hat. *Stem cells* **30** (1): 28-32.

166 Blelloch, R., Venere, M., Yen, J. & Ramalho-Santos, M. (2007). Generation of induced pluripotent stem cells in the absence of drug selection. *Cell stem cell* **1** (3): 245-247.

167 Somers, A. *et al.* (2010). Generation of transgene-free lung disease-specific human induced pluripotent stem cells using a single excisable lentiviral stem cell cassette. *Stem cells* **28** (10): 1728-1740.

168 Woltjen, K. *et al.* (2009). piggyBac transposition reprograms fibroblasts to induced pluripotent stem cells. *Nature* **458** (7239): 766-770.

169 Stadtfeld, M., Nagaya, M., Utikal, J., Weir, G. & Hochedlinger, K. (2008). Induced pluripotent stem cells generated without viral integration. *Science* **322** (5903): 945-949.

170 Okita, K., Hong, H., Takahashi, K. & Yamanaka, S. (2010). Generation of mouse-induced pluripotent stem cells with plasmid vectors. *Nat Protoc* **5** (3): 418-428.

171 Kim, D. *et al.* (2009). Generation of human induced pluripotent stem cells by direct delivery of reprogramming proteins. *Cell stem cell* **4** (6): 472-476.

172 Hong, H. *et al.* (2009). Suppression of induced pluripotent stem cell generation by the p53-p21 pathway. *Nature* **460** (7259): 1132-1135.

173 Kawamura, T. *et al.* (2009). Linking the p53 tumour suppressor pathway to somatic cell reprogramming. *Nature* **460** (7259): 1140-1144.

174 Li, H. *et al.* (2009). The Ink4/Arf locus is a barrier for iPS cell reprogramming. *Nature* **460** (7259): 1136-1139.

175 Marion, R. M. *et al.* (2009). A p53-mediated DNA damage response limits reprogramming to ensure iPS cell genomic integrity. *Nature* **460** (7259): 1149-1153.

176 Utikal, J. *et al.* (2009). Immortalization eliminates a roadblock during cellular reprogramming into iPS cells. *Nature* **460** (7259): 1145-1148.

177 Li, F. *et al.* (2010). Apoptotic caspases regulate induction of iPSCs from human fibroblasts. *Cell stem cell* **7** (4): 508-520.

178 Esteban, M. A. *et al.* (2010). Vitamin C enhances the generation of mouse and human induced pluripotent stem cells. *Cell stem cell* **6** (1): 71-79.

179 Yoshida, Y., Takahashi, K., Okita, K., Ichisaka, T. & Yamanaka, S. (2009). Hypoxia enhances the generation of induced pluripotent stem cells. *Cell stem cell* **5** (3): 237-241.

180 Kang, L., Wang, J., Zhang, Y., Kou, Z. & Gao, S. (2009). iPS cells can support full-term development of tetraploid blastocyst-complemented embryos. *Cell stem cell* **5** (2): 135-138.

181 Tam, P. P. & Rossant, J. (2003). Mouse embryonic chimeras: tools for studying mammalian development. *Development* **130** (25): 6155-6163.

182 Ito, M. *et al.* (2002). NOD/SCID/gamma(c)(null) mouse: an excellent recipient mouse model for engraftment of human cells. *Blood* **100** (9): 3175-3182.

183 Hanna, J. *et al.* (2009). Direct cell reprogramming is a stochastic process amenable to acceleration. *Nature* **462** (7273): 595-601.

184 Okita, K., Ichisaka, T. & Yamanaka, S. (2007). Generation of germline-competent induced pluripotent stem cells. *Nature* **448** (7151): 313-317.

185 Mayshar, Y. *et al.* (2010). Identification and classification of chromosomal aberrations in human induced pluripotent stem cells. *Cell stem cell* **7** (4): 521-531.

186 Laurent, L. C. *et al.* (2011). Dynamic changes in the copy number of pluripotency and cell proliferation genes in human ESCs and iPSCs during reprogramming and time in culture. *Cell stem cell* **8** (1): 106-118.

187 Doi, A. *et al.* (2009). Differential methylation of tissue- and cancer-specific CpG island shores distinguishes human induced pluripotent stem cells, embryonic stem cells and fibroblasts. *Nat Genet* **41** (12): 1350-1353.

188 Kim, K. *et al.* (2010). Epigenetic memory in induced pluripotent stem cells. *Nature* **467** (7313): 285-290.

189 Kim, K. *et al.* (2011). Donor cell type can influence the epigenome and differentiation potential of human induced pluripotent stem cells. *Nat Biotechnol* **29** (12): 1117-1119.

190 Hu, Q., Friedrich, A. M., Johnson, L. V. & Clegg, D. O. (2010). Memory in induced pluripotent stem cells: reprogrammed human retinal-pigmented epithelial cells show tendency for spontaneous redifferentiation. *Stem cells* **28** (11): 1981-1991.

191 Wilson, K. D. *et al.* (2009). MicroRNA profiling of human-induced pluripotent stem cells. *Stem Cells Dev* **18** (5): 749-758.

192 Loewer, S. *et al.* (2010). Large intergenic non-coding RNA-RoR modulates reprogramming of human induced pluripotent stem cells. *Nat Genet* **42** (12): 1113-1117.

193 Polo, J. M. *et al.* (2010). Cell type of origin influences the molecular and functional properties of mouse induced pluripotent stem cells. *Nat Biotechnol* **28** (8): 848-855.

194 Feng, Q. *et al.* (2010). Hemangioblastic derivatives from human induced pluripotent stem cells exhibit limited expansion and early senescence. *Stem cells* **28** (4): 704-712.

195 Kaneko, S. & Yamanaka, S. (2013). To Be Immunogenic, or Not to Be: That's the iPSC Question. *Cell stem cell* **12** (4): 385-386.

196 Kaufman, D. S. (2009). Toward clinical therapies using hematopoietic cells derived from human pluripotent stem cells. *Blood* **114** (17): 3513-3523.

197 Zou, J. *et al.* (2009). Gene targeting of a disease-related gene in human induced pluripotent stem and embryonic stem cells. *Cell stem cell* **5** (1): 97-110.

198 Raya, A. *et al.* (2010). A protocol describing the genetic correction of somatic human cells and subsequent generation of iPS cells. *Nat Protoc* **5** (4): 647-660.

199 Liu, G. H. *et al.* (2012). Progressive degeneration of human neural stem cells caused by pathogenic LRRK2. *Nature* **491** (7425): 603-607.

200 Reinhardt, P. *et al.* (2013). Genetic correction of a LRRK2 mutation in human iPSCs links parkinsonian neurodegeneration to ERK-dependent changes in gene expression. *Cell stem cell* **12** (3): 354-367.

201 Chang, C. J. & Bouhassira, E. E. (2012). Zinc-finger nuclease-mediated correction of alpha-thalassemia in iPS cells. *Blood* **120** (19): 3906-3914.

202 Zou, J., Mali, P., Huang, X., Dowey, S. N. & Cheng, L. (2011). Site-specific gene correction of a point mutation in human iPS cells derived from an adult patient with sickle cell disease. *Blood* **118** (17): 4599-4608.

203 Liu, G. H. *et al.* (2011). Targeted gene correction of laminopathy-associated LMNA mutations in patient-specific iPSCs. *Cell stem cell* **8** (6): 688-694.

204 Howden, S. E. *et al.* (2011). Genetic correction and analysis of induced pluripotent stem cells from a patient with gyrate atrophy. *Proc Natl Acad Sci U S A* **108** (16): 6537-6542.

205 Zou, J. *et al.* (2011). Oxidase-deficient neutrophils from X-linked chronic granulomatous disease iPS cells: functional correction by zinc finger nuclease-mediated safe harbor targeting. *Blood* **117** (21): 5561-5572.

206 Prigione, A., Fauler, B., Lurz, R., Lehrach, H. & Adjaye, J. (2010). The senescence-related mitochondrial/oxidative stress pathway is repressed in human induced pluripotent stem cells. *Stem cells* **28** (4): 721-733.

207 Guo, Y. L., Chakraborty, S., Rajan, S. S., Wang, R. & Huang, F. (2010). Effects of oxidative stress on mouse embryonic stem cell proliferation, apoptosis, senescence, and self-renewal. *Stem Cells Dev* **19** (9): 1321-1331.

208 Ji, A. R. *et al.* (2010). Reactive oxygen species enhance differentiation of human embryonic stem cells into mesendodermal lineage. *Exp Mol Med* **42** (3): 175-186.

209 Schmelter, M., Ateghang, B., Helmig, S., Wartenberg, M. & Sauer, H. (2006). Embryonic stem cells utilize reactive oxygen species as transducers of mechanical strain-induced cardiovascular differentiation. *FASEB J* **20** (8): 1182-1184.

210 Maynard, S. *et al.* (2008). Human embryonic stem cells have enhanced repair of multiple forms of DNA damage. *Stem cells* **26** (9): 2266-2274.

211 Ramalho-Santos, M., Yoon, S., Matsuzaki, Y., Mulligan, R. C. & Melton, D. A. (2002). "Stemness": transcriptional profiling of embryonic and adult stem cells. *Science* **298** (5593): 597-600.

212 Ivanova, N. B. *et al.* (2002). A stem cell molecular signature. *Science* **298** (5593): 601-604.

213 Fong, Y. W. *et al.* (2011). A DNA repair complex functions as an Oct4/Sox2 coactivator in embryonic stem cells. *Cell* **147** (1): 120-131.

214 Momcilovic, O. *et al.* (2010). DNA damage responses in human induced pluripotent stem cells and embryonic stem cells. *PloS one* **5** (10): e13410.

215 Roos, W. P., Christmann, M., Fraser, S. T. & Kaina, B. (2007). Mouse embryonic stem cells are hypersensitive to apoptosis triggered by the DNA damage O(6)-methylguanine due to high E2F1 regulated mismatch repair. *Cell Death Differ* **14** (8): 1422-1432.

216 Filion, T. M. *et al.* (2009). Survival responses of human embryonic stem cells to DNA damage. *J Cell Physiol* **220** (3): 586-592.

217 Barta, T. *et al.* (2010). Human embryonic stem cells are capable of executing G1/S checkpoint activation. *Stem cells* **28** (7): 1143-1152.

218 Dumitru, R. *et al.* (2012). Human embryonic stem cells have constitutively active Bax at the Golgi and are primed to undergo rapid apoptosis. *Mol Cell* **46** (5): 573-583.

219 Oliver, R., Bjoertomt, O., Greenwood, R. & Rothwell, J. (2008). 'Noisy patients'--can signal detection theory help? *Nat Clin Pract Neurol* **4** (6): 306-316.

220 Tietze, F. (1969). Enzymic method for quantitative determination of nanogram amounts of total and oxidized glutathione: applications to mammalian blood and other tissues. *Anal Biochem* **27** (3): 502-522.

221 Rothfuss, O. *et al.* (2009). Parkin protects mitochondrial genome integrity and supports mitochondrial DNA repair. *Hum Mol Genet* **18** (20): 3832-3850.

222 Livak, K. J. & Schmittgen, T. D. (2001). Analysis of relative gene expression data using real-time quantitative PCR and the 2(-Delta Delta C(T)) Method. *Methods* **25** (4): 402-408.

223 Davies, H. *et al.* (2002). Mutations of the BRAF gene in human cancer. *Nature* **417** (6892): 949-954.

224 Steighner, R. J. & Povirk, L. F. (1990). Bleomycin-induced DNA lesions at mutational hot spots: implications for the mechanism of double-strand cleavage. *Proc Natl Acad Sci U S A* **87** (21): 8350-8354.

225 Fung, H. & Demple, B. (2011). Distinct roles of Ape1 protein in the repair of DNA damage induced by ionizing radiation or bleomycin. *J Biol Chem* **286** (7): 4968-4977.

226 Lauber, K. *et al.* (2001). The adapter protein apoptotic protease-activating factor-1 (Apaf-1) is proteolytically processed during apoptosis. *J Biol Chem* **276** (32): 29772-29781.

227 Kabarowski, J. H., Zhu, K., Le, L. Q., Witte, O. N. & Xu, Y. (2001). Lysophosphatidylcholine as a ligand for the immunoregulatory receptor G2A. *Science* **293** (5530): 702-705.

228 Aladjem, M. I. *et al.* (1998). ES cells do not activate p53-dependent stress responses and undergo p53-independent apoptosis in response to DNA damage. *Curr Biol* **8** (3): 145-155.

229 Campbell, C. J. *et al.* (2010). The human stem cell hierarchy is defined by a functional dependence on Mcl-1 for self-renewal capacity. *Blood* **116** (9): 1433-1442.

230 Pastor, W. A. *et al.* (2011). Genome-wide mapping of 5-hydroxymethylcytosine in embryonic stem cells. *Nature* **473** (7347): 394-397.

231 Liu, Y. *et al.* (2006). Genome wide profiling of human embryonic stem cells (hESCs), their derivatives and embryonal carcinoma cells to develop base profiles of U.S. Federal government approved hESC lines. *BMC Dev Biol* **6**: 20.

232 Hauser, P. S., Narayanaswami, V. & Ryan, R. O. (2011). Apolipoprotein E: from lipid transport to neurobiology. *Prog Lipid Res* **50** (1): 62-74.

233 Ikeda, T. *et al.* (1993). Preliminary findings on the variation of serum apolipoprotein levels in neural degenerative disorders. *J Clin Lab Anal* **7** (1): 1-4.

234 Meister, A. (1994). Glutathione-ascorbic acid antioxidant system in animals. *J Biol Chem* **269** (13): 9397-9400.

235 Vukovic, V., Nicklee, T. & Hedley, D. W. (2001). Differential effects of buthionine sulphoximine in hypoxic and non-hypoxic regions of human cervical carcinoma xenografts. *Radiother Oncol* **60** (1): 69-73.

236 Boivin, A. *et al.* (2011). Transient alteration of cellular redox buffering before irradiation triggers apoptosis in head and neck carcinoma stem and non-stem cells. *PloS one* **6** (1): e14558.

237 Held, K. D., Epp, E. R., Awad, S. & Biaglow, J. E. (1991). Postirradiation sensitization of mammalian cells by the thiol-depleting agent dimethyl fumarate. *Radiat Res* **127** (1): 75-80.

238 Wrona, M., Patel, K. & Wardman, P. (2005). Reactivity of 2',7'-dichlorodihydrofluorescein and dihydrorhodamine 123 and their oxidized forms toward carbonate, nitrogen dioxide, and hydroxyl radicals. *Free Radic Biol Med* **38** (2): 262-270.

239 Chen, Q. M. (2000). Replicative senescence and oxidant-induced premature senescence. Beyond the control of cell cycle checkpoints. *Ann N Y Acad Sci* **908**: 111-125.

240 Zenclussen, A. C., Schumacher, A., Zenclussen, M. L., Wafula, P. & Volk, H. D. (2007). Immunology of pregnancy: cellular mechanisms allowing fetal survival within the maternal uterus. *Expert Rev Mol Med* **9** (10): 1-14.

241 Hirano, K. *et al.* (2012). 3-O-sulfated heparan sulfate recognized by the antibody HS4C3 contribute to the differentiation of mouse embryonic stem cells via Fas signaling. *PloS one* **7** (8): e43440.

242 Momcilovic, O. *et al.* (2009). Ionizing radiation induces ataxia telangiectasia mutated-dependent checkpoint signaling and G(2) but not G(1) cell cycle arrest in pluripotent human embryonic stem cells. *Stem cells* **27** (8): 1822-1835.

243 Deng, J. *et al.* (2007). BH3 profiling identifies three distinct classes of apoptotic blocks to predict response to ABT-737 and conventional chemotherapeutic agents. *Cancer cell* **12** (2): 171-185.

244 Sauer, R., Bamberg, M., Hammer, J. & Nemeth, G. (1997). [Strahlentherapie und Onkologie--the publishing organ of German-speaking radio-oncologists]. *Strahlenther Onkol* **173** (2): 57.

245 Asaithamby, A. & Chen, D. J. (2009). Cellular responses to DNA double-strand breaks after low-dose gamma-irradiation. *Nucleic Acids Res* **37** (12): 3912-3923.

246 Lobrich, M., Rydberg, B. & Cooper, P. K. (1995). Repair of x-ray-induced DNA double-strand breaks in specific Not I restriction fragments in human fibroblasts: joining of correct and incorrect ends. *Proc Natl Acad Sci U S A* **92** (26): 12050-12054.

247 Halliwell, B. & Gutteridge, J. M. C. *Free radicals in biology and medicine*. 3rd edn (Clarendon Press ; Oxford University Press, 1999).

248 Booth, M. J. *et al.* (2012). Quantitative sequencing of 5-methylcytosine and 5-hydroxymethylcytosine at single-base resolution. *Science* **336** (6083): 934-937.

249 Muller, F. L., Lustgarten, M. S., Jang, Y., Richardson, A. & Van Remmen, H. (2007). Trends in oxidative aging theories. *Free Radic Biol Med* **43** (4): 477-503.

250 Crespo, F. L., Sobrado, V. R., Gomez, L., Cervera, A. M. & McCreath, K. J. (2010). Mitochondrial reactive oxygen species mediate cardiomyocyte formation from embryonic stem cells in high glucose. *Stem cells* **28** (7): 1132-1142.

251 de Chaves, E. P. & Narayanaswami, V. (2008). Apolipoprotein E and cholesterol in aging and disease in the brain. *Future Lipidol* **3** (5): 505-530.

252 Zhang, P. *et al.* (1997). Thioredoxin peroxidase is a novel inhibitor of apoptosis with a mechanism distinct from that of Bcl-2. *J Biol Chem* **272** (49): 30615-30618.

9. DANKSAGUNG

Ich danke Herrn Prof. Dr. Klaus Schulze-Osthoff dafür, mich in seiner Arbeitsgruppe aufgenommen zu haben und mir große Freiheiten bei der Wahl und Bearbeitung der Themen der dieser Dissertation zugrunde liegenden Promotion gelassen zu haben. Ich danke ihm außerdem für die hervorragenden Arbeitsbedingungen, die großartige Laborausstattung, die mir zur Verfügung stand und letztlich dafür, meine Dissertation mit so viel Geduld gegengelesen zu haben.

Ich danke Herrn Prof. Dr. Sebastian Wesselborg für die Übernahme des Zweitgutachtens und seine Bereitschaft, trotz der großen Entfernung von Düsseldorf nach Tübingen zu reisen, um die mündliche Prüfung abzunehmen.

Ich danke Dr. Oliver Rothfuss für die wunderbare Betreuung meiner Promotion, seine Geduld und seine gute Laune, die mich bei Misserfolgen immer wieder aufmunterte und aufrichtete. Auch über die wissenschaftliche Arbeit hinaus haben mir sein Rat und die Gespräche mit ihm viel bedeutet. Vielen Dank Dir dafür, Oli!

Ich danke Dr. Frank Eßmann für seine zahllosen kritischen und hilfreichen Kommentare, die Software-Notfallhilfe und kollegiale Unterstützung. Danke, Frank!

Ich danke allen Kolleginnen und Kollegen, Ayline, Benjamin & Benjamin, Britta, Dominic, Eva, Franziska, Kerstin, Marianne, Peter, Sebastian und Stephanie für die schöne gemeinsame Zeit und die Unterstützung, die ich von ihnen erfahren habe.

Ich danke meinen Eltern Britta und Peter Lehle sowie meinen Geschwistern Fiona und Nico, meinen Großmüttern Felicitas und Erna, meiner Tante Bini und meinen Cousins Robin und Fabian dafür, dass sie mich immer unterstützt haben und immer für mich da waren. Ihr Rückhalt, ihr Zuspruch und ihre Liebe haben mir erst ermöglicht, diese Promotion und Dissertation durchzuführen bzw. zu verfassen. Ich danke Euch von Herzen dafür!

Ich danke Marie dafür, dass sie mir auch in schwierigen Zeiten den Rücken stärkt und immer ein offenes Ohr für mich hat. Du bist mein Fels in der Brandung und ich bin sehr glücklich darüber, dass Du bei mir bist und immer an meiner Seite stehst!

Abschließend möchte ich Prof. Dr. Marek Los für das Bereitstellen von RNA humaner ES-Zellen, Prof. Dr. Gasser und seiner Arbeitsgruppe für die vielschichtige Zusammenarbeit sowie meinen Mitbewohnern Christian, Jochen und Johanna, meinem besten Freund Benni sowie allen Freunden und Bekannten danken, die mich im Laufe der letzten Jahre unterstützt und begleitet haben. Danke!

10. PUBLIKATIONEN

Lehle S., Hildebrand D.G., Merz B., Malak P.N., Essmann F, Schulze-Osthoff K. & Rothfuss O.C. (2013). LORD-Q: Accurate Long-Run Real-Time PCR-based DNA Damage Quantification. *Nucleic Acids Research*. Manuscript under revision.

Hildebrand D.G., Lehle S., Borst A., Haferkamp S., Essmann F., Schulze-Osthoff K. (2013). α-Fucosidase as a novel convenient biomarker for cellular senescence. *Cell Cycle* **12** (12): Epub ahead of print.

Hildebrand D.G., Alexander E., Hörber S., Lehle S., Obermayer K., Münck N.A., Rothfuss O., Frick J.S., Morimatsu M., Schmitz I., Roth J., Ehrchen J.M., Essmann F., Schulze-Osthoff K. (2013) IκBζ Is a Transcriptional Key Regulator of CCL2/MCP-1. *J Immunol*. **190** (9): 4812-4820.

Konantz M., André M.C., Ebinger M., Grauer M., Wang H., Grzywna S., Rothfuss O.C., Lehle S., Kustikova O.S., Salih H.R., Handgretinger R., Fend F., Baum C., Kanz L., Quintanilla-Martinez L., Schulze-Osthoff K., Essmann F. & Lengerke C. (2012). EVI-1 modulates leukemogenic potential and apoptosis sensitivity in human acute lymphoblastic leukemia. *Leukemia*. **27** (1): 56-65 .

Shanmugasundararaj S., Lehle S., Yamodo H.I., Husain S.S., Tseng C., Nguyen K., Addona G.H. & Miller K.W. (2012) The location and nature of general anesthetic binding sites on the active conformation of firefly luciferase; a time resolved photolabeling study. *PLoS One* **7** (1): e29854.

11. EIDESSTATTLICHE VERSICHERUNG

Hiermit erkläre ich an Eides statt, dass ich die vorliegende Arbeit zum Thema

„Characterization of apoptosis and DNA damage response and in human induced pluripotent stem cells“

eigenständig, ohne unerlaubte Hilfe und nur unter Verwendung der angegebenen Hilfsmittel angefertigt habe. Alle sinngemäß und wörtlich übernommenen Textstellen aus Veröffentlichungen oder aus anderweitigen fremden Äußerungen habe ich als solche kenntlich gemacht.

Tübingen, den 28.05.13 Simon Lehle

12. ERKLÄRUNG ZUM EIGENANTEIL

Die Planung dieses Projekts sowie die experimentelle Ausführung, Auswertung und grafische Darstellung der Ergebnisse wurden von mir bzw. unter meiner Betreuung und mit meiner Zustimmung durchgeführt.

Teile der Experimente, deren Planung und Auswertung der im Kapitel 4.2 dargestellten Ergebnisse wurden von Ayline Wilhelm im Rahmen ihrer Diplomarbeit unter meiner Betreuung durchgeführt. Teile der Abbildungen in diesem Abschnitt gehen auf das von ihr bearbeitete Projekt zurück.

Die Ergebnisse der Kapitel 4.1 und 4.3 sind Teil eines zur Publikation im Journal *Nucleic Acids Research* eingereichten Manuskripts. Die Abbildungen 4.8 bis einschließlich 4.16 sind Teil dieses Manuskripts und aus diesem in modifizierter Form übernommen. Teile der Idee dieses Teilprojekts sowie einzelne Experimente wurden von Dr. Oliver Rothfuss und Dominic Hildebrand mitentwickelt bzw. durchgeführt. Dr. Oliver Rothfuss führte insbesondere die Reprogrammierung der humanen Fibroblasten (Abb. 4.1) und die ChIP-Analysen sowie die zugehörigen qPCR-Analysen, dargestellt in Abbildung 4.16B bzw. 4.16A, durch und war wesentlich an der Erstellung der Abbildungen 4.1 und 4.8 bis 4.16 beteiligt. Des Weiteren waren Benjamin Dannenmann, Mirjam Fröschl und Manuel Cavada unter meiner Betreuung an experimentellen Durchführungen dieses Abschnitts beteiligt.

Der Abschnitt 4.4 ist Gegenstand der Diplomarbeit von Benjamin Dannenmann, welcher an der Planung, experimentellen Durchführung sowie Auswertung der in diesem Abschnitt vorgestellten Ergebnisse unter meiner Betreuung beteiligt war. Weiterhin war Mirjam Fröschl während ihrer Zeit als Praktikantin an der Ausführung und Auswertung von Experimenten beteiligt.